



LUDWIG-MAXIMILIANS-UNIVERSITÄT MÜNCHEN

BACHELOR THESIS

Ward Identities in Many-Body Physics

A Study on the Hubbard Atom

Ward Identitäten in Vielteilchensystemen

Eine Studie des Hubbard Atoms

Chair of Theoretical Solid State Physics[†]

Author

Julia Bialk
j.bialk@campus.lmu.de
LMU Munich

Supervisors

Prof. Dr. Jan von Delft
vondelft@lmu.de
LMU Munich

Nepomuk Ritz
nepomuk.ritz@
physik.uni-muenchen.de
LMU Munich

Benedikt Schneider
schneider.benedikt@physik.uni-
muenchen.de
LMU Munich

Munich, July 24, 2024

[†]https://www.theorie.physik.uni-muenchen.de/171s_th_solidstate_en/

Abstract

Ward identities are exact relations between correlation functions of different order. As they play a fundamental role in gauging the quality of approximations in the context of many body physics, this thesis is dedicated to studying the $U(1)$ Ward identity of the Hubbard atom and its fulfillment for various diagrammatic approaches. First, a general introduction to the topic is given (chapter 1). In chapter 2, the choice of the Hubbard atom as model is illustrated. Next, methods used in this thesis such as the functional field integral for fermionic coherent states, Matsubara formalism and basic principles of diagrammatic perturbation theory are introduced in chapter 3 and 4. These techniques are then applied to the Hubbard atom in chapter 5 to obtain second-order perturbation theory results for Green's function, self-energy and four-point vertex. The second part of the text is concerned with the characterization of symmetries in the path integral formalism. Based on these considerations, the Ward identity corresponding to the $U(1)$ symmetry of the Hubbard atom is derived (chapter 6) and verified (chapter 7). To analyze a violation of the Ward identity in an exemplary manner, expressions for four-point vertex and self-energy were calculated from the Bethe-Salpeter and Schwinger-Dyson equations (chapter 8) and substituted into the identity in chapter 9. Finally, a systematic method of finding analytical and numerical ansatzes for the two-particle irreducible vertex approximation is discussed in chapter 10 and 11.

Ward Identitäten sind exakte Relationen zwischen Korrelationsfunktionen verschiedener Ordnung. Aufgrund der fundamentalen Rolle, die Ward Identitäten bei der Überprüfung der Qualität von Approximationen im Hinblick auf Vielteilchensysteme innehaben, ist diese Bachelorarbeit der Untersuchung der $U(1)$ Ward Identität und ihrer Erfüllung für diagrammatische Störungstheorie im Kontext des Hubbard Atoms gewidmet. Zuerst wird im Kapitel 1 allgemein in das Thema eingeleitet. Im Kapitel 2 wird die Auswahl des Hubbard Atom als exemplarisches Modell erläutert. Es folgt die Vorstellung diverser in dieser Arbeit benutzen Methoden wie beispielsweise das Funktionalintegral für fermionische kohärente Zustände, der Matsubara Formalismus und grundlegende Prinzipien der diagrammatischen Störungstheorie (Kapitel 3 und 4). Danach werden diese Techniken auf das Hubbard Atom angewendet, um Ergebnisse in zweiter Ordnung Störungstheorie zu erhalten (Kapitel 5).

Die zweite Hälfte dieser Arbeit beschäftigt sich zunächst mit der Charakterisierung von Symmetrien im Pfadintegral-Formalismus. Davon ausgehend wird diejenige Ward Identität, die zur $U(1)$ Symmetrie des Hubbard Atoms korrespondiert, hergeleitet (Kapitel 6) und verifiziert (Kapitel 7). Um beispielhaft eine Verletzung der Identität zu analysieren, werden Ausdrücke für Vierpunkt-Vertex und Selbstenergie aus den Bethe-Salpeter- und Schwinger-Dyson Gleichungen abgeleitet (Kapitel 8) und eingesetzt (Kapitel 9). Abschließend wird eine systematische Methode diskutiert, um analytische und numerische Ansätze zur total-irreduziblen Vertex Approximation zu finden (Kapitel 10 und 11).

Acknowledgements

First and foremost, I'd like to thank Nepomuk Ritz and Benedikt Schneider for their great supervision. When faced with problems, I could always count on their advice. Without their help, writing this thesis would not have been possible.

Further, I want to thank Professor Dr. Jan von Delft for giving me the opportunity to write my bachelor's thesis at the chair for theoretical solid state physics at LMU Munich about an interesting topic in a very pleasant environment. I especially appreciated the motivational and positive atmosphere he created among his chair members, which inspired me daily to also try my best during my writing process.

Last, special thanks belongs to all group members of the chair of theoretical solid state physics, who made my time there worthwhile. All in all, everyone was very welcoming which made writing my thesis a great experience.

Contents

1	Introduction	1
2	Brief Overview of the Hubbard Model and Its Limits	2
2.1	Introduction to the Hubbard Model	2
2.2	The Hubbard Atom	3
3	Coherent State Path Integral for the Partition Function	6
3.1	Fermionic Coherent States	6
3.2	Time-Representation of the Fermionic Partition Function	8
3.3	Matsubara Frequency Representation of the Fermionic Partition Function	10
4	Many-Body Perturbation Theory	12
4.1	Matsubara Green's Functions	12
4.2	Self-Energy	16
4.3	Four-Point Vertex	18
5	Second-Order Perturbation Theory for the Hubbard Atom	20
5.1	One-Body Green's Function	20
5.2	Self-Energy	23
5.3	Two-body Green's function	24
5.3.1	Two-Body Green's Function for Spin Arguments ($\uparrow\downarrow; \uparrow\downarrow$)	24
5.3.2	Two-Body Green's Function for Spin Arguments ($\uparrow\uparrow; \uparrow\uparrow$)	26
5.4	Four-point Vertex	27
5.4.1	Four-Point Vertex for Spin Arguments ($\uparrow\uparrow; \uparrow\uparrow$)	27
5.4.2	Four-Point Vertex for Spin Arguments ($\uparrow\downarrow; \uparrow\downarrow$)	28
6	Derivation of Ward Identities for the Hubbard Atom	30
6.1	Symmetry Transformations in the Functional Integral Formalism	30
6.2	U(1) Ward Identity for the Hubbard Atom	33
7	Verification of the U(1) Ward Identity for the Hubbard Atom	37
7.1	U(1) Ward Identity in Second-Order Perturbation Theory	37
7.2	U(1) Ward Identity for Exact Vertex and Self-energy	39
8	Derivation of Self-Energy and Vertex from the Parquet Equations	42
8.1	Basics on Parquet Formalism	42
8.2	Four-Point Vertex from the Bethe-Salpeter Equations	43
8.3	Self-Energy from the Schwinger-Dyson Equation	51
9	Fulfillment of the Ward Identity after BSE and SDE	53
10	Analytical Approximation for the Irreducible Four-Point Vertex	56
11	Numerical Approximation for the Irreducible Four-Point Vertex	63
12	Conclusion and Outlook	66
	Bibliography	67

Appendix	69
A Introduction to Functional Derivation	69
B Evaluation of Matsubara Sums	71

1 Introduction

One of the greatest challenges in the field of theoretical solid state physics is posed by accurately describing interacting many-body systems. Even more so, when trying to make predictions about the behavior of a system of correlated fermions due to e.g. the Pauli exclusion principle. Surprisingly, formulating a Hamiltonian encoding the interactions of a large number of particles in a solid is straightforward. However, deriving exact solutions from this Hamiltonian would require almost unlimited computational effort and therefore approximations need to be made. For one, a model can be chosen which for example only considers specific parts of the complete many-body Hamiltonian. To gain elementary knowledge on theoretical methods in many-body physics, the following is a study of an analytically solvable model that still incorporates interactions: the Hubbard atom. Even for this toy model, expressions of quantities describing particles themselves and their interactions can get very involved. Often, the choice of a suitable model is not enough to characterize a many-body system and one needs to think of further approximations. In that regard, an established method is given by diagrammatic perturbation theory, which allows to depict perturbation expansions graphically in the form of Hugenholtz diagrams. With diagrammatic perturbation theory, quantities such as correlation functions, sometimes also referred to as Green's functions, can be approximated for small interaction strengths. As their name suggests, they relate particles and observables at different points in space and time. Correlation functions are of special physical interest, as they are closely connected to experimental quantities. To provide physically realistic predictions for experiments, of course fundamental principles of physics such as conservation laws need to be regarded. Unfortunately, not all diagrammatic techniques automatically ensure conservation laws. However, there is a way to check their fulfillment by considering Ward identities. Ward identities establish exact relations between different types of correlation functions and correspond directly to conservation laws. By substituting approximated quantities into these identities, we can draw conclusions about the quality of the respective method.

In this thesis, various approaches to diagrammatic perturbation theory are discussed in the context of a case study of the Hubbard atom. Methods usually implemented numerically are performed analytically to obtain mathematical expressions for approximated correlation functions, four-point vertex and self-energy. For these diagrammatic methods, this work aims to analyze the fulfillment of the $U(1)$ Ward identity with the aim of minimizing or fully compensating violations. Therefore, we address the Parquet formalism and the two-particle irreducible vertex approximation. Lastly, it is investigated how a modification of the Parquet approximation for the two-particle irreducible vertex could possibly improve the fulfillment of the $U(1)$ Ward identity.

2 Brief Overview of the Hubbard Model and Its Limits

As this thesis aims to investigate how well Ward identities are fulfilled by a perturbative approximation, a toy model needs to be selected. A suitable choice is given by the Hubbard atom, a limit of the Hubbard model, since it is fully analytically solvable. Thus, the first chapter of this thesis is supposed to serve as an introduction to the Hubbard model and to its limit, the Hubbard atom.

2.1 Introduction to the Hubbard Model

First written down in 1963, the Hubbard model was originally supposed to provide a better understanding of transition metal monoxides such as NiO and FeO. In spite of classical band theory assigning these types of materials metallic behavior, in reality they appear to be insulators, which is explained by the Hubbard model [1]. Surprisingly, a variety of other physical phenomena can be described by the Hubbard model as well. For example, a current area of research involving the Hubbard model is its applicability to the main class of high-temperature superconductors, the ceramic cuprates [2]. Due to its strong versatility, many analytical and numerical techniques have been applied to it. Thus, it often assumes the role of an exemplary model in theoretical solid state physics.

We will begin exploring the properties of the Hubbard model by reviewing the assumptions it makes to characterize interacting fermions. Despite the existence of fermionic and bosonic variants, the following text will concentrate on the fermionic version of the Hubbard model. In terms of lattice geometry, this text will consider a square lattice in 2D. Afterwards, the Hamiltonian will be simply stated, since a full derivation lies beyond the scope of this chapter.

The Hubbard model considers a fixed array of lattice sites, which can either be empty, filled by one fermion with spin up or spin down or filled with two fermions with distinct spin according to the Pauli exclusion principle. These fermions interact with each other, if they meet on the same lattice site. Additionally, fermions are assigned a probability to tunnel to neighboring lattice sites. Lastly, if we assume the interaction strength and energy scale of the tunneling to be the same across the whole lattice, the above assumptions applied to a general many-body Hamiltonian correspond to

$$\hat{H} = -t \sum_{\langle ij \rangle, \sigma} (c_{i\sigma}^\dagger c_{j\sigma} + c_{j\sigma}^\dagger c_{i\sigma}) + U \sum_i c_{i\uparrow}^\dagger c_{i\uparrow} c_{i\downarrow}^\dagger c_{i\downarrow} \quad (2.1)$$

with the indices i and j labeling the lattice sites and the notation $\langle ij \rangle$ standing for neighboring lattice site pairs. The index σ accounts for the spin of the fermions, that is $\sigma \in \{\uparrow, \downarrow\}$. Furthermore, c^\dagger and c represent the fermionic creation and annihilation operators.

Using the definition of the number operator $\hat{n}_{i\sigma} = c_{i\sigma}^\dagger c_{i\sigma}$, the Hamiltonian is rewritten as

$$\hat{H} = -t \sum_{\langle ij \rangle, \sigma} (c_{i\sigma}^\dagger c_{j\sigma} + c_{j\sigma}^\dagger c_{i\sigma}) + U \sum_i \hat{n}_{i\uparrow} \hat{n}_{i\downarrow} \equiv \hat{H}_0 + \hat{H}_{\text{int}}. \quad (2.2)$$

Tunneling of fermionic particles on the lattice is described by the first term, whereas t specifies the probability of a particle 'hopping' to its neighboring site. Normally, t is assumed to be positive. The interaction strength of electrons of distinct spin is given by the variable U . In the case of repulsive interaction, U is positive, whereas negative U implies an attractive interaction. However, this thesis will only consider positive U .

As in the next chapters we will consider symmetries of the Hubbard atom, the most important continuous symmetries are presented in Tab. 2.1.

More detailed information to all entries of Tab. 2.1 can be found in [3]. Symmetries were used in

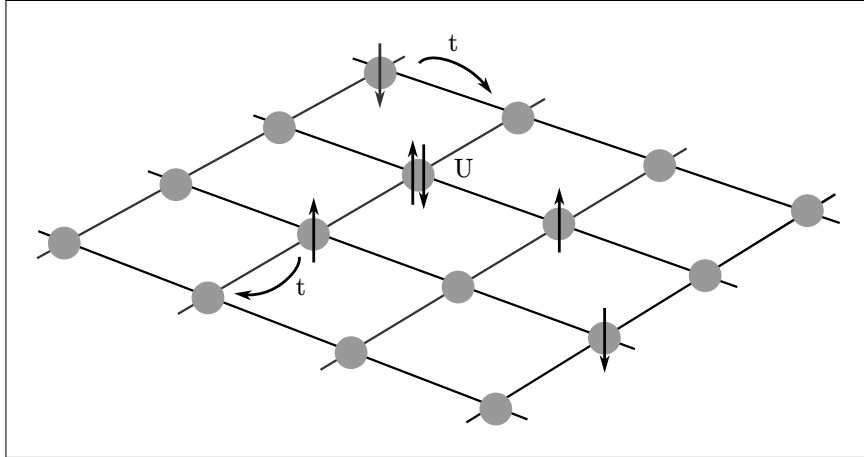


Figure 2.1: Graphic representation of the Hubbard model on a two-dimensional square lattice. An arrow upwards symbolizes an electron with spin up, an arrow downwards an electron with spin down.

continuous symmetry	symmetry group
Gauge symmetry	U(1)
Spin symmetry	SU(2)
Particle-hole-symmetry at half-filling	SU(2)

Table 2.1: Overview of continuous symmetries of the Hubbard Hamiltonian and their corresponding symmetry groups

the Bethe ansatz to solve the Hubbard model in one dimension [4]. Despite seeming simple, no exact solution to the model has been discovered for dimensions higher than one.

Only specific limits of the Hubbard Hamiltonian may be solved easily. Two commonly known limits are characterized by the relation of 'hopping' probability to the interaction scale $\frac{U}{t}$. The limit $\frac{U}{t} \rightarrow 0$ in the case of minimal interaction or very high tunneling probability is called no-interaction or tight-binding limit. In this case, the interaction term \hat{H}_{int} can be neglected and the overall Hamiltonian simplifies to

$$\hat{H} = -t \sum_{\langle ij \rangle, \sigma} (c_{i\sigma}^\dagger c_{j\sigma} + c_{j\sigma}^\dagger c_{i\sigma}). \quad (2.3)$$

A special property of this Hamiltonian is that the corresponding grand canonical operator decouples if the annihilation and creation operators are represented in a momentum basis.

Letting $\frac{U}{t} \rightarrow \infty$ corresponds to no hopping of electrons between lattice sites. From this case of independent lattice sites, the definition of the Hubbard atom can be motivated. As the Hubbard atom represents an important foundation of this thesis, the corresponding limit will be covered in the following section.

2.2 The Hubbard Atom

In the formal limits of infinite interaction strength or vanishing tunneling in example $\frac{U}{t} \rightarrow \infty$, we may neglect the kinetic term in the Hamiltonian completely and simply set $t = 0$. Thus, the Hamiltonian reduces to

$$\hat{H} = U \sum_i \hat{n}_{i\uparrow} \hat{n}_{i\downarrow}. \quad (2.4)$$

This decoupling corresponds to fully independent lattice sites, so they can be treated separately. A

single independent lattice site is called a Hubbard atom. Its Hamiltonian reads as

$$\hat{H}_{\text{atom}} \equiv \hat{H} = U\hat{n}_{\uparrow}\hat{n}_{\downarrow}. \quad (2.5)$$

Our 'atom' may either be empty or filled by one or two fermions represented by the four states $\{|0\rangle, |\downarrow\rangle, |\uparrow\rangle, |\downarrow\uparrow\rangle\}$, which are simultaneously eigenstates of the Hubbard atom Hamiltonian.

Now, some elementary thermodynamic quantities in the grand canonical ensemble are derived. For this purpose, the introduction of a chemical potential μ is necessary, which controls the filling of our lattice site. The grand canonical operator can be formulated as

$$\hat{H}_{\text{GK}} = \hat{H} - \mu\hat{N} = U\hat{n}_{\uparrow}\hat{n}_{\downarrow} - \mu \sum_{\sigma} \hat{n}_{\sigma}. \quad (2.6)$$

After this transformation, the previously identified eigenstates are still eigenstates of the grand canonical Hamiltonian. Applying the Hamilton operator to them, we are able to compute the corresponding eigenvalues:

$$\hat{H}_{\text{GK}}|0\rangle = 0 \cdot |0\rangle = 0 \quad (2.7) \quad \hat{H}_{\text{GK}}|\uparrow\rangle = -\mu \cdot |\uparrow\rangle \quad (2.9)$$

$$\hat{H}_{\text{GK}}|\downarrow\rangle = -\mu \cdot |\downarrow\rangle \quad (2.8) \quad \hat{H}_{\text{GK}}|\downarrow\uparrow\rangle = (U - 2\mu) \cdot |\downarrow\uparrow\rangle \quad (2.10)$$

Taking the previous transformation into consideration, the grand canonical partition function is evaluated by the general formula¹

$$Z_{\text{GK}} = \text{tr} \left(e^{-\beta\hat{H}_{\text{GK}}} \right). \quad (2.11)$$

Inserting the Hubbard atom Hamiltonian results in

$$Z_{\text{GK}} = 1 + 2e^{\beta\mu} + e^{-\beta(U-2\mu)}. \quad (2.12)$$

From this, the expectation values for energy and occupation may be calculated as follows:

$$\langle \hat{N} \rangle = \frac{\text{tr} \left(\hat{N} \cdot e^{-\beta\hat{H}_{\text{GK}}} \right)}{\text{tr} \left(e^{-\beta\hat{H}_{\text{GK}}} \right)} = \frac{2 \left(e^{\beta\mu} + e^{-\beta(U-2\mu)} \right)}{1 + 2e^{\beta\mu} + e^{-\beta(U-2\mu)}} \quad (2.13)$$

$$\langle \hat{H} \rangle = \frac{\text{tr} \left((\hat{H}_{\text{GK}} + \mu\hat{N}) \cdot e^{-\beta\hat{H}_{\text{GK}}} \right)}{\text{tr} \left(e^{-\beta\hat{H}_{\text{GK}}} \right)} = \frac{Ue^{-\beta(U-2\mu)}}{1 + 2e^{\beta\mu} + e^{-\beta(U-2\mu)}} \quad (2.14)$$

To close this chapter, a transformation resulting in a particle-hole symmetric Hamiltonian is going to be introduced. As mentioned in Tab. 2.1, an important continuous symmetry of the Hubbard model is given by the particle-hole symmetry in the case of a half-filled system.

Particle-hole symmetry refers to the Hamiltonian being invariant under the exchange of electrons and empty spaces, also called 'holes'. This exchange switches their occupation number

$$\hat{n}_{e,\sigma} \rightarrow (1 - \hat{n}_{h,\sigma}), \quad (2.15)$$

where the indices 'e' and 'h' stand for electrons and holes. Generally, the Hamiltonian of the Hubbard atom is not symmetric under this transformation but instead transforms as

$$U\hat{n}_{\uparrow}\hat{n}_{\downarrow} \rightarrow U(1 - \hat{n}_{\uparrow})(1 - \hat{n}_{\downarrow}) = U(1 - \hat{n}_{\uparrow} - \hat{n}_{\downarrow} + \hat{n}_{\uparrow}\hat{n}_{\downarrow}). \quad (2.16)$$

¹All expressions and equations in this thesis are formulated in natural units. Therefore, k_B , \hbar and c are all set equal to one.

However, a Hamiltonian invariant under particle-hole exchange

$$\hat{H}' = U \left(\hat{n}_\uparrow - \frac{1}{2} \right) \left(\hat{n}_\downarrow - \frac{1}{2} \right) \quad (2.17)$$

only differing from the original Hubbard atom Hamiltonian of Eq. (2.5) by an additive constant, which doesn't change physical properties, can be constructed. Applying the transformation defined in Eq. (2.15)

$$U \left(\hat{n}_\uparrow - \frac{1}{2} \right) \left(\hat{n}_\downarrow - \frac{1}{2} \right) \rightarrow U \left(1 - \hat{n}_\uparrow - \frac{1}{2} \right) \left(1 - \hat{n}_\downarrow - \frac{1}{2} \right) = U \left(\hat{n}_\uparrow - \frac{1}{2} \right) \left(\hat{n}_\downarrow - \frac{1}{2} \right), \quad (2.18)$$

we can verify that \hat{H}' is indeed particle-hole symmetric. This marks the ending of the quick introduction to the Hubbard model and the Hubbard atom as its limit. In the following chapter, the focus will be on developing methods such as the coherent state path integral to analyze the physical properties of the discussed systems even further.

3 Coherent State Path Integral for the Partition Function

In this section, methods fundamental to later chapters of this thesis are going to be presented. The objective lies in developing a coherent state path integral formulation for the partition function of a fermionic system, whose Hamiltonian includes one-body- as well as two-body-operators. Since it is closely related to statistical mechanics, it is more suitable for us to formulate quantum mechanics in terms of functional integrals than in terms of canonical operators. Especially when later evaluating correlation functions for the Hubbard atom, this connection is going to be very useful. As correlation functions can be expressed in terms of expectation values, a functional integral representation of the partition function is now derived. Previously, the Hubbard atom for fermions was introduced as exemplary model with its Hamiltonian containing two-body operators. Therefore, the resulting functional integral formulation will be restricted to these properties.

3.1 Fermionic Coherent States

Before addressing the main focus of this chapter, the coherent state path integral, some prerequisites have to be introduced. We will start by establishing the concept of coherent states for fermionic particles.

In the previous chapter, the Hamiltonian of the Hubbard model as well as of the Hubbard atom were formulated in terms of annihilation and creation operators. In the following, we are going to look for eigenstates and eigenvectors to these operators. Here, exceptionally \hat{c} and \hat{c}^\dagger denote the fermionic annihilation and creation operators to distinguish them from the Grassmann numbers c and \bar{c} . However, the notation will only be used for this section. In the following sections, the operators will be written as c and c^\dagger .

Taking the effect the creation operator \hat{c}^\dagger has on Fock space states into consideration, it is obvious that the operator cannot have right eigenstates. Applying the creation operator \hat{c}_i^\dagger of state i to a state ψ , increases the minimum number of particles in ψ by 1. Hence, ψ can't be a right eigenstate to \hat{c}_i^\dagger . However, nothing in principle forbids the annihilation operator to have right eigenstates. But, keeping in mind the commutation relations for creation and annihilation operators for fermions

$$\{\hat{c}_i, \hat{c}_j\} = \{\hat{c}_i^\dagger, \hat{c}_j^\dagger\} = 0 \quad (3.1) \quad \{\hat{c}_i, \hat{c}_j^\dagger\} = \delta_{ij} \quad (3.2)$$

the respective eigenvalues $\{c_i\}$ need to possess a quite unusual property: The anticommutativity of the fermionic operators results in anticommuting eigenvalues

$$c_i c_j = -c_j c_i. \quad (3.3)$$

Thus, the eigenvalues can't be complex numbers as usual. Instead, they are defined to be Grassmann numbers and belong to a set of anticommuting numbers, the Grassmann algebra. A detailed explanation on the Grassmann algebra and its characteristics can be found in [5]. In this section, we will not focus on the underlying mathematical structure but rather concentrate on the concept of coherent states and Grassmann computation rules, which will be useful for later chapters. First, the commutation relation of Grassmann numbers and creation and annihilation operators is specified as

$$\{c, \hat{c}\} = \{\bar{c}, \hat{c}^\dagger\} = 0. \quad (3.4)$$

With the Grassmann numbers $\{c_i\}$ the eigenstates of the annihilation operator are defined:

$$|c\rangle \equiv e^{-\sum_i c_i \bar{c}_i} |0\rangle \quad (3.5)$$

Since the creation operator is the adjoint of the annihilation operator, left eigenstates for the creation operator are given by

$$\langle c| = \langle 0| e^{\sum_i \bar{c}_i c_i}. \quad (3.6)$$

Note that in the equation above \bar{c}_i doesn't represent complex conjugates but instead entirely different variables. Multiplication of Eq. (3.5) and Eq. (3.6) gives the overlap of coherent states

$$\langle c|c'\rangle = e^{\sum_i \bar{c}_i c'_i}. \quad (3.7)$$

As the coherent states form a basis in Fock space, deriving a corresponding closure relation results in

$$\int \prod_i (d\bar{c}_i dc_i) e^{-\sum_i \bar{c}_i c_i} |c\rangle \langle c| = \mathbf{1}_{\mathcal{F}}, \quad (3.8)$$

where $\mathbf{1}_{\mathcal{F}}$ stands for the unity operator in Fock space. The exponential factor in the integrand is necessary due to the overcompleteness of the basis of coherent states. A full proof of this identity is for example given in [6].

At last, some computation rules for coherent states will be covered. They will only be mentioned and shortly explained for later reference. Again, formal derivations can be found in [6]. Due to the anticommutativity of Grassmann numbers, squaring a Grassmann number always results in zero:

$$c^2 = 0 \quad (3.9)$$

Therefore, analytic functions on the Grassmann algebra assume the form

$$f(c) = f_0 + f_1 c. \quad (3.10)$$

Differentiation on Grassmann variables is defined as

$$\frac{\partial}{\partial c_i} c_j = \delta_{ij}. \quad (3.11)$$

However, to differentiate more complex expressions the corresponding Grassmann number has to be commuted next to the differential operator, which eventually leads to additional minus signs. There also exists a concept similar to integration called Grassmann integration, although it can not be interpreted in the same way as standard integration. It is denoted in the same way as a normal integral to emphasize the analogy with integration over the complex eigenvalues of bosonic ladder operators. The rules of Grassmann integration are given by:

$$\int (dc) 1 = 0 \quad (3.12) \quad \int (dc) c = 1 \quad (3.13)$$

Again, Grassmann variables need to be commuted next to the differential dc to be integrated, which could introduce additional minus signs. As we will encounter Gaussian integrals in later parts of this text, Gaussian Grassmann integrals are solved as

$$\int \prod_i (d\bar{c}_i dc_i) e^{-\sum_{ij} \bar{c}_i M_{ij} c_j + \sum_i (\bar{\eta}_i c_i + \eta_i \bar{c}_i)} = [\det M]^{-1} e^{\sum_{ij} \bar{\eta}_i M_{ij} \eta_j}, \quad (3.14)$$

where the indices i and j number the Grassmann numbers c and η . Another type of Grassmann integral identity necessary for calculations in the text is

$$\frac{\int \prod_i (d\bar{c}_i dc_i) c_{i_1} \dots c_{i_n} \bar{c}_{j_1} \dots \bar{c}_{j_n} e^{-\sum_{ij} \bar{c}_i M_{ij} c_j}}{\int \prod_i (d\bar{c}_i dc_i) e^{-\sum_{ij} \bar{c}_i M_{ij} c_j}} = \sum_{\mathbf{P}} (-1)^{\mathbf{P}} M_{i_{\mathbf{P}_n}, j_n}^{-1} \dots M_{i_{\mathbf{P}_1}, j_{\mathbf{P}_1}}^{-1}, \quad (3.15)$$

where the index \mathbf{P} stands for all possible permutations. As in the proof of the identity products of Grassmann variables have to be differentiated, a factor $(-1)^{\mathbf{P}}$ arises. Since for Grassmann differentiation the derivative has to be commuted next to the respective variable, the anticommutativity of Grassmann numbers leads to additional minus signs. The factor $(-1)^{\mathbf{P}}$ represents the parity of the permutation \mathbf{P} . Both integral identities are proven formally in [6]. This concludes the quick introduction to coherent states.

3.2 Time-Representation of the Fermionic Partition Function

After reviewing basics on coherent states, we will now derive the coherent state path integral for the partition function. The general outline of the following derivation of the fermionic partition function can be found in [1]. However, further steps have been added for clarity. To begin, let us revisit the definition of the grand canonical partition function and express the trace in terms of the complete set of Fock space states $\{|n\rangle\}$

$$Z = \text{tr} \left(e^{-\beta(\hat{H} - \mu \hat{N})} \right) = \sum_n \langle n | e^{-\beta(\hat{H} - \mu \hat{N})} | n \rangle \quad (3.16)$$

with $\beta = \frac{1}{T}$ and T denoting the temperature. The derivation is limited to a Hamiltonian containing only one-body and two-body operators. Therefore, the most general form of such a Hamiltonian that conserves the particle number will be considered, which reads

$$\hat{H}(c^\dagger, c) = \sum_{ij} h_{ij} c_i^\dagger c_j + \sum_{ijkl} V_{ijkl} c_i^\dagger c_j^\dagger c_k c_l. \quad (3.17)$$

This Hamiltonian is written down in normal-order indicating that all its creation operators stand to the left of its annihilation operators².

Returning to the partition function, we now switch to an integral representation by taking advantage of the closure relation for fermionic coherent states Eq. (3.8). This resolution of unity is inserted into the expression for the partition function

$$Z = \int \prod_i (d\bar{c}_i dc_i) e^{-\sum_i \bar{c}_i c_i} \sum_n \langle n | c \rangle \langle c | e^{-\beta(\hat{H} - \mu \hat{N})} | n \rangle. \quad (3.18)$$

To now get rid of the summation, we can again use a closure relation, this time for the basis $\{|n\rangle\}$:

$$\sum_n |n\rangle \langle n| = \mathbf{1}_{\mathcal{F}} \quad (3.19)$$

However, the factor $\langle n | c \rangle$ in Eq. (3.18) needs to be commuted to the right side of the expression.

²If the Hamiltonian is not normal-ordered, its operators need to be exchanged using commutation relations. For fermions, every permutation of an annihilation and creation operators results in an additional minus sign. For example, the Hubbard atom Hamiltonian is transformed to normal-order by $\hat{H} = U c_\uparrow^\dagger c_\uparrow c_\downarrow^\dagger c_\downarrow = -U c_\uparrow^\dagger c_\downarrow^\dagger c_\uparrow c_\downarrow$

Due to the anticommutativity of Grassmann numbers, this leads to an additional minus sign

$$\begin{aligned} Z &= \int \prod_i (d\bar{c}_i dc_i) e^{-\sum_i \bar{c}_i c_i} \sum_n \langle -c | e^{-\beta(\hat{H}-\mu\hat{N})} | n \rangle \langle n | c \rangle \\ &= \int \prod_i (d\bar{c}_i dc_i) e^{-\sum_i \bar{c}_i c_i} \langle -c | e^{-\beta(\hat{H}-\mu\hat{N})} | c \rangle \end{aligned} \quad (3.20)$$

with $\langle -c | \equiv \langle 0 | e^{-\sum_i \bar{c}_i c_i}$. Comparing the expression of the time evolution operator

$$\hat{U}(t) = e^{-i\hat{H}t}, \quad (3.21)$$

its structure appears to be similar to the argument of the trace in Eq. (3.20). Different are only the prefactors in the exponent and the use of the grand canonical operator \hat{H}_{GK} versus the normal Hamiltonian \hat{H} . Thus, we can interpret the trace as a sum over diagonal elements of the time evolution operator and β as an interval in imaginary time

$$\tau_f - \tau_i = \beta. \quad (3.22)$$

The imaginary-time interval β may be split up into M shorter intervals

$$\beta = M\Delta\tau \quad (3.23)$$

of length $\Delta\tau$. Consequently, the exponent of the trace is approximated by

$$\langle -c | e^{-\beta(\hat{H}-\mu\hat{N})} | c \rangle \approx \langle -c | \prod_{\alpha=0}^{M-1} e^{-\Delta\tau(\hat{H}-\mu\hat{N})} | c \rangle. \quad (3.24)$$

Inserting the closure relation of fermionic coherent states in between each exponential factor leads to

$$\begin{aligned} Z &= \int \prod_{\alpha} \left(\prod_i (d\bar{c}_{i,\alpha} dc_{i,\alpha}) e^{-\sum_i \bar{c}_{i,\alpha} c_{i,\alpha}} \right) \langle c_M | e^{-\Delta\tau(\hat{H}-\mu\hat{N})} | c_{M-1} \rangle \langle c_{M-1} | \dots \langle c_1 | e^{-\Delta\tau(\hat{H}-\mu\hat{N})} | c_0 \rangle \\ &= \int \prod_{\alpha=0}^{M-1} \left(\prod_i (d\bar{c}_{i,\alpha} dc_{i,\alpha}) e^{-\sum_i \bar{c}_{i,\alpha} c_{i,\alpha}} \langle c_{\alpha+1} | e^{-\Delta\tau(\hat{H}-\mu\hat{N})} | c_{\alpha} \rangle \right), \end{aligned} \quad (3.25)$$

where the index α numbers the resolutions of unity inserted. Furthermore, the additional minus sign of $\langle -c |$ was absorbed into the definition of the factor $\langle c_M |$. Since \hat{H} and \hat{N} are expressed in a normal-ordered second-quantized representation, the coherent states are eigenstates of both operators. Therefore, we can apply the operators to the states $\{c_i\}$ ³:

$$\begin{aligned} Z &= \int \prod_{\alpha=0}^{M-1} \left(\prod_i (d\bar{c}_{i,\alpha} dc_{i,\alpha}) e^{-\sum_i \bar{c}_{i,\alpha} c_{i,\alpha}} e^{\sum_i \bar{c}_{i,\alpha+1} c_{i,\alpha} - \Delta\tau(H(\bar{c}_{\alpha+1}, c_{\alpha}) - \mu N(\bar{c}_{\alpha+1}, c_{\alpha}))} \right) \\ &= \int \prod_{\alpha=0}^{M-1} (d(\bar{c}_{\alpha}, c_{\alpha})) e^{-\Delta\tau \sum_{\alpha=0}^{M-1} (\Delta\tau^{-1}(\bar{c}_{\alpha} - \bar{c}_{\alpha+1})c_{\alpha} + H(\bar{c}_{\alpha+1}, c_{\alpha}) - \mu N(\bar{c}_{\alpha+1}, c_{\alpha}))}, \end{aligned} \quad (3.26)$$

where the short notation

³In an exemplary manner, the quartic term of the Hamiltonian \hat{V} in Eq.(3.17) is applied to the coherent states $\langle c_{\alpha+1} | e^{-\Delta\tau \sum_{ijkl} V_{ijkl} c_i^{\dagger} c_j^{\dagger} c_k c_l} | c_{\alpha} \rangle = e^{-\Delta\tau \sum_{ijkl} V_{ijkl} \bar{c}_{i,\alpha+1} \bar{c}_{j,\alpha+1} c_{k,\alpha} c_{l,\alpha}} \langle c_{\alpha+1} | c_{\alpha} \rangle = e^{-\Delta\tau V(\bar{c}_{\alpha+1}, c_{\alpha})} e^{\sum_i \bar{c}_{i,\alpha+1} c_{i,\alpha}}$. Here, the overlap between coherent states was evaluated as in Eq. (3.7)

$$c_\alpha \equiv \{c_{i,\alpha}\} \quad (3.27) \quad d(\bar{c}_\alpha, c_\alpha) \equiv \prod_i (d\bar{c}_{i,\alpha} dc_{i,\alpha}) \quad (3.28)$$

has been adopted. Now, choosing the split-up time intervals infinitesimally small, that is taking the limit $\Delta\tau \rightarrow 0, M \rightarrow \infty$, sum and differential quotient in Eq. (3.26) can be identified with integral and derivative as shown below:

$$\Delta\tau \sum_{\alpha=0}^{M-1} \dots \rightarrow \int_0^\beta d\tau \dots \quad (3.29) \quad \frac{\bar{c}_{\alpha+1} - \bar{c}_\alpha}{\Delta\tau} = \partial_\tau \bar{c}_\alpha \quad (3.30)$$

Also, we need to keep the antiperiodic boundary conditions

$$\bar{c}(0) = -\bar{c}(\beta) \quad (3.31) \quad c(0) = -c(\beta) \quad (3.32)$$

in mind. Lastly, the final version of the coherent state path integral for the fermionic partition function is given by

$$Z = \int D(\bar{c}, c) e^{-S[\bar{c}, c]} \quad (3.33)$$

with the measure

$$D(\bar{c}, c) = \lim_{M \rightarrow \infty} \prod_{\alpha=0}^{M-1} d(\bar{c}_\alpha, c_\alpha) \quad (3.34)$$

and the action

$$S[\bar{c}, c] = \int_0^\beta d\tau (\bar{c} \partial_\tau c + H(\bar{c}, c) - \mu N(\bar{c}, c)). \quad (3.35)$$

A more explicit expression for the action S

$$S[\bar{c}, c] = \int_0^\beta d\tau \left(\sum_{ij} \bar{c}_i(\tau) [(\partial_\tau - \mu)\delta_{ij} + h_{ij}] c_j(\tau) + \sum_{ijkl} V_{ijkl} \bar{c}_i(\tau) \bar{c}_j(\tau) c_k(\tau) c_l(\tau) \right) \quad (3.36)$$

is obtained by inserting the Hamiltonian from Eq. (3.17).

3.3 Matsubara Frequency Representation of the Fermionic Partition Function

Perturbative calculations on the Hubbard atom in the next chapters will be performed in frequency representation. Hence, we will transform Eq. (3.33) with the Matsubara frequencies. For fermions they are defined as

$$\omega_n = \frac{(2n+1)\pi}{\beta} \quad n \in \mathbb{Z}. \quad (3.37)$$

With these Matsubara frequencies, the function $c(\tau)$ can be expanded

$$c(\tau) = \frac{1}{\sqrt{\beta}} \sum_{\omega_n} c_n e^{-i\omega_n \tau} \quad (3.38)$$

with the coefficients

$$c_n = \frac{1}{\sqrt{\beta}} \int_0^\beta d\tau c(\tau) e^{i\omega_n \tau}. \quad (3.39)$$

Substituting Eq. (3.37) and Eq. (3.38) into the time representation of the partition function yields the Matsubara frequency representation. First, the expansions will be inserted into the action S

from Eq. (3.36). To simplify the calculations, one-body and two-body part of the action will be covered separately. Expanding the Grassmann numbers in terms of their Matsubara frequency representations in the one-body part S_0 , leads to

$$\begin{aligned} S_0 &= \int_0^\beta d\tau \left(\sum_{ij} \bar{c}_i(\tau) ((\partial_\tau - \mu)\delta_{ij} + h_{ij}) c_j(\tau) \right) \\ &= \frac{1}{\beta} \int_0^\beta d\tau \sum_{ij} \left(\sum_{\omega_{n_1}} \bar{c}_{in_1} e^{+i\omega_{n_1}\tau} \right) ((-i\omega_{n_2} - \mu)\delta_{ij} + h_{ij}) \left(\sum_{\omega_{n_2}} c_{jn_2} e^{-i\omega_{n_2}\tau} \right). \end{aligned} \quad (3.40)$$

Now the terms are regrouped, such that the integral over τ can be evaluated easily:

$$\begin{aligned} S_0 &= \int_0^\beta d\tau \frac{1}{\beta} \sum_{ij, \omega_{n_i}} \bar{c}_{in_1} (-i\omega_{n_2} - \mu) c_{in_2} e^{i(\omega_{n_1} - \omega_{n_2})\tau} + \int_0^\beta d\tau \frac{1}{\beta} \sum_{ij, \omega_{n_i}} \bar{c}_{in_1} h_{ij} c_{jn_2} e^{i(\omega_{n_1} - \omega_{n_2})\tau} \\ &= \delta_{n_1 n_2} \left(\sum_{ij, \omega_{n_i}} \bar{c}_{in_1} (-i\omega_{n_2} - \mu) c_{in_2} \right) + \delta_{n_1 n_2} \left(\sum_{ij, \omega_{n_i}} \bar{c}_{in_1} h_{ij} c_{jn_2} \right) \\ &= \sum_{ij, n} \bar{c}_{in} ((-i\omega_n - \mu)\delta_{ij} + h_{ij}) c_{jn} \end{aligned} \quad (3.41)$$

A similar procedure will be used to derive the Matsubara frequency representation for the two-body part of the action S_{int} . Again, we insert the expansions:

$$\begin{aligned} S_{\text{int}} &= \int_0^\beta d\tau \sum_{ijkl} V_{ijkl} \bar{c}_i(\tau) \bar{c}_j(\tau) c_k(\tau) c_l(\tau) \\ &= \int_0^\beta d\tau \frac{1}{\beta^2} \sum_{ijkl} \left(\sum_{\omega_{n_1}} \bar{c}_{in_1} e^{+i\omega_{n_1}\tau} \sum_{\omega_{n_2}} \bar{c}_{jn_2} e^{+i\omega_{n_2}\tau} \sum_{\omega_{n_3}} c_{kn_3} e^{-i\omega_{n_3}\tau} \sum_{\omega_{n_4}} c_{ln_4} e^{-i\omega_{n_4}\tau} \right). \end{aligned} \quad (3.42)$$

This time, the regrouping of the integral will be skipped and rather the expression after imaginary-time integration will be shown. The arising integrals are analogous to the ones for one-body action and therefore they produce delta functions, which simplify S_{int} to

$$S_{\text{int}} = \frac{1}{\beta} \sum_{ijkl, n_i} V_{ijkl} \bar{c}_{in_1} \bar{c}_{jn_2} c_{kn_3} c_{ln_4} \delta_{n_1+n_2; n_3+n_4}. \quad (3.43)$$

The frequency representation of the total action then reads

$$S[\bar{c}, c] = \sum_{ij, n} \bar{c}_{in} [(-i\omega_n - \mu)\delta_{ij} + h_{ij}] c_{jn} + \frac{1}{\beta} \sum_{ijkl, n_i} V_{ijkl} \bar{c}_{in_1} \bar{c}_{jn_2} c_{kn_3} c_{ln_4} \delta_{n_1+n_2; n_3+n_4}. \quad (3.44)$$

With Eq. (3.44), we can formulate the partition function in Matsubara frequency representation

$$Z = \int D(\bar{c}, c) e^{-S[\bar{c}, c]} \quad (3.45)$$

with the measure

$$D(\bar{c}, c) = \prod_n d(\bar{c}_n, c_n). \quad (3.46)$$

Having derived the functional integral as an important formulation for the next sections, we are finally ready to address perturbation theory. Fundamental concepts to this topic are going to be introduced in the subsequent chapter.

4 Many-Body Perturbation Theory

Before applying perturbation theory to the Hubbard atom, some important preliminaries on perturbation theory are going to be covered. As a lot of problems in many-body physics are not analytically solvable due to the high complexity arising from interactions between particles, one has to think of suitable approximation strategies such as perturbation theory. It is based on decomposing the Hamiltonian (or alternatively the action) of a system

$$\hat{H} = \hat{H}_0 + \hat{V} \quad (4.1)$$

into a solvable one-body part \hat{H}_0 and an interaction part \hat{V} . Supposing that the physical system is continuous in some parameter [6], which is ‘small’ compared to other quantities of the system, a perturbative expansion in terms of orders of this parameter can be used to describe the system. Sometimes, it is advantageous to represent contributions to such expansions graphically. This is called a diagrammatic approach to perturbation theory. How to generate and interpret suitable diagrams will be explained in the next section.

4.1 Matsubara Green’s Functions

Often, to obtain information about a system experimentally the response to external perturbations is measured. Mathematically, this is described by response functions. These are closely related to Green’s functions or correlation functions. There are many different kinds of Green’s functions, but since we will work in the grand canonical ensemble, the Matsubara Green’s function is the best choice for the following perturbation calculations. The Matsubara Green’s function is the thermal average of a time-ordered product of creation and annihilation operators depending on imaginary time. Since all perturbation expansions of the subsequent text will be based on the functional integral formulation, the Matsubara Green’s function is defined in terms of Grassmann variables [7]

$$G^{(n)} = -(-1)^n \langle c_{i_1} \dots \bar{c}_{i_n} \rangle = -\frac{(-1)^n}{Z} \int \mathcal{D}(\bar{c}, c) c_{i_1} \dots \bar{c}_{i_n} e^{-S}. \quad (4.2)$$

For the partition function Z , the action S and the measure, the same definitions and short notations as in chapter 3 are used. The index $i_n, n \in \mathbb{N}$ numbers the particles. Here, the time-ordering of the field variables is already implicit because of the properties of the functional integral. An example would be the non-interacting single-particle Green’s function, also called the bare propagator

$$G_{0,ij} = -\langle c_i \bar{c}_j \rangle_0 = -\frac{\int \mathcal{D}(\bar{c}, c) c_i \bar{c}_j e^{-S_0}}{\int \mathcal{D}(\bar{c}, c) e^{-S_0}} = -\frac{1}{Z_0} \int \mathcal{D}(\bar{c}, c) c_i \bar{c}_j e^{-S_0} \quad (4.3)$$

with the one-body action defined as:

$$S_0 = \int_0^\beta d\tau \left(\sum_{ij} \bar{c}_i(\tau) ((\partial_\tau - \mu)\delta_{ij} + h_{ij}) c_j(\tau) \right). \quad (4.4)$$

Thus, the integral Eq. (4.3) is just a Gaussian integral and can be solved exactly. In general, an integral with an integrand consisting of an exponential factor that is at most quadratic in the field variables multiplied by a polynomial of field variables is evaluated as covered in section 2.1.

Applying the identity Eq. (3.15) to Eq. (4.3), leads to

$$G_{0,ij} = -(S_0^{-1})_{ij} = - \left(\int_0^\beta d\tau (\partial_\tau - \mu) \delta_{ij} + h_{ij} \right)^{-1}, \quad (4.5)$$

where $(S_0)_{ij}$ is short for the matrix element corresponding to the one-body action. With this, we can write S_0 in terms of the bare propagator as

$$S_0 = - \sum_{ij} \bar{c}_i (G_0^{-1})_{ij} c_j \quad (4.6)$$

To reformulate the interaction part, we define the bare vertex $\Gamma_{0|ij;kl}$, which denotes the interaction strength between particles. It is related to the previous form of the interaction part of the action as

$$S_{\text{int}} = \int_0^\beta d\tau \sum_{ijkl} V_{ijkl} \bar{c}_i(\tau) \bar{c}_j(\tau) c_k(\tau) c_l(\tau) = -\frac{1}{4} \sum_{ijkl} \Gamma_{0|ij;kl} \bar{c}_i \bar{c}_l c_k c_j. \quad (4.7)$$

Taking Eq. (4.6) and Eq. (4.7) into consideration, the full action S is rewritten as

$$S = - \sum_{ij} \bar{c}_i (G_0^{-1})_{ij} c_j - \frac{1}{4} \sum_{ijkl} \Gamma_{0|ik;jl} \bar{c}_i \bar{c}_l c_k c_j. \quad (4.8)$$

In the last expression, the interaction strength is now described by the bare vertex Γ_0 .

Previously, it was mentioned that resorting to graphic representations can be helpful to formally organize the perturbation series. In condensed matter physics, the formalism of Hugenholtz diagrams is often used for this purpose. Regarding Hugenholtz diagrams, this thesis is going to follow the convention defined in [7]. According to this formalism the bare propagator G_0 is represented by \longleftarrow and the full single-particle Green's function $G^{(2)}$, which is also called the full propagator, by \longleftarrow . Moreover, the bare vertex is represented by $\begin{array}{c} \diagup \\ \times \\ \diagdown \end{array}$.

After this brief introduction to Green's functions, let us now focus on quantities of interest, which we will compute up to a given order in the following chapters. The first of these quantities is the single-particle Green's function. As stated in Eq. (4.3), it is evaluated as

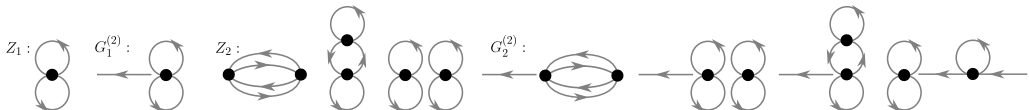
$$G_{ij} = -\langle c_i \bar{c}_j \rangle = -\frac{1}{Z} \int D(\bar{c}, c) c_i \bar{c}_j e^{-S}. \quad (4.9)$$

In practice, the action is separated into the two parts Eq. (4.6) and Eq. (4.7) and one expands the interaction part

$$G_{ij} = -\frac{1}{Z_0} \cdot \frac{Z_0}{Z} \int D(\bar{c}, c) c_i \bar{c}_j e^{-S_0} \left(\sum_{r=0}^{\infty} \frac{(-1)^r}{r!} (S_{\text{int}})^r \right). \quad (4.10)$$

We have expanded by Z_0 , as the factor $\frac{Z_0}{Z}$ cancels disconnected diagrams⁴. What a disconnected diagram is will be explained later. For now, one can just say the expansion simplifies the graphical representation of the expression. Inserting the two-body action from Eq. (4.7) to calculate the r -th

⁴Below, this is illustrated exemplary for the first few orders. By comparison to the disconnected diagrams of $G^{(2)}$, one observes that the diagrams of Z match them. Therefore, it should be plausible that Z as a denominator cancels disconnected diagrams. However, this is nowhere near a rigorous proof. For this purpose, one should refer to the literature as for example [6].



order contribution to G_{ij} , averages over products of Grassmann variables have to be evaluated with Gaussian integrals again. This can be done conveniently by using Wick's theorem. How this is done, will be covered in the following paragraph.

A full derivation of Wick's theorem lies beyond the scope of this thesis, so only its general statement is going to be covered. A proof by induction is for example provided in [8]. To understand the general statement of Wick's theorem, the concept of contractions of field variables needs to be established. A contraction of Grassmann variables is represented by [6]

$$\overline{\tilde{c}_i \tilde{c}_j} = \langle \tilde{c}_i \tilde{c}_j \rangle_0 \quad (4.11)$$

with $\tilde{c}_i \in \{c_i, \bar{c}_i\}$. As we will work with functional integrals, only the definition in terms of Grassmann numbers is needed. Contractions of Grassmann variables are evaluated as:

$$\overline{c_i(\tau) \bar{c}_j(\tau')} = -G_{0;ij}(\tau - \tau') \quad (4.12)$$

$$\overline{\bar{c}_i(\tau) \bar{c}_j(\tau')} = \overline{c_i(\tau) c_j(\tau')} = 0 \quad (4.13)$$

In Eq. (4.12), $G_{0;ij}(\tau - \tau')$ represents the single-particle non-interacting Green's function. For a Hamiltonian not depending on τ , G only depends on the imaginary-time difference $(\tau - \tau')$. All Hamiltonians considered in this thesis are imaginary-time-independent, so we restrict ourselves to the case $G_{0;ij}(\tau, \tau') = G_{0;ij}(\tau - \tau')$. Contractions of the type Eq. (4.13) are zero, which is due to the definition of a contraction as an expectation value. Expectation values of two creation or annihilation operators vanish for every Fock state. Thus, the same holds for expectation values of Grassmann variables corresponding to these operators. Now, the main statement of Wick's theorem [6]

$$\langle c_{i_1} \dots c_{i_n} \bar{c}_{j_1} \dots \bar{c}_{j_n} \rangle_0 = \sum \text{all complete contractions} \quad (4.14)$$

can be addressed. A complete contraction refers to contracting all Grassmann variables $\{c_{i_1} \dots c_{i_n}\}$ with $\{\bar{c}_{j_1} \dots \bar{c}_{j_n}\}$ and multiplying them. To evaluate the expression on the left-hand side of Eq. (4.14), one needs to sum over all possible products of pair contractions $\langle \tilde{c}_i \tilde{c}_j \rangle_0$ generated by permuting the indices j_1 to j_n . Applying this together with Eq. (4.2) to the evaluation of Green's functions, the n -th order non-interacting Green's function is given by

$$G_{0|\alpha_1, \dots, \alpha_n; \alpha'_1, \dots, \alpha'_n}^{(2n)}(\tau_1, \dots, \tau_n; \tau'_1, \dots, \tau'_n) = \sum_{\text{P}} (-1)^{\text{P}} \delta_{\alpha_{\text{P}_1} \alpha'_1} \dots \delta_{\alpha_{\text{P}_n} \alpha'_n} G_{0|\alpha'_1}(\tau_{\text{P}_1} - \tau'_1) \dots G_{0|\alpha'_n}(\tau_{\text{P}_n} - \tau'_n), \quad (4.15)$$

where the index P denotes all permutations of the indices 1 to n . Again, due to the permutations of Grassmann numbers a sign factor $(-1)^{\text{P}}$ is needed. If Grassmann numbers are commuted an odd number of times, an additional minus sign arises.

This statement suggests a graphical representation. Specific rules can be determined to generate Hugenholtz diagrams for the r -th order term of the perturbation expansion of $G^{(n)}$ for a system containing only two-body interactions. These rules are found in detail in [6]. For completeness, they will be summarized briefly. For each complete contraction, one draws r vertices with 4 legs, each corresponding to a field variable of the two-body interaction .

Furthermore, one represents the arguments of the Green's function $\{\bar{c}_{i_1}, \dots, \bar{c}_{i_n}\}$ as n external points $\beta'_i \xrightarrow{\alpha'_i}$ and the arguments $\{c_{j_1}, \dots, c_{j_n}\}$ as n external points $\alpha_i \xrightarrow{\beta_i}$.

Each contraction of two field variables corresponds to a propagator $\tau', \alpha' \xrightarrow{\tau, \alpha}$ connecting either external points or vertices corresponding to the respective field variables, which are contracted. Examples of such diagrams are shown in Fig. 4.1.

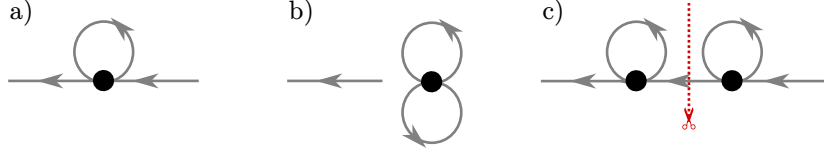


Figure 4.1: (a) First-order contribution to the single-particle Green's function $G^{(1)}$. This is a connected diagram with $n_L = 1$. (b) Also a first-order contribution to $G^{(1)}$. However, it is disconnected with $n_L = 2$. (c) Example for an one-particle reducible diagram. Cutting the propagator in the middle, yields two subdiagrams.

Converting a diagram back to an analytical expression, each propagator, external point and vertex are assigned time and particle labels, if not already denoted in the diagram. Each bare vertex corresponds to a factor $\Gamma_{0|ij;kl}$ and each propagator to a factor $G_{0;ij}$. These factors are then multiplied. Afterwards, one sums over all internal particles and integrates r times over all τ_i from 0 to β .

Described above is how to generate diagrams for the Matsubara Green's function $G^{(n)}(\tau)$ in imaginary-time representation. Diagrammatic depiction of $G^{(n)}(\omega_n)$ depending on Matsubara frequencies ω_n works in a similar way. Instead of assigning time labels, frequency labels are assigned to each propagator. Because of frequency conservation, the sum of frequencies assigned to propagators entering a vertex must be equal to the sum of frequencies assigned to propagators leaving the vertex. Furthermore, to convert a diagram in frequency representation back to a mathematical expression, instead of integrating over τ one sums over all internal frequencies.

In general, one can group diagrams into connected and disconnected ones. Connected means, that all vertices and external points are connected to each other by propagators. Another way to classify diagrams is by their reducibility. An n -particle reducible diagram means that n lines would have to be cut to split it into two disconnected diagrams. Examples are given in Fig. 4.1).

To close this introduction on Green's functions, we will briefly talk about their generating functionals. Originally, the expression of the Matsubara Green's function was only stated in Eq. (4.2). However, it turns out that this expression may be generated from a functional

$$Z[\bar{J}, J] \equiv \langle e^{-\int_0^\beta d\tau \sum_\alpha [\bar{J}_\alpha(\tau)c_\alpha(\tau) + \bar{c}_\alpha(\tau)J_\alpha(\tau)]} \rangle. \quad (4.16)$$

This generating function is given by adding source terms J_α and \bar{J}_α , which are also Grassmann variables, to the action. More details on this and the following expressions can be found in [6]. Based on Eq. (4.16), the n -particle Green's function is generated [6]

$$G_{\alpha_1, \dots, \alpha_n; \alpha'_1, \dots, \alpha'_n}^{(2n)}(\tau_1, \dots, \tau_n; \tau'_1, \dots, \tau'_n) = (-1)^{-n+1} \frac{\delta^{2n} Z[\bar{J}, J]}{\delta \bar{J}_{\alpha_1}(\tau_1) \dots \delta \bar{J}_{\alpha_n}(\tau_n) \delta J_{\alpha'_1}(\tau'_1) \dots \delta J_{\alpha'_n}(\tau'_n)} \Big|_{\bar{J}=J=0} \quad (4.17)$$

using functional derivatives with respect to the source fields. Note, that the generating function $Z[\bar{J}, J]$ appears to be the grand canonical partition function with additional source terms \bar{J}, J . In thermodynamics however, the grand potential W , which is the natural logarithm of the partition function, has higher physical significance. Thus, it is only natural to wonder, if there is a similar relation between Green's functions and the grand potential with additional source terms, which reads

$$W[\bar{J}, J] \equiv \ln(Z[\bar{J}, J]). \quad (4.18)$$

In fact, the grand potential with sources is the generating function for connected Green's functions.

This is known in literature as the Linked Cluster theorem [6]. The n -particle connected Green's function is then calculated as

$$G_{\alpha_1, \dots, \alpha_n; \alpha'_1, \dots, \alpha'_n}^{(2n), c}(\tau_1, \dots, \tau_n; \tau'_1, \dots, \tau'_n) = (-1)^{n+1} \frac{\delta^{2n} W[\bar{J}, J]}{\delta \bar{J}_{\alpha_1}(\tau_1) \dots \delta \bar{J}_{\alpha_n}(\tau_n) \delta J_{\alpha'_1}(\tau'_1) \dots \delta J_{\alpha'_n}(\tau'_n)} \Big|_{\bar{J}=J=0}. \quad (4.19)$$

As thermodynamic quantities are derived from the grand potential instead of from the partition function, it is in most cases sufficient to only consider connected Green's function, which only consist of connected diagram contributions.

We are now able to compute n -particle Green's functions, expand them in perturbation series and represent them diagrammatically. Additionally, the same shall be done for the self-energy and vertex. We will focus on this in the next section.

4.2 Self-Energy

To define the self-energy as well as its properties, we will need an additional generating function for the one-particle irreducible vertex. It is obtained by a Legendre-transformation of the generating function of connected Green's functions $W[\bar{J}, J]$ [6]

$$\Gamma[\bar{\phi}_\alpha(\tau), \phi_\alpha(\tau)] = -W[\bar{J}, J] - \sum_\gamma \int_0^\beta d\tau' [\bar{\phi}_\gamma(\tau') J_\gamma(\tau')] + \bar{J}_\gamma(\tau') \phi_\gamma(\tau'), \quad (4.20)$$

where the new variables ϕ and $\bar{\phi}$ are called field averages in the presence of source fields and evaluated as $\phi_\alpha = \langle c_\alpha \rangle_{\bar{J}, J}$ and similarly $\bar{\phi}_\alpha$. The vertex function is then given by functionally differentiating the generating function analogous to the derivation of the Green's functions [6]:

$$\Gamma_{\alpha_1, \dots, \alpha_n; \alpha'_1, \dots, \alpha'_n}^{(m+n)}(\tau_1, \dots, \tau_n; \tau'_1, \dots, \tau'_n) = \frac{\delta^{m+n} \Gamma[\bar{\phi}_\alpha(\tau), \phi_\alpha(\tau)]}{\delta \bar{\phi}_{\alpha_1}(\tau_1) \dots \delta \bar{\phi}_{\alpha_m}(\tau_m) \delta \phi_{\alpha'_1}(\tau'_1) \dots \delta \phi_{\alpha'_n}(\tau'_n)} \Big|_{\bar{J}=J=0} \quad (4.21)$$

Here, m is almost always equal to n due to particle conservation at each interaction vertex.

From the two-point vertex function, the self-energy Σ is defined as the difference between the interacting and the non-interacting vertex function $\tilde{\Gamma}_{\bar{\phi}\phi}$

$$\Gamma_{\alpha_1, \alpha'_1}^{(2)}(\tau_1, \tau'_1) \equiv \tilde{\Gamma}_{\alpha_1, \alpha'_1} - \Sigma_{\alpha_1, \alpha'_1}(\tau_1, \tau'_1). \quad (4.22)$$

Thus, the self-energy contains all information about the interactions of the system on the one particle level. As we will later want to calculate the self-energy up to a certain order from a perturbation series of the single-particle Green's function, it is necessary to relate both quantities. Therefore, the explicit expression corresponding to the two-point vertex is obtained as

$$\Gamma_{\alpha_1, \alpha'_1}^{(2)}(\tau_1, \tau'_1) = \frac{\delta^2}{\delta \bar{\phi}_{\alpha_1} \delta \phi_{\alpha'_1}} \left(-W[\bar{J}, J] - \sum_\gamma \int_0^\beta d\tau' [\bar{\phi}_\gamma(\tau') J_\gamma(\tau')] + \bar{J}_\gamma(\tau') \phi_\gamma(\tau') \right) \Big|_{\bar{J}=J=0} \quad (4.23)$$

from the generating function. In the following, time arguments are suppressed for ease of notation and sums over repeated indices are implicit. Evaluating the derivatives with respect to ϕ and $\bar{\phi}$,

results in

$$\begin{aligned}
 \Gamma_{\alpha_1, \alpha'_1}^{(2)} &= \frac{\delta}{\delta \bar{\phi}_{\alpha_1}} \left(-\frac{\delta W}{\delta \bar{J}_{\beta_1}} \frac{\delta \bar{J}_{\beta_1}}{\delta \phi_{\alpha'_1}} - \frac{\delta \bar{J}_{\beta_1}}{\delta \phi_{\alpha'_1}} \phi_{\beta_1} - \bar{J}_{\alpha'_1} \right) \Big|_{\bar{J}=J=0} \\
 &= \frac{\delta}{\delta \bar{\phi}_{\alpha_1}} \left(-\frac{\delta W}{\delta \bar{J}_{\beta_1}} \left(\frac{\delta^2 \Gamma}{\delta \bar{\phi}_{\beta_1} \delta \phi_{\alpha'_1}} \right) + \left(\frac{\delta^2 \Gamma}{\delta \bar{\phi}_{\beta_1} \delta \phi_{\alpha'_1}} \right) \frac{\delta W}{\delta \bar{J}_{\beta_1}} - \bar{J}_{\alpha'_1} \right) \Big|_{\bar{J}=J=0} \\
 &= -\frac{\delta \bar{J}_{\alpha'_1}}{\delta \bar{\phi}_{\alpha_1}} \Big|_{\bar{J}=J=0}.
 \end{aligned} \tag{4.24}$$

By functionally differentiating the grand potential W with respect to ϕ and J

$$\frac{\delta^2 W}{\delta \phi_{\alpha_1}(\tau_1) \delta J_{\alpha'_1}(\tau'_1)} = \delta(\tau_1 - \tau'_1) \tag{4.25}$$

we generate a delta-function. Applying the chain rule to $\frac{\delta^2 W}{\delta \phi_{\alpha_1}(\tau_1) \delta J_{\alpha'_1}(\tau'_1)}$, leads to

$$\delta(\tau_1 - \tau'_1) = \frac{\delta^2 W}{\delta \bar{J}_{\beta_1} \delta J_{\alpha'_1}} \frac{\delta \Gamma}{\delta \bar{\phi}_{\beta_1} \delta \phi_{\alpha_1}}. \tag{4.26}$$

Thus, the two partial derivatives on the right-hand side of Eq. (4.26) need to be inverse to each other. Taking the limit $(J, \bar{J}) \rightarrow 0$, we can relate the two-point vertex and the two-point Green's function as

$$(G_{\beta_1 \alpha'_1}^{(2)})^{-1} = \Gamma_{\beta_1 \alpha'_1}^{(2)}. \tag{4.27}$$

Hence, the single-particle connected Green's function and the self energy are related as

$$(G^{(2)})^{-1} = (G_0)^{-1} - \Sigma. \tag{4.28}$$

Multiplying Eq. (4.28) by the non-interacting Green's function G_0 from the left and by the interacting Green's function G from the right, results in a recursive relation

$$G^{(2)} = G_0 + G_0 \Sigma G^{(2)} \tag{4.29}$$

called the Dyson equation. Graphically, the self-energy Σ is represented as $\textcircled{\Sigma}$. With this, the Dyson equation is depicted as shown in 4.2.



Figure 4.2: Diagrammatic representation of the Dyson equation.

In fact, the self-energy sums amputated one-particle irreducible diagrams between external points $(\alpha_1 \tau_1)$ and $(\alpha'_1 \tau'_1)$. Amputating a diagram means removing the contribution of its external 'legs', which are propagators connected to arguments of a Green's function. Drawing and evaluating Hugenholtz diagrams for the self-energy is done by the same principles as for the Green's functions. There will be concrete examples in the next chapter, when perturbation theory is applied to the Hubbard atom.

4.3 Four-Point Vertex

After introducing the self-energy, now the same shall be done for the four-point vertex. Physically, the four-point vertex encodes the full interaction between two particles. One may think, that the information about two particle interaction strength is specified by $\Gamma_0^{(2)}$, the prefactor of the two-body interaction Eq. (4.8). In fact, this is not the case, as there are additional contributions to the interaction such as quantum fluctuations, which are not considered by Γ_0 . In preparation to investigating the interaction between electrons of the Hubbard atom in the next chapter, a relation between the four-point vertex and the four-point Green's function $G^{(4)}$ will be derived. In the following derivation, we compute $G^{(4),c}$ and compare it to the expression for $\Gamma^{(4)}$. We will do so by differentiating generating functions Eq. (4.17) and Eq. (4.19). The derivatives with respect to the source terms are evaluated using product rule and chain rule. For the derivatives to act on Grassmann numbers, they need to be commuted next to the respective variable they act on. The additional sign changes arising from these permutations were taken into account as well:

$$\begin{aligned}
 G_{\alpha_1\alpha_2;\alpha'_1\alpha'_2}^{(4),c} &= \frac{\delta^4 \ln(Z)}{\delta \bar{J}_{\alpha_1} \delta \bar{J}_{\alpha_2} \delta J_{\alpha'_2} \delta J_{\alpha'_1}} \Big|_{\bar{J}=J=0} = \frac{\delta^3}{\delta \bar{J}_{\alpha_1} \delta \bar{J}_{\alpha_2} \delta J_{\alpha'_2}} \left(\frac{1}{Z} \frac{\delta Z}{\delta J_{\alpha'_1}} \right) \Big|_{\bar{J}=J=0} \\
 &= \frac{\delta^2}{\delta \bar{J}_{\alpha_1} \delta \bar{J}_{\alpha_2}} \left(-\frac{1}{Z^2} \frac{\delta Z}{\delta J_{\alpha'_2}} \frac{\delta Z}{\delta J_{\alpha'_1}} + \frac{1}{Z} \frac{\delta^2 Z}{\delta J_{\alpha'_2} \delta J_{\alpha'_1}} \right) \Big|_{\bar{J}=J=0} \\
 &= \langle c_{\alpha_2} \bar{c}_{\alpha'_1} \rangle \langle c_{\alpha_1} \bar{c}_{\alpha'_2} \rangle - \langle c_{\alpha_1} \bar{c}_{\alpha'_1} \rangle \langle c_{\alpha_2} \bar{c}_{\alpha'_2} \rangle + \langle c_{\alpha_1} c_{\alpha_2} \bar{c}_{\alpha'_1} \bar{c}_{\alpha'_2} \rangle \\
 &= G_{\alpha_2\alpha'_1}^{(2)} G_{\alpha_1\alpha'_2}^{(2)} - G_{\alpha_1\alpha'_1}^{(2)} G_{\alpha_2\alpha'_2}^{(2)} + G_{\alpha_1\alpha_2;\alpha'_1\alpha'_2}^{(4)}
 \end{aligned} \tag{4.30}$$

Above, the first few partial derivatives were evaluated exemplary using the chain rule and product rule. In the last step, the source terms were set equal to zero. With no source terms present, fermionic correlation function of odd order vanish. Therefore, we are left with only three terms on the left-hand side of Eq. (4.30). Now, the only thing left to do is to relate the connected Green's function $G^{(4),c}$ to the vertex $\Gamma^{(4)}$. Again, we differentiate a generating function Eq. (4.21) to obtain the expression

$$\begin{aligned}
 \Gamma_{\beta'_1\beta'_2;\beta_1\beta_2}^{(4)} &= \frac{\delta^4 \Gamma}{\delta \phi_{\beta'_1} \delta \phi_{\beta'_2} \delta \phi_{\beta_2} \delta \phi_{\beta_1}} \Big|_{\bar{J}=J=0} = \frac{\delta^3}{\delta \phi_{\beta'_1} \delta \phi_{\beta'_2} \delta \phi_{\beta_2}} \left(-\bar{J}_{\beta_1} \right) \Big|_{\bar{J}=J=0} \\
 &= \frac{\delta^2}{\delta \phi_{\beta'_1} \delta \phi_{\beta'_2}} \left(\frac{\delta^2 W}{\delta \bar{J}_{\beta_1} \delta J_{\alpha_1}} \right) \Big|_{\bar{J}=J=0} \\
 &= \left(G_{\alpha_1\beta_1'}^{(2)} \right)^{-1} \left(G_{\alpha_2\beta_2'}^{(2)} \right)^{-1} G_{\alpha_1\alpha_2;\alpha'_1\alpha'_2}^{(4),c} \left(G_{\beta_1\alpha_1'}^{(2)} \right)^{-1} \left(G_{\beta_2\alpha_2'}^{(2)} \right)^{-1}
 \end{aligned} \tag{4.31}$$

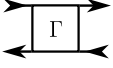
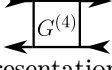
for the four-point vertex. To simplify expressions, which occur after the partial differentiation, some results derived in section 4.2 were used. Setting $J = 0$, correlation functions of odd order vanish. As it is not necessary to distinguish between connected and disconnected Green's functions on the one-particle level, the second equality follows. What remains to be done, is solving Eq. (4.31) for $G^{(4),c}$:

$$G_{\alpha_1\alpha_2;\alpha'_1\alpha'_2}^{(4),c} = G_{\alpha_1\beta_1'}^{(2)} G_{\alpha_2\beta_2'}^{(2)} \Gamma_{\beta'_1\beta'_2;\beta_1\beta_2}^{(4)} G_{\beta_1\alpha_1'}^{(2)} G_{\beta_2\alpha_2'}^{(2)} \tag{4.32}$$

Inserting this into Eq. (4.30) yields the exact relation

$$G_{\alpha_1\alpha_2;\alpha'_1\alpha'_2}^{(4)} = G_{\alpha_1\alpha_1'}^{(2)} G_{\alpha_2\alpha_2'}^{(2)} - G_{\alpha_2\alpha_1'}^{(2)} G_{\alpha_1\alpha_2'}^{(2)} + G_{\alpha_1\beta_1'}^{(2)} G_{\alpha_2\beta_2'}^{(2)} \Gamma_{\beta'_1\beta'_2;\beta_1\beta_2}^{(4)} G_{\beta_1\alpha_1'}^{(2)} G_{\beta_2\alpha_2'}^{(2)} \tag{4.33}$$

between the four-point vertex and the four-point Green's function. To represent this equation

diagrammatically, it is common to introduce additional symbols corresponding to the vertex and four-point Green's function. One draws the four-point vertex as  and the four-point correlation function as .

The diagrammatic representation of Eq. (4.33) is then given by:

$$\begin{array}{c} \text{---} \rightarrow \\ \left[G^{(4)} \right] \\ \leftarrow \text{---} \end{array} = \begin{array}{c} \rightarrow \\ \leftarrow \end{array} - \begin{array}{c} \uparrow \\ \downarrow \end{array} + \begin{array}{c} \text{---} \rightarrow \\ \left[\Gamma \right] \\ \leftarrow \text{---} \end{array}$$

Figure 4.3: Diagrammatic representation of the relation between vertex and four-point correlation function.

This concludes the explanation of basics on many-body perturbation theory. We will refer back to many formulas and principles developed in this chapter in later calculations. Next up is using perturbation techniques on an exemplary model, the Hubbard atom.

5 Second-Order Perturbation Theory for the Hubbard Atom

Now, the diagrammatic methods established in chapter 4 are going to be used on the Hubbard atom introduced in section 4.1. This system is chosen specifically, as there exists an exact solution, which can then later be compared to the expressions obtained from perturbation theory in the context of Ward identities.

The quantities needed for this comparison are self-energy Σ and four-point vertex $\Gamma^{(4)}$ that can be derived from one-body and two-body Green's functions $G^{(2)}$ and $G^{(4)}$ as explained in section 4.2 and 4.3. Therefore, the perturbation series of $G^{(2)}$, $G^{(4)}$, Σ and $\Gamma^{(4)}$ will be evaluated up to second-order in the interaction strength $\frac{U}{\beta}$.⁵

At first, let us reformulate the Matsubara frequency representation of the action Eq. (3.44) as

$$\begin{aligned} S[\bar{c}, c] &= \sum_{ij,n} \bar{c}_{in} [(-i\omega_n - \mu)\delta_{ij} + h_{ij}] c_{jn} + \frac{1}{\beta} \sum_{ijkl, n_i} V_{ijkl} \bar{c}_{in_1} \bar{c}_{jn_2} c_{kn_3} c_{ln_4} \delta_{n_1+n_2; n_3+n_4} \\ &= \sum_{\sigma, n} \bar{c}_{\sigma, n} (-i\omega_n - \mu) c_{\sigma, n} - \frac{U}{\beta} \sum_{\{n_i\}} \bar{c}_{\uparrow n_1} \bar{c}_{\downarrow n_2} c_{\uparrow n_3} c_{\downarrow n_4} \delta_{n_1+n_2; n_3+n_4} \end{aligned} \quad (5.1)$$

in terms of the properties of the Hubbard atom Hamiltonian $\hat{H}_{\text{GK}} = U\hat{n}_{\uparrow}\hat{n}_{\downarrow} - \mu(\hat{n}_{\uparrow} + \hat{n}_{\downarrow})$. Here, the sum over σ represents a summation over spins $\sigma \in \{\uparrow, \downarrow\}$. Splitting the Hubbard atom action up into interaction part S_{int} and bare part S_0 and expanding $e^{-S_{\text{int}}}$ as in Eq. (4.10) yields

$$\begin{aligned} e^{-S_{\text{int}}} &\approx 1 + \frac{U}{\beta} \sum_{\{n_i\}} \bar{c}_{\uparrow n_1} \bar{c}_{\downarrow n_2} c_{\uparrow n_3} c_{\downarrow n_4} \delta_{n_1+n_2; n_3+n_4} \\ &\quad + \frac{U^2}{2\beta^2} \sum_{\{n_i\}} \bar{c}_{\uparrow n_1} \bar{c}_{\downarrow n_2} c_{\uparrow n_3} c_{\downarrow n_4} \delta_{n_1+n_2; n_3+n_4} \sum_{\{m_i\}} \bar{c}_{\uparrow m_1} \bar{c}_{\downarrow m_2} c_{\uparrow m_3} c_{\downarrow m_4} \delta_{m_1+m_2; m_3+m_4} \end{aligned} \quad (5.2)$$

With the expression above, let us now compute the perturbation series up to second-order of the one-body Green's function.

5.1 One-Body Green's Function

The general expression corresponding to the time-representation of the one-body Green's function is given by Eq. (4.9). Because of its periodicity, it can be expanded as a Fourier series

$$G^{(2)}(\tau) = \frac{1}{\beta} \sum_{n=-\infty}^{\infty} e^{-i\omega_n \tau} G^{(2)}(\omega_n) \quad (5.3) \quad G^{(2)}(\omega_n) = \int_0^{\beta} d\tau e^{i\omega_n \tau} G^{(2)}(\tau) \quad (5.4)$$

in terms of the Matsubara frequencies as defined in Eq. (3.37) with $n \in \mathbb{Z}$. Inserting the definition of the Green's function in time representation and the expansions of Grassmann numbers in terms of Matsubara frequencies Eq. (3.38) and Eq. (3.39), results in

$$G_{\sigma, \sigma'}^{(2)}(\omega_n) = -\langle c_{\sigma n} \bar{c}_{\sigma' n} \rangle \quad (5.5)$$

⁵It may seem unusual to expand in $\frac{U}{\beta}$, as it is not a dimensionless quantity. This is due to the convention chosen throughout this thesis, which entails that the dimensions of all correlation functions match accordingly. Therefore, it makes sense to expand in $\frac{U}{\beta}$.

with spin indices σ and σ' . This is the quantity we are calculating in the following. Note, that the Hubbard atom Hamiltonian doesn't contain any spin-flip terms. Thus, for the two-point correlation function $G_{\sigma,\sigma'}^{(2)}(\omega_n)$ only the case $\sigma = \sigma'$ needs to be considered, since correlation functions with distinct spin components would vanish. Explicitly, $G_{\sigma}^{(2)}(\omega_n)$ then reads

$$G_{\sigma}^{(2)}(\omega_n) = -\frac{Z_0}{Z} \frac{1}{Z_0} \int D(\bar{c}, c) c_{\sigma n} \bar{c}_{\sigma n} e^{-S_0} \left(1 - S_{\text{int}} + \frac{1}{2} (S_{\text{int}})^2 + \mathcal{O}\left(\frac{U^3}{\beta^3}\right) \right). \quad (5.6)$$

For the expansion of S_{int} , one inserts Eq. (5.1) above. To begin, the zero-order contribution G_0 is evaluated as

$$G_0^{(2)}(\omega_n) = -\frac{Z_0}{Z} \frac{1}{Z_0} \int D(\bar{c}, c) c_{\sigma n} \bar{c}_{\sigma n} e^{-\sum_{\sigma,n} \bar{c}_{\sigma,n} (-i\omega_n - \mu) c_{\sigma,n}}. \quad (5.7)$$

The integral is solved as

$$G_0^{(2)}(\omega_n) = \frac{1}{i\omega_n + \mu} \quad (5.8)$$

by applying identity Eq. (3.15). Diagrammatically, this corresponds to the bare propagator:



Figure 5.1: Zero-order contribution to the one-body Greens function for the Hubbard atom.

Next, we focus on higher-order contributions. The first-order of $G_{\sigma}^{(2)}$ reads

$$\begin{aligned} G_{1|\sigma}^{(2)}(\omega_n) &= -\frac{Z_0}{Z} \frac{1}{Z_0} \int D(\bar{c}, c) c_{\sigma n} \bar{c}_{\sigma n} e^{-S_0} \frac{U}{\beta} \sum_{\{n_i\}} \bar{c}_{\uparrow n_1} \bar{c}_{\downarrow n_2} c_{\uparrow n_3} c_{\downarrow n_4} \delta_{n_1+n_2; n_3+n_4} \\ &= -\frac{U}{\beta} \sum_{\{n_i\}} \langle c_{\sigma n} \bar{c}_{\sigma n} \bar{c}_{\uparrow n_1} \bar{c}_{\downarrow n_2} c_{\uparrow n_3} c_{\downarrow n_4} \rangle \delta_{n_1+n_2; n_3+n_4} \frac{Z_0}{Z} \\ &= -\frac{U}{\beta} \sum_{\{n_i\}} \langle c_{\sigma n} c_{\uparrow n_3} c_{\downarrow n_4} \bar{c}_{\sigma n} \bar{c}_{\uparrow n_1} \bar{c}_{\downarrow n_2} \rangle \delta_{n_1+n_2; n_3+n_4} \frac{Z_0}{Z}, \end{aligned} \quad (5.9)$$

where in the last step, the product of Grassmann variables was brought into anti-normal-order. As for this a total of four pair-permutations of Grassmann variables were conducted, there is no sign reversal to the expression.

The thermal average is then evaluated using Wick's theorem, which was introduced in section 4.1. Without loss of generality, we can assume $\sigma = \uparrow$, as the correlation function for $\sigma = \downarrow$ would be numerically equivalent with vertically flipped diagrams. Applying Wick's theorem, leads to

$$\begin{aligned} \langle c_{\uparrow n} c_{\uparrow n_3} c_{\downarrow n_4} \bar{c}_{\uparrow n} \bar{c}_{\uparrow n_1} \bar{c}_{\downarrow n_2} \rangle &= -\langle c_{\uparrow n} \bar{c}_{\uparrow n} \rangle_0 \langle c_{\uparrow n_3} \bar{c}_{\uparrow n_1} \rangle_0 \langle c_{\downarrow n_4} \bar{c}_{\downarrow n_2} \rangle_0 \delta_{n_1 n_3} \delta_{n_2 n_4} \\ &\quad + \langle c_{\uparrow n} \bar{c}_{\uparrow n_1} \rangle_0 \langle c_{\uparrow n_3} \bar{c}_{\uparrow n} \rangle_0 \langle c_{\downarrow n_4} \bar{c}_{\downarrow n_2} \rangle_0 \delta_{n n_1} \delta_{n n_3} \delta_{n_2 n_4}, \end{aligned} \quad (5.10)$$

where the first summand represents a disconnected diagram, whereas the diagram of second summand is connected. Because of the factor $\frac{Z_0}{Z}$, only connected diagrams need to be considered. This is explained in section 4.1. The Hugenholtz diagram corresponding to the connected term according to the rules discussed in section 4.1 is given by:

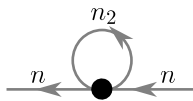


Figure 5.2: First-order contribution to the one-body correlation function for the Hubbard atom.

Inserting Eq. (5.10) back into Eq. (5.9), one obtains the first-order contribution to the one-body

Green's function

$$G_{1|\sigma}^{(2)}(\omega_n) = -\frac{U}{\beta} G_0^2(\omega_n) \sum_{n_2} G_0(\omega_{n_2}) = -\frac{U}{\beta(i\omega_n + \mu)^2} \sum_{n_2} \frac{1}{i\omega_{n_2} + \mu}, \quad (5.11)$$

where in the last step the bare propagator from Eq. (5.8) was inserted. What remains to be done, is the evaluation of the sum \sum_{n_2} . Sums of this type are called Matsubara frequency sums and are analytically evaluated with the help of a weighting function h and a contour integral in the complex plane, which is explained in more detail in appendix B. In this chapter, only the solutions to occurring Matsubara sums are written out explicitly. Following the procedure given in appendix B, the first-order contribution $G_{1|\sigma}^{(2)}(\omega_n)$ is evaluated as

$$G_{1|\sigma}^{(2)}(\omega_n) = -\frac{U}{(i\omega_n + \mu)^2} \frac{e^{\beta\mu}}{1 + e^{\beta\mu}}. \quad (5.12)$$

To compute the second-order contribution to $G_\sigma^{(2)}$, one proceeds in the same way illustrated above for the first-order. There are three distinct types of connected diagrams corresponding to second-order contributions:

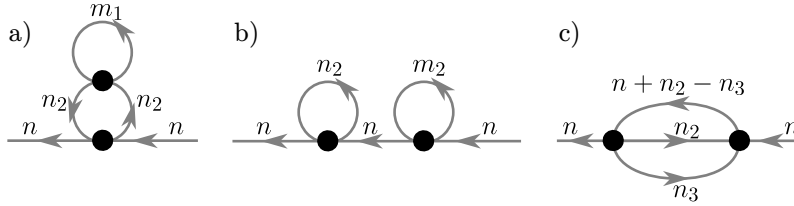


Figure 5.3: Second-order contributions to the one-body Green's function for the Hubbard atom. Again, both spins corresponding to the input arguments were chosen as \uparrow .

Mathematically, the first diagram Fig. 5.3a is expressed as

$$G_{2,1|\sigma}^{(2)} = \frac{U^2}{\beta^2} G_0^2(\omega_n) \sum_{n_2} G_0^2(\omega_{n_2}) \sum_{i\omega_{m_1}} G_0(\omega_{m_1}). \quad (5.13)$$

Note, that the factor $\frac{1}{2}$ was canceled, as the term of the diagram shown in Fig. 5.3 contributes two times to the one-body Green's function, as exchanging the roles of the vertices leads to the same diagram, just flipped horizontally. However, in terms of mathematical expressions this flipped diagram is equivalent to the diagram shown in Fig. 5.3. The factor 2 due to the possibility of exchanging the vertices arises for the following contributions to $G_\sigma^{(2)}$ as well.

Evaluating both Matsubara frequency sums from Eq. (5.13), $G_{2,1|\sigma}^{(2)}$ is given by

$$G_{2,1}^{(2)} = -\frac{e^{2\beta\mu} U^2 \beta}{(1 + e^{\beta\mu})^3 (i\omega_n + \mu)^2}. \quad (5.14)$$

Another diagram corresponding to $G_2^{(2)}$ can be seen in Fig. 5.3b. It is transformed into

$$G_{2,2|\sigma}^{(2)} = \frac{U^2}{\beta^2} G_0^3(\omega_n) \sum_{n_2} G_0(\omega_{n_2}) \sum_{m_2} G_0(\omega_{m_2}) = \frac{e^{2\beta\mu} U^2}{(1 + e^{\beta\mu})^2 (i\omega_n + \mu)^3}. \quad (5.15)$$

Lastly, there is a third type of diagram representing a part of $G_\sigma^{(2)}$, namely Fig. 5.3c: In terms of

equations, the third contribution reads

$$G_{2,3|\sigma}^{(2)} = -\frac{U^2}{\beta^2} G_0^2(\omega_n) \sum_{n_3} \left(G_0(\omega_{n_3}) \sum_{n_2} G_0(\omega_{n_2}) G_0(\omega_n + \omega_{n_2} - \omega_{n_3}) \right). \quad (5.16)$$

Applying residue theorem to the frequency sums, one obtains

$$G_{2,3|\sigma}^{(2)} = -\frac{e^{\beta\mu} U^2 \beta}{(1 + e^{\beta\mu})^2 (i\omega_n + \mu)^3}. \quad (5.17)$$

Now, all contributions to $G_\sigma^{(2)}$ derived above are added. The one-particle Green's function up to second-order in $\frac{U}{\beta}$ is thus expanded as

$$G_{2|\sigma}^{(2)} = \frac{1}{i\omega_n + \mu} - \frac{U e^{\beta\mu}}{(i\omega_n + \mu)^2 (1 + e^{\beta\mu})} + \frac{e^{\beta\mu} U^2 (1 + e^{2\beta\mu} + e^{\beta\mu} (2 - \beta(i\omega_n + \mu)))}{(1 + e^{\beta\mu})^3 (i\omega_n + \mu)^3}. \quad (5.18)$$

From this expression, one can determine the self-energy up to second-order, which is the aim of the next subsection.

5.2 Self-Energy

Revisiting the Dyson equation Eq. (4.29), the self-energy is composed of the one-particle irreducible parts of diagrams of the one-body Green's function. Hence, we assign self-energy contributions to the diagrams from the previous section. The self-energy can be expanded in orders of $\frac{U}{\beta}$ as well:

$$\Sigma = \Sigma_1 + \Sigma_2 + \mathcal{O}\left(\frac{U^3}{\beta^3}\right) \quad (5.19)$$

Therefore, the Dyson equation is expanded as

$$G \approx G_0 + G_0 (\Sigma_1 + \Sigma_2) (G_0 + G_0 (\Sigma_1 + \Sigma_2)) \approx G_0 + G_0 \Sigma_1 G_0 + G_0 \Sigma_1 G_0 \Sigma_1 G_0 + G_0 \Sigma_2 G_0. \quad (5.20)$$

Thus, the diagrams shown in Fig. 5.2, Fig. 5.3a, Fig. 5.3b and Fig. 5.3c can be related to the self-energy. From them, the first-order contribution Σ_1 and the second-order contribution Σ_2 are extracted. Diagrammatically, one has to 'cut off' or amputate external Green's functions:

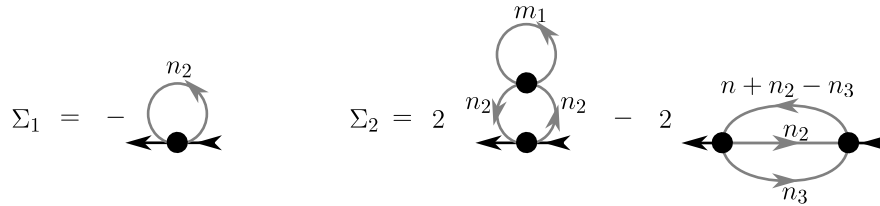


Figure 5.4: First- and second-order contributions to the self-energy for the Hubbard atom.

For the Hubbard atom, the amputation of the Green's function 'legs' is simply done by dividing by the expressions corresponding to the respective propagators. The self-energy may therefore be expressed as

$$\Sigma_\sigma(\omega_n) = -\frac{U e^{\beta\mu}}{(1 + e^{\beta\mu})} - \frac{e^{\beta\mu} U^2 (-1 + e^{\beta\mu} (-1 + \beta(i\omega_n + \mu)))}{(1 + e^{\beta\mu})^3 (i\omega_n + \mu)} + \mathcal{O}\left(\frac{U^3}{\beta^3}\right). \quad (5.21)$$

As the self-energy is not dependent on the spin argument σ , it has the same mathematical value for $\sigma = \uparrow$ and $\sigma = \downarrow$.

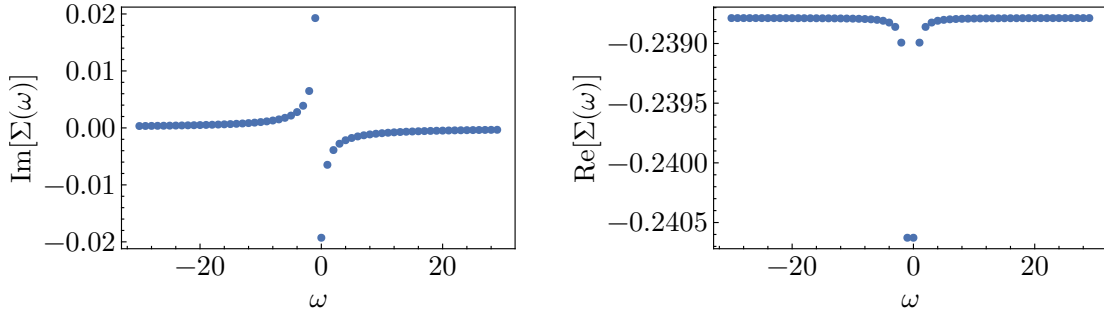


Figure 5.5: Real and imaginary part of the self-energy from second-order perturbation theory for $\beta = 1$, $U = 0.5$, $\mu = -0.3$.

5.3 Two-body Green's function

We proceed in the same way as for the one-body Green's function to derive the vertex according to Eq. (4.33). Expanding the exponential factor $e^{-S_{\text{int}}}$, the starting point for the perturbative series of $G^{(4)}$ is given by

$$G_{\sigma_1\sigma_2;\sigma_3\sigma_4}^{(4)}(\omega_{n_1}, \omega_{n_2}, \omega_{n_3}, \omega_{n_4}) = \frac{Z_0}{Z} \frac{1}{Z_0} \int D(\bar{c}, c) c_{\sigma_1 n_1} c_{\sigma_2 n_2} \bar{c}_{\sigma_3 n_3} \bar{c}_{\sigma_4 n_4} e^{-S_0} \times \left(1 - S_{\text{int}} + \frac{1}{2} (S_{\text{int}})^2 + \mathcal{O}\left(\frac{U^3}{\beta^3}\right) \right) \delta_{n_1+n_2; n_3+n_4}. \quad (5.22)$$

This time, we have to distinguish different combinations of spins σ_1 to σ_4 . There are two possible cases which do not vanish:

$$\begin{aligned} \text{case 1: } & \sigma_1 = \sigma_3; \sigma_2 = \sigma_4 \neq \sigma_1 \\ \text{case 2: } & \sigma_1 = \sigma_2 = \sigma_3 = \sigma_4 \end{aligned} \quad (5.23)$$

5.3.1 Two-Body Green's Function for Spin Arguments ($\uparrow\downarrow; \uparrow\downarrow$)

At first, case 1 from Eq. (5.23) is treated. Without loss of generality, we can assume the spin arguments to be $\sigma_1 = \sigma_3 = \uparrow; \sigma_2 = \sigma_4 = \downarrow$. Other combinations of spins according to case 1 would result in flipped diagrams and identical mathematical expressions. Taking only the first-order term of Eq. (5.22) into consideration, one needs to evaluate

$$G_{1|\uparrow\downarrow; \uparrow\downarrow}^{(4)}(\omega_{n_i}) = \frac{Z_0}{Z} \frac{U}{\beta} \sum_{\{m_i\}} \langle c_{\uparrow, n_1} c_{\downarrow, n_2} c_{\uparrow, m_3} c_{\downarrow, m_4} \bar{c}_{\uparrow, n_3} \bar{c}_{\downarrow, n_4} \bar{c}_{\uparrow, m_1} \bar{c}_{\downarrow, m_2} \rangle_0 \delta_{n_1+n_2; n_3+n_4} \delta_{m_1+m_2; m_3+m_4}. \quad (5.24)$$

In first-order there is only one connected diagram representing $G_1^{(4)}$, which is depicted in Fig. 5.6.

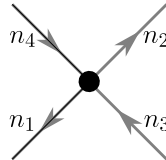


Figure 5.6: First-order contribution to the two-body Green's function ($\uparrow\downarrow; \uparrow\downarrow$) for the Hubbard atom.

Transforming it into a mathematical expression, reads

$$G_{1|\uparrow\downarrow; \uparrow\downarrow}^{(4)}(\omega_{n_i}) = \frac{U}{\beta} G_0(\omega_{n_1}) G_0(\omega_{n_2}) G_0(\omega_{n_3}) G_0(\omega_{n_4}). \quad (5.25)$$

Because of frequency conservation, the Matsubara frequency ω_{n_4} can be expressed as $\omega_{n_1} + \omega_{n_2} - \omega_{n_3}$. Next, the second-order contribution

$$G_{2|\uparrow\downarrow;\uparrow\downarrow}^{(4)}(\omega_{n_i}) = \frac{Z_0}{Z} \frac{U^2}{2\beta^2} \sum_{\{m_i, l_i\}} \langle c_{\uparrow, n_1} c_{\downarrow, n_2} c_{\uparrow, m_3} c_{\downarrow, m_4} c_{\uparrow, l_3} c_{\downarrow, l_4} \bar{c}_{\uparrow, n_3} \bar{c}_{\downarrow, n_4} \bar{c}_{\uparrow, m_1} \bar{c}_{\downarrow, m_2} \bar{c}_{\uparrow, l_1} \bar{c}_{\downarrow, l_2} \rangle_0 \quad (5.26)$$

$$\times \delta_{n_1+n_2; n_3+n_4} \delta_{m_1+m_2; m_3+m_4} \delta_{l_1+l_2; l_3+l_4}$$

is analyzed. We are once again only considering connected diagrams. There are twelve connected diagrams, but only six distinct diagram types, as half of them can be generated from the others by exchanging vertices. Below, they will be listed with their corresponding equations:

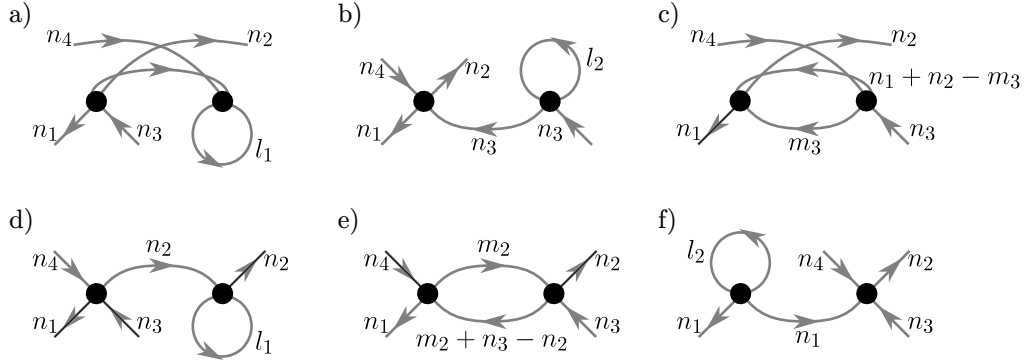


Figure 5.7: Second-order contributions to the two-body Green's function ($\uparrow\downarrow\uparrow\downarrow$) for the Hubbard atom.

Expression Fig. 5.7a:

$$G_{2,1|\uparrow\downarrow;\uparrow\downarrow}^{(4)}(\omega_{n_i}) = -\frac{U^2}{\beta^2} G_0(\omega_{n_1}) G_0(\omega_{n_2}) G_0(\omega_{n_3}) G_0(\omega_{n_4}) \sum_{l_1} G_0(\omega_{l_1}) \quad (5.27)$$

$$= -\frac{U^2 e^{\beta\mu}}{\beta(1+e^{\beta\mu})} \frac{1}{(i\omega_{n_1} + \mu)(i\omega_{n_2} + \mu)(i\omega_{n_3} + \mu)(i\omega_{n_1} + i\omega_{n_2} - i\omega_{n_3} + \mu)^2}$$

Expression Fig. 5.7b:

$$G_{2,2|\uparrow\downarrow;\uparrow\downarrow}^{(4)}(\omega_{n_i}) = -\frac{U^2}{\beta^2} G_0(\omega_{n_1}) G_0(\omega_{n_2}) G_0(\omega_{n_3})^2 G_0(\omega_{n_4}) \sum_{l_2} G_0(\omega_{l_2}) \quad (5.28)$$

$$= -\frac{U^2 e^{\beta\mu}}{\beta(1+e^{\beta\mu})} \frac{1}{(i\omega_{n_1} + \mu)(i\omega_{n_2} + \mu)(i\omega_{n_3} + \mu)^2 (i\omega_{n_1} + i\omega_{n_2} - i\omega_{n_3} + \mu)}$$

Expression Fig. 5.7c:

$$G_{2,3|\uparrow\downarrow;\uparrow\downarrow}^{(4)}(\omega_{n_i}) = \frac{U^2}{\beta^2} G_0(\omega_{n_1}) G_0(\omega_{n_2}) G_0(\omega_{n_3}) G_0(\omega_{n_4}) \sum_{m_3} (G_0(\omega_{m_3}) G_0(\omega_{n_1} + \omega_{n_2} - \omega_{m_3})) \quad (5.29)$$

$$= \frac{U^2 (e^{\beta\mu} - 1)}{\beta(1+e^{\beta\mu})(2\mu + i\omega_{n_1} + i\omega_{n_2})} \frac{1}{(i\omega_{n_1} + \mu)(i\omega_{n_2} + \mu)(i\omega_{n_3} + \mu)(i\omega_{n_1} + i\omega_{n_2} - i\omega_{n_3} + \mu)}$$

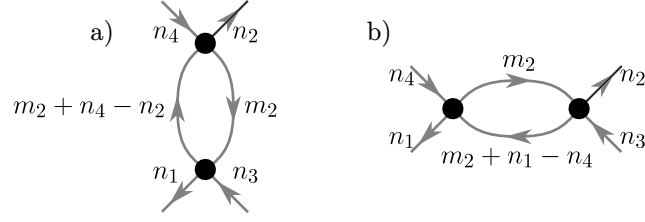


Figure 5.8: Second-order contributions to the two-body Green's function($\uparrow\uparrow\uparrow$) for the Hubbard atom

Expression Fig. 5.7d:

$$\begin{aligned} G_{2,4|\uparrow\downarrow;\uparrow\downarrow}^{(4)}(\omega_{n_i}) &= -\frac{U^2}{\beta^2} G_0(\omega_{n_1}) G_0(\omega_{n_2})^2 G_0(\omega_{n_3}) G_0(\omega_{n_4}) \sum_{l_1} G_0(\omega_{l_1}) \\ &= -\frac{U^2 e^{\beta\mu}}{\beta(1+e^{\beta\mu}) (i\omega_{n_1} + \mu)(i\omega_{n_2} + \mu)^2 (i\omega_{n_3} + \mu)(i\omega_{n_1} + i\omega_{n_2} - i\omega_{n_3} + \mu)} \end{aligned} \quad (5.30)$$

Expression Fig. 5.7e:

$$\begin{aligned} G_{2,5|\uparrow\downarrow;\uparrow\downarrow}^{(4)}(\omega_{n_i}) &= \frac{U^2}{\beta^2} G_0(\omega_{n_1}) G_0(\omega_{n_2}) G_0(\omega_{n_3}) G_0(\omega_{n_4}) \sum_{m_2} (G_0(\omega_{m_2}) G_0(\omega_{m_2} - \omega_{n_2} + \omega_{n_3})) \\ &= -\delta_{n_2 n_3} \frac{U^2 e^{\beta\mu}}{(1+e^{\beta\mu})^2 (i\omega_{n_1} + \mu)^2 (i\omega_{n_3} + \mu)^2} \end{aligned} \quad (5.31)$$

Expression Fig. 5.7f:

$$\begin{aligned} G_{2,6|\uparrow\downarrow;\uparrow\downarrow}^{(4)}(\omega_{n_i}) &= -\frac{U^2}{\beta^2} G_0(\omega_{n_1})^2 G_0(\omega_{n_2}) G_0(\omega_{n_3}) G_0(\omega_{n_4}) \sum_{m_2} G_0(\omega_{m_2}) \\ &= -\frac{U^2 e^{\beta\mu}}{\beta(1+e^{\beta\mu}) (i\omega_{n_1} + \mu)^2 (i\omega_{n_2} + \mu)(i\omega_{n_3} + \mu)(i\omega_{n_1} + i\omega_{n_2} - i\omega_{n_3} + \mu)} \end{aligned} \quad (5.32)$$

Adding these terms would yield the second-order contribution to the connected two-particle Green's function for spin arguments as in case 1.

5.3.2 Two-Body Green's Function for Spin Arguments ($\uparrow\uparrow;\uparrow\uparrow$)

After computing $G^{(4)}$ for the spin combination defined in the first case, we proceed accordingly for the spin combinations in case 2 from Eq. (5.23). Without loss of generality $\sigma_1 = \sigma_2 = \sigma_3 = \sigma_4 = \uparrow$ is assumed. Again, we only consider connected diagrams. If all spin components are chosen equal, there are no contributions in first-order to $G^{(4)}$. In second-order, one can only draw two connected diagram types, which are depicted in Fig. 5.8. Below are again written down the equations derived from both diagrams.

Expression Fig. 5.8a:

$$\begin{aligned} G_{2,1|\uparrow\uparrow;\uparrow\uparrow}^{(4)}(\omega_{n_i}) &= -\frac{U^2}{\beta^2} G_0(\omega_{n_1}) G_0(\omega_{n_2}) G_0(\omega_{n_3}) G_0(\omega_{n_4}) \sum_{m_2} (G_0(\omega_{m_2}) G_0(\omega_{m_2} + \omega_{n_1} - \omega_{n_3})) \\ &= \delta_{n_1 n_3} \frac{U^2 e^{\beta\mu}}{(1+e^{\beta\mu})^2 (i\omega_{n_1} + \mu)^2 (i\omega_{n_2} + \mu)^2} \end{aligned} \quad (5.33)$$

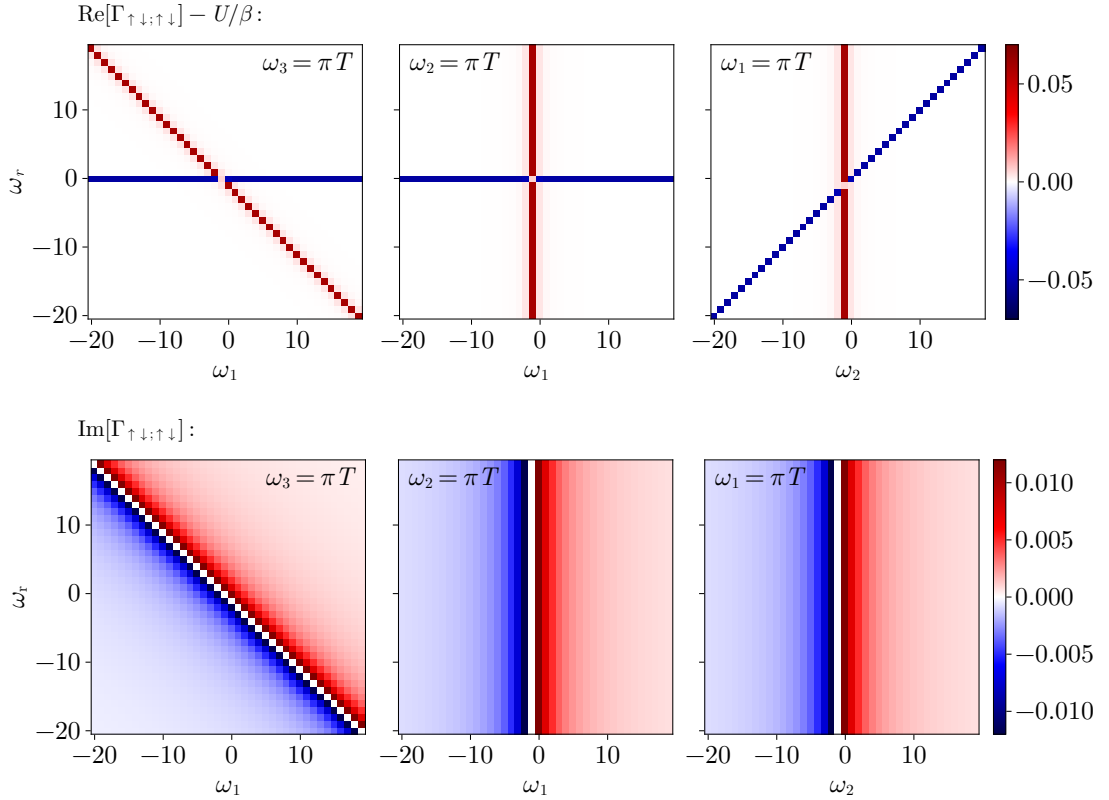


Figure 5.9: Four-point vertex $\Gamma_{\uparrow\downarrow;\uparrow\downarrow}$ in second-order perturbation theory for chemical potential $\mu = -0.8$, $\beta = 1$ and $U = 0.5$. ω_r stands for the frequency index, for which the frequency was not set equal to $\frac{\pi}{\beta}$ and not plotted along the x-axis.

Expression Fig. 5.8b:

$$\begin{aligned}
 G_{2,2|\uparrow\uparrow;\uparrow\uparrow}^{(4)}(\omega_{n_i}) &= \frac{U^2}{\beta^2} G_0(\omega_{n_1}) G_0(\omega_{n_2}) G_0(\omega_{n_3}) G_0(\omega_{n_4}) \sum_{m_2} (G_0(\omega_{m_2}) G_0(\omega_{m_2} + \omega_{n_3} - \omega_{n_2})) \\
 &= -\delta_{n_2 n_3} \frac{U^2 e^{\beta\mu}}{(1 + e^{\beta\mu})^2} \frac{1}{(i\omega_{n_1} + \mu)^2 (i\omega_{n_3} + \mu)^2}
 \end{aligned} \tag{5.34}$$

With above diagrams and expressions, we are finally able to calculate the four-point vertex up to second-order in $\frac{U}{\beta}$. This is illustrated in the next section.

5.4 Four-point Vertex

As the four-point vertex is a quantity which will be used to check Ward identities for the Hubbard atom later, it is the last quantity for which a perturbation expansion up to second-order will be determined. According to Eq. (4.33), the vertex can be related to the two-body Green's function by amputating parts corresponding to the one-body connected Green's function. Again, we need to distinguish between the different cases Eq. (5.23) for the spin of the arguments of $G^{(4)}$.

5.4.1 Four-Point Vertex for Spin Arguments ($\uparrow\downarrow;\uparrow\downarrow$)

To begin, we will concentrate on case 1 ($\sigma_1 = \sigma_3 = \uparrow; \sigma_2 = \sigma_4 = \downarrow$). Comparing the diagrams of $G^{(2)}$ in section 5.1 and of $G^{(4)}$ in section 5.3, following diagrams are part of the vertex in first and second-order:

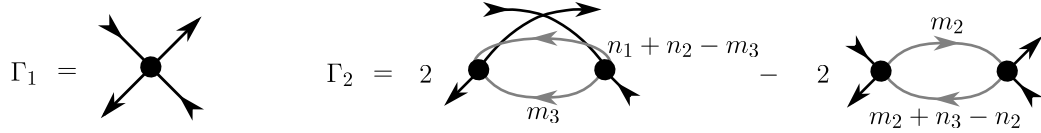


Figure 5.10: Second-order contributions to the four-point vertex($\uparrow\downarrow\uparrow\downarrow$) for the Hubbard atom

After amputation, we obtain a mathematical expression for the four-point vertex

$$\Gamma_{\uparrow\downarrow;\uparrow\downarrow}(\omega_{n_i}) = \frac{U}{\beta} + \frac{U^2}{\beta} \left(\frac{e^{\beta\mu} - 1}{(1 + e^{\beta\mu})(2\mu + i(\omega_{n_1} + \omega_{n_2}))} \right) - \delta_{n_2 n_3} \left(\frac{U^2 e^{\beta\mu}}{(1 + e^{\beta\mu})^2} \right) + \mathcal{O} \left(\frac{U^3}{\beta^3} \right). \quad (5.35)$$

Again, we just divide by the one-body Green's functions, which are 'cut' in order to generate the vertex diagrams from the diagrams of $G^{(4)}$. The real and imaginary part of the above vertex contribution are depicted in Fig. 5.9.

5.4.2 Four-Point Vertex for Spin Arguments ($\uparrow\uparrow;\uparrow\uparrow$)

Repeating this whole procedure for case 2, in which all spins of the arguments of $G^{(4)}$ are equal, the vertex corresponding to this spin combination is given by:

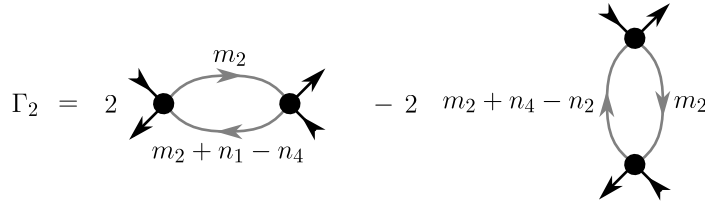


Figure 5.11: Second-order contributions to the four-point vertex($\uparrow\uparrow\uparrow\uparrow$) for the Hubbard atom

Translating these diagrams into a formula, results in

$$\Gamma_{\uparrow\uparrow;\uparrow\uparrow}(\omega_{n_i}) = \left(\frac{U^2 e^{\beta\mu}}{(1 + e^{\beta\mu})^2} \right) (\delta_{n_1 n_3} - \delta_{n_2 n_3}) + \mathcal{O} \left(\frac{U^3}{\beta^3} \right). \quad (5.36)$$

The result for $\Gamma_{\uparrow\uparrow;\uparrow\uparrow}$ is illustrated in Fig. 5.12.

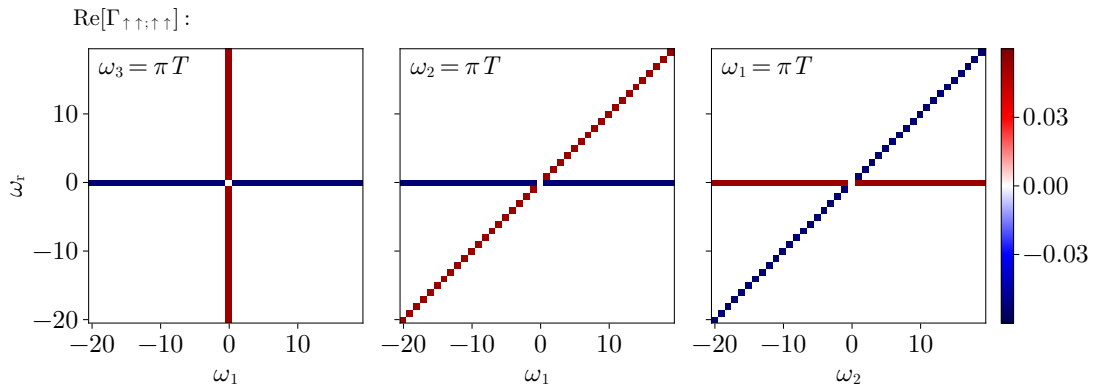


Figure 5.12: Real part of the four-point vertex $\Gamma_{\uparrow\uparrow;\uparrow\uparrow}$ in second-order perturbation theory for chemical potential $\mu = -0.8$, $\beta = 1$ and $U = 0.5$. The imaginary part of $\Gamma_{\uparrow\uparrow;\uparrow\uparrow}$ in second-order perturbation theory is equal to 0. ω_r stands for the frequency index, for which the frequency was not set equal to $\frac{\pi}{\beta}$ and not plotted along the x-axis.

Now, we have acquired all preliminary results necessary for the actual topic of this thesis, the Ward identities. At last, in the subsequent chapter symmetries are covered from a functional field perspective. This will also serve as our starting point for the derivation of Ward identities for the Hubbard atom.

6 Derivation of Ward Identities for the Hubbard Atom

In this section, a general formalism to derive Ward identities from functional integrals will be introduced. This functional ansatz is then employed to find the Ward identity corresponding to the U(1)-symmetry of the Hubbard atom. Before covering the methods necessary for the following derivations, let's first address the definition of Ward identities in general. First discovered in 1950 by John Clive Ward [9], they were further developed by Takahashi [10] and are therefore sometimes also referred to as Ward-Takahashi identities. Depending on the respective literature, there may be slight differences between Ward identities and Ward-Takahashi identities in terms of their exact definition and applicability range. In this thesis, we will refer to all exact relations between correlation functions of different order as Ward identities. Ward identities originate from symmetries of a system, which we will see later. As Ward identities are exact and always supposed to hold due to their dependence on fundamental symmetries of the respective physical system, one can for example use them to verify the quality of an approximation by substituting the approximated quantities into a Ward identity and checking, if it still holds true.

However, in order to do this we need to be able to associate symmetries with their corresponding Ward identities. Thus, the next subsection is dedicated to developing such an approach in the path integral formalism.

6.1 Symmetry Transformations in the Functional Integral Formalism

Starting point for the derivation of a method to obtain Ward identities from symmetry transformations is the partition function with additional source terms

$$Z[\bar{J}, J] = \int D(\bar{c}, c) e^{-S[\bar{c}, c] + \int d^4x (\bar{J}_n c_n + \bar{c}_m J_m)}. \quad (6.1)$$

The definitions of the formula symbols are the same as in chapter 4.1, whereas the only change is the additional integration of the source terms over the four-vector $x = (\tau, \mathbf{x})^T$. Furthermore, Einstein sum convention is used, which means one sums over repeated indices. Therefore, a summation over n, m numbering the Grassmann numbers is implicit. Now, let us consider an infinitesimal transformation of Grassmann variables

$$c_n(x) \mapsto c'_n(x) = c_n(x) + \epsilon F_n[c_k, x] \quad (6.2)$$

$$\bar{c}_m(x) \mapsto \bar{c}'_m(x) = \bar{c}_m(x) + \epsilon \bar{F}_m[\bar{c}_l, x]. \quad (6.3)$$

Above, ϵ is a small parameter and k, l index coherent states. Next, we express the partition function Z in terms of c'_n and $\bar{c}'_m(x)$. This is done by simply relabeling the Grassmann variables in Eq. (6.1) to obtain

$$\begin{aligned} Z'[\bar{J}, J] &= \int D(\bar{c}', c') e^{-S[\bar{c}', c'] + \int d^4x (\bar{J}_n c'_n + \bar{c}'_m J_m)} \\ &= \int D(\bar{c}, c) \left| \det \frac{\delta \bar{c}'_m(y)}{\delta \bar{c}_m(x)} \right| \left| \det \frac{\delta c'_n(y)}{\delta c_n(x)} \right| \\ &\quad \times e^{-S[\bar{c}, c] + \int d^4x (\bar{J}_n c_n + \bar{c}_m J_m) + \epsilon \int d^4x [\bar{J}_n F_n + \bar{F}_m J_m - \frac{\delta S}{\delta \bar{c}_m} \bar{F}_m - \frac{\delta S}{\delta c_n} F_n]}, \end{aligned} \quad (6.4)$$

where in the last step, the integration measure was transformed, which generated the determinant of the Jacobians for \bar{c}'_n and c'_n as additional factors. Besides, the transformations Eq. (6.2), Eq.

(6.3) were inserted and the action S was expanded around \bar{c}_n and c_n up to first-order in ϵ . For explicit representations of the transformation determinants

$$\left| \det \frac{\delta \bar{c}'_{m'}(y)}{\delta \bar{c}_m(x)} \right| = e^{\text{tr} \log(1 + \epsilon \frac{\delta \bar{F}_m}{\delta \bar{c}_m})}, \quad (6.5)$$

we make use of the identity $\log(\det(A)) = \text{tr}(\log(A))$ for an arbitrary matrix A . Here, we also calculated the functional derivative $\frac{\delta \bar{c}'_{m'}(y)}{\delta \bar{c}_m(x)}$. Now, natural logarithm and exponential function are expanded up to first-order in ϵ and the trace is evaluated:

$$\left| \det \frac{\delta \bar{c}'_{m'}(y)}{\delta \bar{c}_m(x)} \right| = 1 + \left(\epsilon \int d^4x \sum_m \frac{\delta \bar{F}_m}{\delta \bar{c}_m} \right) + \mathcal{O}(\epsilon^2) \quad (6.6)$$

Accordingly, the transformation determinant corresponding to c'_n and c_n is given by

$$\left| \det \frac{\delta c'_n(y)}{\delta c_n(x)} \right| = 1 + \left(\epsilon \int d^4x \sum_n \frac{\delta F_n}{\delta c_n} \right) + \mathcal{O}(\epsilon^2). \quad (6.7)$$

Eq. (6.6) and Eq. (6.7) are substituted into Z' and the expression is again expanded to only contain terms up to first-order in ϵ :

$$\begin{aligned} Z'[\bar{J}, J] &= \int D(\bar{c}, c) e^{-S[\bar{c}, c] + \int d^4x (\bar{J}_n c_n + \bar{c}_m J_m)} \\ &\times \left(1 + \epsilon \int d^4x \sum_{n,m} \left(\frac{\delta F_n}{\delta c_n} + \frac{\delta \bar{F}_m}{\delta \bar{c}_m} \right) + \bar{F}_m J_m - \frac{\delta S}{\delta \bar{c}_m} \bar{F}_m + \bar{J}_n F_n - \frac{\delta S}{\delta c_n} F_n \right) + \mathcal{O}(\epsilon^2) \end{aligned} \quad (6.8)$$

Since originally the transformation of the variables c_n, \bar{c}_m to c'_n, \bar{c}'_m was just a relabeling, the above expression needs to be equal to Eq. (6.1). Therefore, setting $Z[\bar{J}, J] = Z'[\bar{J}, J]$ leads to

$$\begin{aligned} 0 &= \int D(\bar{c}, c) e^{-S[\bar{c}, c] + \int d^4x (\bar{J}_n c_n + \bar{c}_m J_m)} \\ &\times \int d^4x \left(\sum_{n,m} \left(\frac{\delta F_n}{\delta c_n} + \frac{\delta \bar{F}_m}{\delta \bar{c}_m} \right) + \bar{F}_m J_m - \frac{\delta S}{\delta \bar{c}_m} \bar{F}_m + \bar{J}_n F_n - \frac{\delta S}{\delta c_n} F_n \right). \end{aligned} \quad (6.9)$$

This is a highly important result and we will refer back to it later. Before proceeding with the derivation, let us now briefly cover some terminology in the context of symmetry transformations. Generally, a transformation is called a symmetry of a system, if it leaves its action invariant. In quantum field theory, one can distinguish between internal and external symmetry transformations. The former refers to transformations only affecting the fields c, \bar{c} , whereas the latter includes a transformation of the four-vector x describing space-time. Additionally, symmetry transformations which leave the measure invariant are called non-anomalous, and ones that do change the measure are called anomalous. In this thesis, only non-anomalous internal symmetries will be covered. Lastly, symmetries can either be global or local. The transformation corresponding to a global symmetry does not depend on the space-time point x , whereas in the case of a local symmetry the transformation parameters are dependent on x .

Let us now consider a local non-anomalous symmetry and simplify Eq. (6.9) according to this assumption. As the measure is invariant under a non-anomalous transformation, the partial derivatives which arise from transforming $D(\bar{c}', c')$ to $D(\bar{c}, c)$ vanish. Therefore, we are left with

$$0 = \int D(\bar{c}, c) e^{-S[\bar{c}, c] + \int d^4x (\bar{J}_n c_n + \bar{c}_m J_m)} \int d^4x \left(\bar{F}_m J_m - \frac{\delta S}{\delta \bar{c}_m} \bar{F}_m + \bar{J}_n F_n - \frac{\delta S}{\delta c_n} F_n \right). \quad (6.10)$$

Now, let us consider some terms in Eq. (6.10) separately. More specifically, we try to relate the expression to the Noether current. As a quick reminder, the Noether theorem tells us that from every symmetry of the action there arises a conserved quantity, which is called the Noether current. In the following, we are concerned with finding a field-theoretical version of this quantity. Thus, we reformulate the action terms in Eq. (6.10) as

$$\begin{aligned} & \int d^4x \left(\frac{\delta S}{\delta \bar{c}_m} \bar{F}_m + \frac{\delta S}{\delta c_n} F_n \right) \epsilon(x) \\ &= \int d^4x \left[\left(\frac{\partial \mathcal{L}}{\partial \bar{c}_m} - \partial_\mu \frac{\partial \mathcal{L}}{\partial (\partial_\mu \bar{c}_m)} \right) \bar{F}_m + \left(\frac{\partial \mathcal{L}}{\partial c_n} - \partial_\mu \frac{\partial \mathcal{L}}{\partial (\partial_\mu c_n)} \right) F_n \right] \theta(x), \end{aligned} \quad (6.11)$$

where θ denotes the transformation parameter, which is dependent on the space-time point x in the case of a local symmetry transformation and the Lagrangian \mathcal{L} corresponding to the action S . Greek indices like μ in Eq. (6.11) number the indices of four-vectors from 0 to 3. In the second step, the Euler-Lagrange equations for fields were inserted for the variation of the action. Next, we apply chain rule:

$$\begin{aligned} \int d^4x \left(\frac{\delta S}{\delta \bar{c}_m} \bar{F}_m + \frac{\delta S}{\delta c_n} F_n \right) \theta(x) &= \int d^4x \left[\frac{\partial \mathcal{L}}{\partial \bar{c}_m} \bar{F}_m + \frac{\partial \mathcal{L}}{\partial (\partial_\mu \bar{c}_m)} \partial_\mu \bar{F}_m - \partial_\mu \left(\frac{\partial \mathcal{L}}{\partial (\partial_\mu \bar{c}_m)} \bar{F}_m \right) \right. \\ &\quad \left. + \frac{\partial \mathcal{L}}{\partial c_n} F_n + \frac{\partial \mathcal{L}}{\partial (\partial_\mu c_n)} \partial_\mu F_n - \partial_\mu \left(\frac{\partial \mathcal{L}}{\partial (\partial_\mu c_n)} F_n \right) \right] \theta(x) \end{aligned} \quad (6.12)$$

Regrouping some terms in Eq. (6.12), we can formulate them as one derivative of the Lagrangian density with respect to the transformation parameter

$$\begin{aligned} & \frac{\partial \mathcal{L}}{\partial \bar{c}_m} \bar{F}_m + \frac{\partial \mathcal{L}}{\partial (\partial_\mu \bar{c}_m)} \partial_\mu \bar{F}_m + \frac{\partial \mathcal{L}}{\partial c_n} F_n + \frac{\partial \mathcal{L}}{\partial (\partial_\mu c_n)} \partial_\mu F_n \\ &= \frac{\partial \mathcal{L}(\bar{c} + \epsilon \theta \bar{F}, c + \epsilon \theta F, \partial_\mu (\bar{c} + \epsilon \theta \bar{F}), \partial_\mu (c + \epsilon \theta F))}{\epsilon \partial \theta} \\ &= \frac{1}{\epsilon} (\mathcal{L}(\bar{c}', c', \partial_\mu \bar{c}', \partial_\mu c') - \mathcal{L}(\bar{c}, c, \partial_\mu \bar{c}, \partial_\mu c)) = \frac{1}{\epsilon} \delta \mathcal{L}. \end{aligned} \quad (6.13)$$

We define this variation of the Lagrangian density as

$$\frac{1}{\epsilon} \delta \mathcal{L} \equiv \partial_\mu J_0. \quad (6.14)$$

Substituting this back into Eq. (6.13), the partial derivatives of the action are given by

$$\begin{aligned} \int d^4x \left(\frac{\delta S}{\delta \bar{c}_m} \bar{F}_m + \frac{\delta S}{\delta c_n} F_n \right) \theta(x) &= \int d^4x \partial_\mu \left(J_0 - \frac{\partial \mathcal{L}}{\partial (\partial_\mu \bar{c}_m)} \bar{F}_m - \frac{\partial \mathcal{L}}{\partial (\partial_\mu c_n)} F_n \right) \theta(x) \\ &= - \int d^4x \partial_\mu j^\mu \theta(x), \end{aligned} \quad (6.15)$$

where the Noether current was defined as $j^\mu \equiv \frac{\partial \mathcal{L}}{\partial (\partial_\mu \bar{c}_m)} \bar{F}_m + \frac{\partial \mathcal{L}}{\partial (\partial_\mu c_n)} F_n - J_0$. Inserting this into our original expression Eq. (6.10) and taking the fact into consideration that $\theta(x)$ is an arbitrary function of x , for a local non-anomalous symmetry the identity

$$\int D(\bar{c}, c) e^{-S[\bar{c}, c] + \int d^4x (\bar{J}_n c_n + \bar{c}_m J_m)} (\bar{F}_m J_m + \bar{J}_n F_n + \partial_\mu j^\mu) = 0 \quad (6.16)$$

must hold. This identity is now written out explicitly for specific symmetry transformations fulfilling

the conditions specified in the former paragraph. We demonstrate this by considering the U(1) symmetry transformation for the Hubbard atom in the next section.

6.2 U(1) Ward Identity for the Hubbard Atom

Various symmetries of the Hubbard model are listed in Tab. 2.1. To each continuous symmetry there is a corresponding symmetry transformation, Noether current and ultimately a corresponding Ward identity. At first, we will focus on the U(1) symmetry, which describes the invariance of the Hubbard atom action under the addition of a global phase to all Grassmann fields, as its transformation is rather simple compared to the other symmetries. In particular, the U(1) transformation reads:

$$c'_\sigma = e^{i\phi} c_\sigma \quad (6.17) \quad \bar{c}'_\sigma = e^{-i\phi} \bar{c}_\sigma \quad (6.18)$$

with σ denoting the spin and $\phi \in [0, 2\pi)$. If ϕ is replaced by $\epsilon \ll 1$, the transformations F and \bar{F} are given by:

$$F_\sigma = i c_\sigma \quad (6.19) \quad \bar{F}_\sigma = -i \bar{c}_\sigma \quad (6.20)$$

To derive the Noether current for this case, we first need an expression for the Lagrangian, which is related to the action by time differentiation, as there isn't any dependence on space in the Hubbard atom action. In time representation, the action for the Hubbard atom is defined as

$$S[\bar{c}, c] = \int_0^\beta d\tau (\bar{c} \partial_\tau c + H(\bar{c}, c) - \mu N(\bar{c}, c)). \quad (6.21)$$

Inserting the expressions from chapter 1 and differentiating with respect to τ , yields the Lagrangian

$$\mathcal{L} = \sum_\sigma \bar{c}_\sigma \partial_\tau c_\sigma - U \bar{c}_\uparrow \bar{c}_\downarrow c_\uparrow c_\downarrow - \mu (\bar{c}_\uparrow c_\uparrow + \bar{c}_\downarrow c_\downarrow). \quad (6.22)$$

Let us now derive an expression for the Noether current for this specific Lagrangian. The value of J_0 is determined by the variation of the Lagrangian under U(1) transformation. Substituting the transformed variables $\bar{c}'_\sigma, c'_\sigma$, the Lagrangian is invariant under a U(1) symmetry transformation:

$$\mathcal{L}(\bar{c}', c') = e^{-i\phi} e^{i\phi} \left(\sum_\sigma \bar{c}_\sigma \partial_\tau c_\sigma \right) - e^{-i\phi} e^{-i\phi} e^{i\phi} e^{i\phi} U \bar{c}_\uparrow \bar{c}_\downarrow c_\uparrow c_\downarrow - e^{-i\phi} e^{i\phi} \mu (\bar{c}_\uparrow c_\uparrow + \bar{c}_\downarrow c_\downarrow) = \mathcal{L}(\bar{c}, c) \quad (6.23)$$

and therefore

$$\delta \mathcal{L} = 0 \quad \Rightarrow \quad J_0 = 0. \quad (6.24)$$

According to Eq. (6.15), the Noether current

$$j_\mu = j_\tau = -i \sum_\sigma \bar{c}_\sigma c_\sigma \quad (6.25)$$

is obtained. Let us reconsider Eq. (6.10) for the U(1) symmetry:

$$\begin{aligned} & \int D(\bar{c}, c) e^{-S[\bar{c}, c] + \int d^4x (\bar{J}_n c_n + \bar{c}_m J_m)} \partial_\tau j^\tau \\ &= - \int D(\bar{c}, c) e^{-S[\bar{c}, c] + \int d^4x (\bar{J}_n c_n + \bar{c}_m J_m)} (-i \bar{c}_\sigma J_\sigma + i \bar{J}_\sigma c_{\sigma'}) \end{aligned} \quad (6.26)$$

From the above expression, we can obtain relations between correlation functions by differentiating with respect to the source terms and setting them to zero at the end. Both sides of Eq. (6.26) are treated separately. We first differentiate the left-hand side with respect to the sources:

$$\begin{aligned} & \frac{\delta}{\delta \bar{J}_1} \frac{\delta}{\delta J_2} \left(\int D(\bar{c}, c) e^{-S[\bar{c}, c] + \int d^4x (\bar{J}_n c_n + \bar{c}_m J_m)} \partial_\tau j^\tau \right) \Big|_{\bar{J}=J=0} \\ &= - \int D(\bar{c}, c) e^{-S[\bar{c}, c] + \int d^4x (\bar{J}_n c_n + \bar{c}_m J_m)} \partial_\tau j^\tau (c_1 \bar{c}_2) \Big|_{\bar{J}=J=0} = -\partial_\tau \langle j^\tau c_1 \bar{c}_2 \rangle \end{aligned} \quad (6.27)$$

Differentiating the right-hand side yields

$$\begin{aligned} & -\frac{\delta}{\delta \bar{J}_1} \frac{\delta}{\delta J_2} \left(\int D(\bar{c}, c) e^{-S[\bar{c}, c] + \int d^4x (\bar{J}_n c_n + \bar{c}_m J_m)} (-i\bar{c}_\sigma J_\sigma + i\bar{J}_{\sigma'} c_{\sigma'}) \right) \Big|_{\bar{J}=J=0} \\ &= -\frac{\delta}{\delta \bar{J}_1} \left(\int D(\bar{c}, c) e^{-S[\bar{c}, c] + \int d^4x (\bar{J}_n c_n + \bar{c}_m J_m)} (-\bar{c}_2 (-i\bar{c}_\sigma J_\sigma + i\bar{J}_{\sigma'} c_{\sigma'}) + i\bar{c}_2 \delta(\tau - \tau_2)) \right) \Big|_{\bar{J}=J=0} \\ &= - \int D(\bar{c}, c) e^{-S[\bar{c}, c] + \int d^4x (\bar{J}_n c_n + \bar{c}_m J_m)} (i\bar{c}_2 c_1 \delta(\tau - \tau_1) \\ &+ c_1 \bar{c}_2 (-i\bar{c}_\sigma J_\sigma + i\bar{J}_{\sigma'} c_{\sigma'}) + i c_1 \bar{c}_2 \delta(\tau - \tau_2)) \Big|_{\bar{J}=J=0} = i \langle c_1 \bar{c}_2 \rangle \delta(\tau - \tau_1) - i \langle c_1 \bar{c}_2 \rangle \delta(\tau - \tau_2), \end{aligned} \quad (6.28)$$

where the relation $\frac{\delta J_n(\tau_n)}{\delta J_i(\tau_i)} = \delta(\tau_n - \tau_i) \delta_{n,i}$, which is a general rule in functional differentiation, was used to generate the δ functions. Considering both sides of the equation, we obtain the relation

$$-\partial_\tau \langle j_\tau c_1(\tau_1) \bar{c}_2(\tau_2) \rangle = i \delta(\tau - \tau_1) \langle c_1(\tau_1) \bar{c}_2(\tau_2) \rangle - i \delta(\tau - \tau_2) \langle c_1(\tau_1) \bar{c}_2(\tau_2) \rangle \quad (6.29)$$

between thermal averages of field variables. Finally, we insert the Noether current Eq. (6.25). The U(1) Ward identity for the Hubbard atom in time representation is then given by

$$\partial_\tau \sum_\sigma \langle \bar{c}_\sigma c_\sigma c_1(\tau_1) \bar{c}_2(\tau_2) \rangle = \delta(\tau - \tau_1) \langle c_1(\tau_1) \bar{c}_2(\tau_2) \rangle - \delta(\tau - \tau_2) \langle c_1(\tau_1) \bar{c}_2(\tau_2) \rangle. \quad (6.30)$$

Next, the U(1) Ward identity is reformulated in Matsubara frequency space. To start, the left-hand side of Eq. (6.30) is Fourier transformed with the transformation rules Eq. (3.38), Eq. (3.39) and Eq. (5.3), Eq.(5.4):

$$\begin{aligned} & \partial_\tau \sum_\sigma \langle \bar{c}_\sigma c_\sigma c_1(\tau_1) \bar{c}_2(\tau_2) \rangle \\ &= -\partial_\tau \sum_\sigma \frac{1}{\beta^3} \int_0^\beta d\tau d\tau_1 d\tau_2 e^{i\omega_n \tau} e^{i\omega_{n_1} \tau_1} e^{i\omega_{n_2} \tau_2} \\ &\times \frac{1}{\beta^2} \sum_{\omega_{n'}, \omega_{n''}, \omega_{n_1'}, \omega_{n_2'}} e^{-i\omega_{n'} \tau} e^{-i\omega_{n_1'} \tau_1} e^{i\omega_{n_2'} \tau_2} e^{i\omega_{n''} \tau} \langle c_\sigma(\omega_{n'}) c_1(\omega_{n_1'}) \bar{c}_\sigma(\omega_{n''}) \bar{c}_2(\omega_{n_2'}) \rangle \end{aligned} \quad (6.31)$$

At first, the expression was brought into anti-normal-order and the transformations were inserted. Next, the partial derivative with respect to τ and the integrals over imaginary-time components are

evaluated as

$$\begin{aligned}
 & \sum_{\sigma, n'} (i\omega_{n'} - i\omega_{n'} - i\omega_{n_1} + i\omega_{n_2} + (\mu - \mu)) \langle c_{\sigma}(\omega_{n'}) c_1(\omega_{n'_1}) \bar{c}_{\sigma}(\omega_{n'} + \omega_{n_1} - \omega_{n_2}) \bar{c}_2(-\omega_{n_2}) \rangle \\
 &= \sum_{\sigma, n'} \left(([G_0^{(2)}(\omega_{n'})]^{-1} - (G_0^{(2)}(\omega_{n'} + \omega_{n_1} - \omega_{n_2}))^{-1}) G_{\sigma 1; \sigma 2}^{(4)}(\omega_{n'}, \omega_{n_1}, \omega_{n'} + \omega_{n_1} - \omega_{n_2}, \omega_{n_2}) \right).
 \end{aligned} \tag{6.32}$$

To express the factors $i\omega$ arising from the partial time derivative in frequency space in terms of non-interacting Green's functions, $0 = \mu - \mu$ was added. Let us now transform the right-hand side of Eq. (6.30) as

$$\begin{aligned}
 & \delta(\tau - \tau_1) \langle c_1(\tau_1) \bar{c}_2(\tau_2) \rangle - \delta(\tau - \tau_2) \langle c_1(\tau_1) \bar{c}_2(\tau_2) \rangle \\
 &= \frac{1}{\beta^4} \int_0^{\beta} \left[d\tau d\tau_1 d\tau_2 e^{i\omega_n \tau} e^{i\omega_{n_1} \tau_1} e^{i\omega_{n_2} \tau_2} \sum_{n'_1, n'_2} e^{-i\omega_{n_1} \tau_1} e^{i\omega_{n_2} \tau_2} \right. \\
 & \quad \left. \times \left(\delta(\tau - \tau_1) \langle c_1(\omega_{n'_1}) \bar{c}_2(\omega_{n'_2}) \rangle - \delta(\tau - \tau_2) \langle c_1(\omega_{n'_1}) \bar{c}_2(\omega_{n'_2}) \rangle \right) \right] \\
 &= G^{(2)}(\omega_{n_2}) \delta_{12} \delta_{n_2 n'} - G^{(2)}(\omega_{n_1}) \delta_{12} \delta_{n_1 n'}.
 \end{aligned} \tag{6.33}$$

After transforming to frequency space, we now want to express the U(1) Ward identity in terms of vertex and self-energy. Thus, we reformulate the four-point correlation function in Eq. (6.32) in terms of the four-point vertex by using relation Eq. (4.33), which in Matsubara frequency space is given by

$$\begin{aligned}
 & G_{\sigma 1; \sigma 2}^{(4)}(\omega_{n'}, \omega_{n_1}, \omega_{n'} + \omega_{n_1} - \omega_{n_2}, \omega_{n_2}) \delta_{n'+n_1; n+n'+n_2} \\
 &= G_{\sigma}^{(2)}(\omega_{n'}) G_1^{(2)}(\omega_{n_1}) \delta_{12} \delta_{n_1 n_2} - G_2^{(2)}(\omega_{n_2}) G_1^{(2)}(\omega_{n_1}) \delta_{1\sigma} \delta_{2\sigma} \delta_{n' n_2} \\
 &+ G_{\sigma}^{(2)}(\omega_{n'}) G_1^{(2)}(\omega_{n_1}) \Gamma_{\sigma 1; \sigma 2}(\omega_{n'}, \omega_{n_1}, \omega_{n'} + \omega_{n_1} - \omega_{n_2}, \omega_{n_2}) G_{\sigma}^{(2)}(\omega_{n'} + \omega_{n_1} - \omega_{n_2}) G_2^{(2)}(\omega_{n_2}).
 \end{aligned} \tag{6.34}$$

Substituting the above expression into Eq. (6.32), yields the U(1) Ward identity in terms of the four-point vertex

$$\begin{aligned}
 & \sum_{\sigma, n'} \left([G_0^{(2)}(\omega_{n'})]^{-1} - [G_0^{(2)}(\omega_{n'} + \omega_{n_1} - \omega_{n_2})]^{-1} \right) \left(G_{\sigma}^{(2)}(\omega_{n'}) G_1^{(2)}(\omega_{n_1}) \delta_{12} \delta_{n_1 n_2} \right. \\
 & \quad \left. - G_2^{(2)}(\omega_{n_2}) G_1^{(2)}(\omega_{n_1}) \delta_{1\sigma} \delta_{2\sigma} \delta_{n' n_2} \right. \\
 & \quad \left. + G_{\sigma}^{(2)}(\omega_{n'}) G_1^{(2)}(\omega_{n_1}) \Gamma_{\sigma 1; \sigma 2}(\omega_{n'}, \omega_{n_1}, \omega_{n'} + \omega_{n_1} - \omega_{n_2}, \omega_{n_2}) G_{\sigma}^{(2)}(\omega_{n'} + \omega_{n_1} - \omega_{n_2}) G_2^{(2)}(\omega_{n_2}) \right) \\
 &= G^{(2)}(\omega_{n_2}) \delta_{12} \delta_{n_2 n'} - G^{(2)}(\omega_{n_1}) \delta_{12} \delta_{n_1 n'}.
 \end{aligned} \tag{6.35}$$

Lastly, we would also like to include the self-energy in the Ward identity. Hence, expression Eq. (6.35) is multiplied by $[G^{(2)}(\omega_{n_1})]^{-1} [G^{(2)}(\omega_{n_2})]^{-1}$. The right-hand side of the equation then reads

$$[[G^{(2)}(\omega_{n_1})]^{-1} \delta_{12} - [G^{(2)}(\omega_{n_2})]^{-1} \delta_{12}]. \tag{6.36}$$

For the left-hand side of the expression, the multiplication results in

$$\begin{aligned}
 & \sum_{\sigma, n'} \left([G_0^{(2)}(\omega_{n'})]^{-1} - [G_0^{(2)}(\omega_{n'} + \omega_{n_1} - \omega_{n_2})]^{-1} \right) \left(G_\sigma^{(2)}(\omega_{n'}) \left(G_1^{(2)}(\omega_{n_2}) \right)^{-1} \delta_{12} \delta_{n_1 n_2} \right. \\
 & \quad \left. - G_2^{(2)}(\omega_{n'}) \left(G_1^{(2)}(\omega_{n_2}) \right)^{-1} \delta_{1\sigma} \delta_{2\sigma} \delta_{n' n_2} \delta_{n_1 n_2} \right) \\
 & \quad + G_\sigma^{(2)}(\omega_{n'}) \Gamma_{\sigma_1; \sigma_2}(\omega_{n'}, \omega_{n_1}, \omega_{n'} + \omega_{n_1} - \omega_{n_2}, \omega_{n_2}) G_\sigma^{(2)}(\omega_{n'} + \omega_{n_1} - \omega_{n_2}) \\
 & = 0 - \left([G_0^{(2)}(\omega_{n_2})]^{-1} - [G_0^{(2)}(\omega_{n_1})]^{-1} \right) + \sum_{\sigma, n'} \left([G_0^{(2)}(\omega_{n'})]^{-1} - [G_0^{(2)}(\omega_{n'} + \omega_{n_1} - \omega_{n_2})]^{-1} \right) \\
 & \quad \times G_\sigma^{(2)}(\omega_{n'}) \Gamma_{\sigma_1; \sigma_2}(\omega_{n'}, \omega_{n_1}, \omega_{n'} + \omega_{n_1} - \omega_{n_2}, \omega_{n_2}) G_\sigma^{(2)}(\omega_{n'} + \omega_{n_1} - \omega_{n_2}).
 \end{aligned} \tag{6.37}$$

Revisiting the definition of the self-energy from the two-point correlation function $\Sigma = [G_0^{(2)}]^{-1} - [G^{(2)}]^{-1}$, the whole equation is reformulated dependent on Σ as

$$\begin{aligned}
 & \sum_{\sigma, n'} \left([G_0^{(2)}(\omega_{n'})]^{-1} - [G_0^{(2)}(\omega_{n'} + \omega_{n_1} - \omega_{n_2})]^{-1} \right) \\
 & \quad \times G_\sigma^{(2)}(\omega_{n'}) \Gamma_{\sigma_1; \sigma_2}(\omega_{n'}, \omega_{n_1}, \omega_{n'} + \omega_{n_1} - \omega_{n_2}, \omega_{n_2}) G_\sigma^{(2)}(\omega_{n'} + \omega_{n_1} - \omega_{n_2}) \\
 & = \left([G^{(2)}(\omega_{n_1})]^{-1} - [G_0^{(2)}(\omega_{n_1})]^{-1} \right) + \left([G_0^{(2)}(\omega_{n_2})]^{-1} - [G^{(2)}(\omega_{n_2})]^{-1} \right)
 \end{aligned} \tag{6.38}$$

by adding the term $\left([G_0^{(2)}(\omega_{n_2})]^{-1} - [G_0^{(2)}(\omega_{n_1})]^{-1} \right)$. Finally, the U(1) Ward identity in Matsubara frequency space in terms of the four-point vertex and self-energy is

$$\begin{aligned}
 & \sum_{\sigma, n'} \left([G_0^{(2)}(\omega_{n'})]^{-1} - [G_0^{(2)}(\omega_{n'} + \omega_{n_1} - \omega_{n_2})]^{-1} \right) \\
 & \quad \times G_\sigma^{(2)}(\omega_{n'}) \Gamma_{\sigma_1; \sigma_2}(\omega_{n'}, \omega_{n_1}, \omega_{n'} + \omega_{n_1} - \omega_{n_2}, \omega_{n_2}) G_\sigma^{(2)}(\omega_{n'} + \omega_{n_1} - \omega_{n_2}) \\
 & = \Sigma_1(\omega_{n_2}) - \Sigma_1(\omega_{n_1}).
 \end{aligned} \tag{6.39}$$

Deriving the above equation concludes chapter 6. In the next section, we will insert the perturbation expansions derived in chapter 5 and compare this to the substitution of the exact expressions.

7 Verification of the U(1) Ward Identity for the Hubbard Atom

As Ward identities are exact relations, they are expected to hold for the exact solutions, as well as for each order in perturbation theory respectively. Therefore, the results from chapter 5 are used to check the Ward identity derived in 6.2. Furthermore, as mentioned in section 2.1, there exists an exact expression for the vertex and self-energy of the Hubbard atom, which will also be substituted into the U(1) Ward identity.

7.1 U(1) Ward Identity in Second-Order Perturbation Theory

In this section, first- and second-order of the self-energy and four-point vertex are inserted into Eq. (6.39). Whereas in the previous chapters the convention of double indices with a letter corresponding to the respective quantity and a number numbering the frequency arguments of these quantities was used, in this section we resort to just numbers as frequency indices, since we are not considering specific diagrams and thus do not need to distinguish between different vertices. Therefore, the change from double indices to single indices provides an ease of notation. This goes along with changing the notation of Kronecker-delta symbols from containing frequency indices to containing the frequencies themselves, such that it is still clear, if frequencies or numbers are the arguments of the respective Kronecker-deltas.

Expanding the Ward identity Eq. (6.39) in terms of orders of $\frac{U}{\beta}$, reads⁶

$$\begin{aligned} & (i\omega_2 - i\omega_1) \sum_{\sigma, \omega} [G_0(\omega) + G_{1|\sigma}(\omega) + G_{2|\sigma}(\omega)] [\Gamma_{1|\sigma_1; \sigma_2} + \Gamma_{2|\sigma_1; \sigma_2}(\omega, \omega_1, \omega + \omega_1 - \omega_2, \omega_2)] \\ & \quad \times [G_0(\omega + \omega_1 - \omega_2) + G_{1|\sigma}(\omega + \omega_1 - \omega_2) + G_{2|\sigma}(\omega + \omega_1 - \omega_2)] \\ & = [\Sigma_{1|1}(\omega_{n_2}) + \Sigma_{2|1}(\omega_{n_2})] - [\Sigma_{1|1}(\omega_1) + \Sigma_{2|1}(\omega_1)] + \mathcal{O}\left(\frac{U^3}{\beta^3}\right). \end{aligned} \quad (7.1)$$

Above, the first index of each quantity denotes its order in the interaction strength. For some orders, spin indices and frequency arguments were omitted, as the terms do not explicitly depend on them. Now, let us analyze each order separately, starting with zero-order in $\frac{U}{\beta}$. It is trivially fulfilled, as zero-order contributions do not exist for vertex and self-energy. Next, the first-order terms are investigated, which are given by

$$(i\omega_2 - i\omega_1) \sum_{\sigma, \omega} G_0(\omega) \Gamma_{1|\sigma_1; \sigma_2} G_0(\omega + \omega_1 - \omega_2) = \Sigma_{1|1}(\omega_{n_2}) - \Sigma_{1|1}(\omega_{n_1}). \quad (7.2)$$

Since for the Hubbard atom the first-order contribution to the self-energy is frequency-independent, the right-hand side of Eq. (7.2) yields

$$\Sigma_{1|1}(\omega_{n_2}) - \Sigma_{1|1}(\omega_{n_1}) = -\frac{Ue^{\beta\mu}}{(1 + e^{\beta\mu})} + \frac{Ue^{\beta\mu}}{(1 + e^{\beta\mu})} = 0. \quad (7.3)$$

Now, the left-hand side of the equation is considered. First, the spin sum over σ

$$\begin{aligned} & (i\omega_2 - i\omega_1) \sum_{\omega} [G_0(\omega) \Gamma_{1|\uparrow\downarrow; \uparrow\downarrow} G_0(\omega + \omega_1 - \omega_2) + G_0(\omega) \Gamma_{1|\downarrow\downarrow; \downarrow\downarrow} G_0(\omega + \omega_1 - \omega_2)] \\ & = (i\omega_2 - i\omega_1) \sum_{\omega} [G_0(\omega) \Gamma_{1|\uparrow\downarrow; \uparrow\downarrow} G_0(\omega + \omega_1 - \omega_2)] \end{aligned} \quad (7.4)$$

⁶Why an expansion in $\frac{U}{\beta}$ makes sense, even though it is not a dimensionless quantity, was covered in chapter 5.

is written out explicitly. Without loss of generality, spin index $1 = \downarrow$ and $2 = \downarrow$ is assumed. As we are not considering magnetic fields, $\Gamma_{|\downarrow\downarrow;\downarrow\downarrow}$ is equal to $\Gamma_{|\uparrow\uparrow;\uparrow\uparrow}$ and vanishes in first-order. In the next step, the perturbation theory results from chapter 4 are inserted and the Matsubara frequency sum over ω is computed as

$$\begin{aligned} & (i\omega_2 - i\omega_1) \sum_{\omega} \left[G_0(\omega) \Gamma_{|\uparrow\downarrow;\uparrow\downarrow} G_0(\omega + \omega_1 - \omega_2) \right] \\ &= (i\omega_2 - i\omega_1) \frac{U}{\beta} \sum_{\omega} \left[\frac{1}{i\omega + \mu} \frac{1}{i\omega + i\omega_1 - i\omega_2 + \mu} \right] = (i\omega_2 - i\omega_1) \frac{U}{\beta} \left[\frac{e^{\beta\mu}}{1 + e^{\beta\mu}} - \frac{e^{\beta\mu}}{1 + e^{\beta\mu}} \right] = 0 \end{aligned} \quad (7.5)$$

using the techniques described in appendix B. Upon summation, it was proven that the U(1)-Ward identity is fulfilled in first-order as well.

We proceed accordingly for the second-order perturbation theory results. The Ward identity in second-order in the interaction strength is given by

$$\begin{aligned} & (i\omega_2 - i\omega_1) \sum_{\sigma, \omega} G_0(\omega) \Gamma_{1|\sigma_1; \sigma_2} G_{1|\sigma}(\omega + \omega_1 - \omega_2) \\ &+ G_0(\omega) \Gamma_{2|\sigma_1; \sigma_2}(\omega, \omega_1, \omega + \omega_1 - \omega_2, \omega_2) G_0(\omega + \omega_1 - \omega_2) + G_{1|\sigma}(\omega) \Gamma_{1|\sigma_1; \sigma_2} G_0(\omega + \omega_1 - \omega_2) \\ &= \Sigma_{2|1}(\omega_2) - \Sigma_{2|1}(\omega_1). \end{aligned} \quad (7.6)$$

Again, each side of the equation is considered separately. At first, the self-energy terms on the right-hand side are subtracted as

$$\Sigma_{2|1}(\omega_2) - \Sigma_{2|1}(\omega_1) = \frac{U^2 e^{\beta\mu} (i\omega_1 - i\omega_2)}{(e^{\beta\mu} + 1)^2 (\mu + i\omega_1)(\mu + i\omega_2)}. \quad (7.7)$$

Next, let us focus on the left-hand side, which consists of three distinct types of summands. The first summand reads

$$\begin{aligned} & (i\omega_2 - i\omega_1) \sum_{\sigma, \omega} G_0(\omega) \Gamma_{1|\sigma_1; \sigma_2} G_{1|\sigma}(\omega + \omega_1 - \omega_2) \\ &= (i\omega_2 - i\omega_1) \sum_{\omega} G_0(\omega) \Gamma_{1|\uparrow\downarrow; \uparrow\downarrow} G_1(\omega + \omega_1 - \omega_2) \\ &= - \sum_{\omega} \frac{(i\omega_2 - i\omega_1) U^2 e^{\beta\mu}}{\beta (e^{\beta\mu} + 1) (\mu + i\omega) (\mu + (i\omega_1 - i\omega_2 + i\omega))^2} = \frac{\beta U^2 e^{2\beta\mu}}{(e^{\beta\mu} + 1)^3}. \end{aligned} \quad (7.8)$$

Again, we assumed spin indices $1 = \downarrow$ and $2 = \downarrow$. Similarly, we evaluate the third summand of Eq. (7.6), which equates to Eq. (7.8) with shifted frequency arguments

$$\begin{aligned} & (i\omega_2 - i\omega_1) \sum_{\sigma, \omega} G_{1|\sigma}(\omega) \Gamma_{1|\sigma_1; \sigma_2} G_0(\omega + \omega_1 - \omega_2) \\ &= (i\omega_2 - i\omega_1) \sum_{\omega} G_1(\omega) \Gamma_{1|\uparrow\downarrow; \uparrow\downarrow} G_0(\omega + \omega_1 - \omega_2) \\ &= - \sum_{\omega} \frac{(i\omega_2 - i\omega_1) U^2 e^{\beta\mu}}{\beta (e^{\beta\mu} + 1) (\mu + i\omega)^2 (\mu + i(\omega_1 - \omega_2 + \omega))} = - \frac{\beta U^2 e^{2\beta\mu}}{(e^{\beta\mu} + 1)^3}. \end{aligned} \quad (7.9)$$

It is apparent that the terms Eq. (7.8) and Eq. (7.9) cancel each other. What remains to be done,

is calculating the second summand from Eq. (7.6)

$$\begin{aligned}
 & (i\omega_2 - i\omega_1) \sum_{\sigma, \omega} G_0(\omega) \Gamma_{2|\sigma_1; \sigma_2}(\omega, \omega_1, \omega + \omega_1 - \omega_2, \omega_2) G_{0|\sigma}(\omega + \omega_1 - \omega_2) \\
 &= (i\omega_2 - i\omega_1) \sum_{\omega} G_0(\omega) \Gamma_{2|\downarrow\downarrow; \downarrow\downarrow}(\omega, \omega_1, \omega + \omega_1 - \omega_2, \omega_2) G_{0|\sigma}(\omega + \omega_1 - \omega_2) \\
 &+ (i\omega_2 - i\omega_1) \sum_{\omega} G_0(\omega) \Gamma_{2|\uparrow\uparrow; \uparrow\uparrow}(\omega, \omega_1, \omega + \omega_1 - \omega_2, \omega_2) G_0(\omega + \omega_1 - \omega_2),
 \end{aligned} \tag{7.10}$$

which should then be equal to the difference between self-energies Eq. (7.7). As the Hubbard atom Hamiltonian is SU(2) symmetric, $\Gamma_{2|\downarrow\downarrow; \downarrow\downarrow}$ is mathematically equivalent to $\Gamma_{2|\uparrow\uparrow; \uparrow\uparrow}$. Inserting the result for the vertex contribution with all spins equal reads

$$\begin{aligned}
 & \sum_{\omega} \frac{(i\omega_2 - i\omega_1) U^2 e^{\beta\mu} (\delta_{\omega_1 - \omega_2} - \delta_{\omega_2 - \omega})}{(e^{\beta\mu} + 1)^2 (\mu + i\omega)(\mu + i(\omega_1 - \omega_2 + \omega))} \\
 &= \frac{U^2 e^{\beta\mu} (\omega_1 - \omega_2)}{(e^{\beta\mu} + 1)^2 (\omega_1 - i\mu)(\mu + i\omega_2)}.
 \end{aligned} \tag{7.11}$$

Finally, the term from Eq. (7.10) containing the vertex $\Gamma_{2|\uparrow\downarrow; \uparrow\downarrow}$ is evaluated as

$$\sum_{\omega} \frac{U^2 (\omega_1 - \omega_2) (-1 + e^{2\beta\mu} - e^{\beta\mu} \beta \delta_{\omega - \omega_2} (2\mu + i(\omega + \omega_1)))}{\beta (e^{\beta\mu} + 1)^2 (\mu + i\omega)(2\mu + i(\omega + \omega_1))(i\mu - \omega - \omega_1 + \omega_2)} = 0. \tag{7.12}$$

Note, that the left-hand side of the Ward identity only depends on vertex components with all spin arguments equal. In fact, this is not only the case for the second-order but for all orders in the interaction strength and the exact quantities. The reason for this is the SU(2) symmetry of the Hubbard atom 2.1, as this leads to another Ward identity with which the above statement can be proven. However, this lies beyond the scope of this thesis. This statement can for example be inferred from the form of the SU(2) Ward identity for the Anderson impurity model, which is described by the Hubbard model Hamiltonian with an additional term representing a bath, derived in [11].

Adding all non-zero terms from the left-hand side of the U(1) Ward identity Eq. (7.6), we obtain

$$\begin{aligned}
 & (i\omega_2 - i\omega_1) \sum_{\sigma, \omega} G_0 \Gamma_{1|\sigma_1; \sigma_2} G_{1|\sigma} + G_0 \Gamma_{2|\sigma_1; \sigma_2} G_{0|\sigma} + G_{1|\sigma} \Gamma_{1|\sigma_1; \sigma_2} G_0 \\
 &= \frac{U^2 e^{\beta\mu} (\omega_1 - \omega_2)}{(e^{\beta\mu} + 1)^2 (\omega_1 - i\mu)(\mu + i\omega_2)},
 \end{aligned} \tag{7.13}$$

which is indeed equal to the right-hand side of the identity Eq. (7.7). Therefore, it was proven that, as expected, the Ward identity holds in second-order perturbation theory.

7.2 U(1) Ward Identity for Exact Vertex and Self-energy

If the U(1) Ward identity for the Hubbard atom has been derived correctly, it should be fulfilled for the exact solutions to vertex and self-energy. The exact quantities used in the text are derived in [12]. As the expressions for the exact vertex and self-energy are rather complex for general chemical potential, only the case of $\mu = -\frac{U}{2}$ at half-filling is considered. Under this assumption, the exact single-particle Green's function and self-energy are given by [12]:

$$G^{(2)}(\omega) = -\frac{4i\omega}{U^2 + 4\omega^2} \tag{7.14}$$

$$\Sigma(\omega) = -\frac{iU(U - 2i\omega)}{4\omega} \tag{7.15}$$

Above, spin indices were omitted, as for the Hubbard atom without magnetic fields the single-particle Green's function and the self-energy don't depend on the spin components. Next, the expressions for the exact vertex components of the Hubbard atom will be stated. Even for the half-filled system, the exact vertex component with distinct spin components [12]

$$\begin{aligned} \Gamma_{\uparrow\downarrow;\uparrow\downarrow}(\omega_1, \omega_2, \omega_3, \omega_1 + \omega_2 - \omega_3) &= -\frac{U^2 (U^2 + 4\omega_1^2) (U^2 + 4\omega_2^2) \delta_{\omega_2 - \omega_3}}{32\omega_1^2 \omega_2^2 (e^{\frac{\beta U}{2}} + 1)} \\ &+ \frac{U^2 (U^2 + 4\omega_1^2) (U^2 + 4\omega_2^2) \delta_{\omega_1 - \omega_3} \tanh\left(\frac{\beta U}{4}\right)}{64\omega_1^2 \omega_2^2} + \frac{U^2 e^{\frac{\beta U}{2}} (U^2 + 4\omega_1^2) (U^2 + 4\omega_3^2) \delta_{\omega_1 + \omega_2}}{32\omega_1^2 \omega_3^2 (e^{\frac{\beta U}{2}} + 1)} \quad (7.16) \\ &+ \frac{-3U^5 - 4U^3 (\omega_1^2 - \omega_3 (\omega_1 + \omega_2) + \omega_1 \omega_2 + \omega_2^2 + \omega_3^2) + 16U \omega_1 \omega_2 \omega_3 (\omega_1 + \omega_2 - \omega_3)}{16\beta \omega_1 \omega_2 \omega_3 (\omega_1 + \omega_2 - \omega_3)} \end{aligned}$$

is a rather lengthy expression. The last exact quantity required for verifying the Ward identity at half-filling is the vertex contribution with all spin components equal [12]

$$\Gamma_{\uparrow\uparrow;\uparrow\uparrow}(\omega_1, \omega_2, \omega_3, \omega_1 + \omega_2 - \omega_3) = \frac{U^2 (U^2 + 4\omega_1^2) (U^2 + 4\omega_2^2) (\delta_{\omega_1 - \omega_3} - \delta_{\omega_2 - \omega_3})}{64\omega_1^2 \omega_2^2}. \quad (7.17)$$

Due to frequency conservation at each vertex, the vertex components only depend on three Matsubara frequency arguments. As indicated above, these exact quantities are substituted into the U(1) Ward identity Eq. (6.39). Similar to before, both sides of the equation are treated separately. First, the difference between self-energy terms on the right hand-side of the equation is calculated as

$$\Sigma(\omega_2) - \Sigma(\omega_1) = -\frac{U^2 (i\omega_1 - i\omega_2)}{4\omega_1 \omega_2}. \quad (7.18)$$

Again, evaluating the left-hand side of the expression is more complex. We start with the summand containing the vertex contribution with equal spins

$$\begin{aligned} &(i\omega_2 - i\omega_1) \sum_{\omega} G(\omega) \Gamma_{\uparrow\uparrow;\uparrow\uparrow}(\omega, \omega_1, \omega + \omega_1 - \omega_2, \omega_2) G(\omega + \omega_1 - \omega_2) \\ &= \frac{U^2 (U^2 + 4\omega_1^2) (\omega + \omega_1 - \omega_2) (\delta_{\omega - \omega_2} - \delta_{\omega_1 - \omega_2})}{4\omega \omega_1^2 (U^2 + 4(\omega + \omega_1 - \omega_2)^2)} \quad (7.19) \\ &= -\frac{U^2 (i\omega_1 - i\omega_2)}{4\omega_1 \omega_2}. \end{aligned}$$

As the vertex with all spins equal is proportional to a sum of Kronecker-deltas, there is no need to compute the frequency sum. Besides, the summand proportional to $\delta_{\omega_1 - \omega_2}$ equals zero due to the prefactor $(i\omega_2 - i\omega_1)$. The result from Eq. (7.19) is equal to the left-hand side of the Ward identity Eq. (7.18). Under these conditions, the summand of the vertex component for spins $\uparrow\downarrow\uparrow\downarrow$ must vanish, if the Ward identity is fulfilled for the half-filled system. Indeed, this is the case, as we will calculate in the following. To start, the contribution

$$\begin{aligned} &\sum_{\omega} G(\omega) \Gamma_{\uparrow\uparrow;\uparrow\uparrow}(\omega, \omega_1, \omega + \omega_1 - \omega_2, \omega_2) G(\omega + \omega_1 - \omega_2) \\ &= \frac{4\omega (3U^5 + 4U^3 (\omega^2 + \omega(\omega_1 - \omega_2) + \omega_1^2 - \omega_1 \omega_2 + \omega_2^2) - 16U \omega \omega_1 \omega_2 (\omega + \omega_1 - \omega_2))}{\beta \omega_1 \omega_2 (4\omega (U^2 + 4\omega^2) (U^2 + 4(\omega + \omega_1 - \omega_2)^2))} \\ &- \frac{\beta U^2 e^{\frac{\beta U}{2}} \delta_{\omega + \omega_1}}{2\omega (e^{\frac{\beta U}{2}} + 1) (\omega + \omega_1 - \omega_2)} + \frac{\beta U^2 (U^2 + 4\omega_1^2) \delta_{\omega - \omega_2} (\omega + \omega_1 - \omega_2)}{2\omega \omega_1^2 (e^{\frac{\beta U}{2}} + 1) (U^2 + 4(\omega + \omega_1 - \omega_2)^2)} \quad (7.20) \\ &- \frac{\beta U^2 (U^2 + 4\omega_1^2) \delta_{\omega_1 - \omega_2} \tanh\left(\frac{\beta U}{4}\right) (\omega + \omega_1 - \omega_2)}{4\omega \omega_1^2 (U^2 + 4(\omega + \omega_1 - \omega_2)^2)} \end{aligned}$$

is explicitly written out in terms of the frequency arguments. Evaluated, the expression Eq. (7.20) reads

$$-\frac{\beta U^2 e^{\frac{\beta U}{2}}}{2\omega_1 \omega_2 (e^{\frac{\beta U}{2}} + 1)} + \frac{\beta U^2}{2\omega_1 \omega_2 (e^{\frac{\beta U}{2}} + 1)} + \frac{\beta U^2 (e^{\frac{\beta U}{2}} - 1)}{2\omega_1 \omega_2 (e^{\frac{\beta U}{2}} + 1)} = 0. \quad (7.21)$$

Hence, the U(1) Ward identity is fulfilled for the exact vertex and self-energy, which was to be expected. Moreover, it can be used to gauge the quality of approximations as proposed at the beginning of chapter 6. Specifically, the text will examine approximations for the vertex and self-energy motivated by the Parquet formalism, which is the topic of the next section.

8 Derivation of Self-Energy and Vertex from the Parquet Equations

In the last chapter, it was proven that, besides the exact solutions for the vertex and self-energy, the quantities from second-order perturbation theory fulfill the U(1) Ward identity. Let us now address other approximation methods for the four-point vertex and self-energy and examine the fulfillment of the U(1) Ward identity. Given that the U(1) Ward identity represents particle conservation, it can be used to gauge the accuracy of approximation methods. In the following, we will analyze approximations obtained from the Parquet formalism, which is introduced in the next subsection.

8.1 Basics on Parquet Formalism

Regarding the calculations in chapter 5, with increasing order in the interaction strength the complexity of perturbation theory increases as well. This is a general principle in many-body physics, so it is not feasible to calculate diagrams up to arbitrary order to characterize the properties of a system. The Parquet formalism provides the opportunity to only consider subsets of diagrams and one is able to generate higher-order terms to physical quantities much more efficiently. As the Parquet formalism plays a fundamental role throughout the rest of this thesis, elementary knowledge on the Parquet formalism is covered in the following. This introductory section is mostly a short summary of chapter 2.3 from [7] but without derivations of the respective equations.

In chapter 4, reducibility was presented as a way of classifying diagrams. Furthermore, the self-energy was defined as the sum of one-particle irreducible diagrams. In the Parquet formalism, diagrams are categorized by their two-particle reducibility. There are three distinct ways to separate two-particle reducible diagrams by cutting two propagator lines, which correspond to three different channels, namely the antiparallel a, the parallel p and the transverse-antiparallel t channel. How to divide diagrams into these three groups, can be best understood graphically. Therefore, exemplary diagrams from the four-point vertex of the Hubbard atom in second-order and the respective classification into one of the three channels are shown in Fig. 8.1. Of course, there are also diagrams which cannot be separated into subdiagrams by cutting two propagators that together form the fully irreducible part R .

To connect the self-energy, a one-particle irreducible quantity, and the four-point vertex, a two-particle reducible quantity, one needs exact relations for both. The vertex can be obtained from the Bethe-Salpeter equations in each channel [7]:

$$\gamma_{a|12;34} = I_{a|15;64} G_{67} G_{85} \Gamma_{72;38} \quad (8.1)$$

$$\gamma_{p|12;34} = \frac{1}{2} I_{p|12;68} G_{65} G_{87} \Gamma_{57;34} \quad (8.2)$$

$$\gamma_{t|12;34} = -I_{t|52;64} G_{67} G_{85} \Gamma_{17;38} \quad (8.3)$$

Here, all indices are multi-indices and include spin as well as frequency. Moreover, Einstein sum convention is used and thus summation over repeating indices is implicit. Above, γ_r , $r \in \{a, p, t\}$ represent the two-particle reducible vertices in each channel and the irreducible parts I_r are calculated as $I_r = R + \sum_{r' \neq r} \gamma_{r'}$. Neither the Bethe-Salpeter equation nor any of the following relations are derived in this thesis. For a more detailed discussion, one should refer to [7]. As any diagram is either two-particle reducible in only one channel or totally two-particle irreducible, the

four-point vertex can be written as [7]

$$\Gamma = R + \sum_{r \in \{a,p,t\}} \gamma_r. \quad (8.4)$$

This is also called the Parquet decomposition of the vertex. Regarding the one-particle reducible self-energy, the Schwinger-Dyson equation [7]

$$\Sigma_{13} = -\Gamma_{0|12;34} G_{24} - \frac{1}{2} \Gamma_{0|12;68} G_{42} G_{87} G_{65} \Gamma_{57;34} \quad (8.5)$$

is considered. Note that both the Bethe-Salpeter equations and the Schwinger-Dyson equation depend on the four-point vertex, one-particle Green's function and therefore implicitly on the self-energy, see Eq. (4.28). In the Parquet formalism, one chooses initial values for the self-energy, the two-particle reducible vertices and the two-particle irreducible vertex R . These initial values are inserted into the Bethe-Salpeter equation to obtain an expression for the full four-point vertex. Next, the vertex from the Bethe-Salpeter equation is substituted into the Schwinger-Dyson equation for an expression of the self-energy. The new vertex and self-energy are in the next iteration again inserted into the Bethe-Salpeter and Schwinger-Dyson equation. With each iteration of this cycle, the approximations for the four-point vertex and the self-energy improve. Normally, the process described above is done numerically.

One finds that the results can depend strongly on the choice of the approximation for the two-particle irreducible contribution to the four-point vertex R . Most commonly, the Parquet approximation $R = \frac{U}{\beta} \equiv \Gamma_0$ is chosen. While the Parquet approximation only takes the first-order two-particle irreducible diagram into consideration, the next actual contribution arises in fourth-order in the interaction strength. As a matter of fact, the Parquet approximation possesses a lot of useful properties such as fulfilling crossing symmetry. Therefore, it is in some practical applications reasonable to neglect higher-order diagrams.

Nevertheless, self-energy and four-point vertex from the Parquet iteration with the Parquet approximation as irreducible vertex contribution do not automatically fulfill Ward identities. This originates from the fact that Parquet mixes different-order diagrams and therefore exact relations, which are fulfilled for each order respectively, do not hold anymore. As Ward identities directly correspond to conservation laws, in order to have a physically realistic approximation they should hold for the approximated quantities. In this thesis, we search for an alternative to the Parquet approximation, which ensures that vertex and self-energy of the Hubbard atom fulfill the U(1) Ward identity and therefore the particle conservation law. Our approach is to perform one Parquet iteration analytically starting from the second-order perturbation theory results for the Hubbard atom. By inserting the approximated quantities from this iteration into the U(1) Ward identity, the deviation is computed. This deviation is then used to improve on the two-particle irreducible vertex R . The rest of this chapter is dedicated to obtaining approximations for the self-energy and the four-point vertex from the Bethe-Salpeter and Schwinger-Dyson equations.

8.2 Four-Point Vertex from the Bethe-Salpeter Equations

At first, second-order self-energy and four-point vertex are substituted into the Bethe-Salpeter equations. However, to obtain a valid four-point vertex for the Hubbard atom in the absence of magnetic fields specific symmetry requirements need to be fulfilled. When performing multiple numerical Parquet iterations, the Bethe-Salpeter equations preserve these symmetries. However, when inserting second-order perturbation theory, the result depends on the order of contraction of

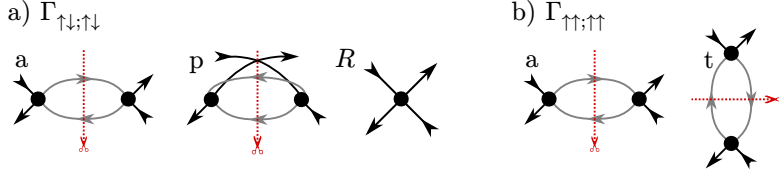


Figure 8.1: (a) Two-particle reducible diagrams in the antiparallel channel a, parallel channel p and two-particle irreducible Parquet approximation R for $\Gamma_{\uparrow\downarrow;\uparrow\downarrow}$ in second-order. For this vertex contribution, there is no t-channel diagram in second-order (b) Two-particle reducible diagrams in the antiparallel channel a and transverse-antiparallel channel t for $\Gamma_{\uparrow\uparrow;\uparrow\uparrow}$ in second-order. For this vertex contribution there is no p-channel diagram in second-order.

the irreducible vertex in each channel with the full vertex resulting in the symmetry properties of the four-point vertex not being fulfilled anymore. The reason for this is that some diagrams that would be needed to preserve the symmetries are only generated one iteration later. To begin with, the vertex is computed from the usual version of the Bethe-Salpeter equations as defined in [7]. Only afterwards, we will consider the necessary symmetrization.

Let us specify the inputs to the Bethe-Salpeter equations. In this chapter, particle-hole symmetric expressions are used, for which the chemical potential μ is set to $-\frac{U}{2}$:

$$G_0(\omega) = \frac{1}{-\frac{U}{2} + i\omega} \quad (8.6) \quad \Sigma(\omega) = -\frac{U}{2} - \frac{iU^2}{4\omega} \quad (8.7)$$

$$\Gamma_{\uparrow\downarrow;\uparrow\downarrow}(\omega_1, \omega_2, \omega_3) = \frac{U}{\beta} + \frac{1}{4}U^2(\delta_{\omega_1+\omega_2} - \delta_{\omega_2-\omega_3}) \quad (8.8)$$

$$\Gamma_{\uparrow\uparrow;\uparrow\uparrow}(\omega_1, \omega_2, \omega_3) = \frac{1}{4}U^2(\delta_{\omega_1-\omega_3} - \delta_{\omega_2-\omega_3}) \quad (8.9)$$

As with frequency conservation the fourth frequency argument of the vertex is automatically determined from the other three, it suffices to only specify the first three arguments. The single-particle Green's function in second-order is calculated from the self-energy according to Eq. (4.28). Starting with the antiparallel channel, Eq. (8.1) is rewritten for the Hubbard atom as

$$\gamma_{a|12;34} = I_{a|15;74} G_7 G_5 \Gamma_{72;35} \delta_{67} \delta_{85}. \quad (8.10)$$

We split the above equation into two parts considering the vertices $\gamma_{a|\uparrow\downarrow;\uparrow\downarrow}$ and $\gamma_{a|\uparrow\uparrow;\uparrow\uparrow}$ separately. Writing out the spin sum and applying frequency conservation, $\gamma_{a|\uparrow\downarrow;\uparrow\downarrow}$ becomes

$$\gamma_{a|\uparrow\downarrow;\uparrow\downarrow}(\omega_1, \omega_2, \omega_3) = \sum_{\omega_5} I_{a|\uparrow\downarrow;\uparrow\downarrow}(\omega_1, \omega_5, \omega_5 + \omega_3 - \omega_2) G(\omega_5 + \omega_3 - \omega_2) G(\omega_5) \Gamma_{\uparrow\downarrow;\uparrow\downarrow}(\omega_5 + \omega_3 - \omega_2, \omega_2, \omega_3). \quad (8.11)$$

An overview of all diagrams necessary to build the irreducible part of Eq. (8.11) and the following calculations is given in Fig. 8.1.

Inserting the irreducible vertex in the antiparallel channel, the vertex and Green's function, the

two-particle reducible vertex in the antiparallel channel is computed as

$$\begin{aligned}
 \gamma_{\text{a}|\uparrow\downarrow;\uparrow\downarrow}(\omega_1, \omega_2, \omega_3) &= \delta_{\omega_2 - \omega_3} \left(\frac{U^2 (\beta U e^{\frac{\beta U}{2}} + e^{\beta U} - 1)}{8 (e^{\frac{\beta U}{2}} + 1)^2} + \frac{U^4 \omega_1^2}{(U^2 + 4\omega_1^2)^2} - \frac{U (\beta U e^{\frac{\beta U}{2}} + e^{\beta U} - 1)}{2\beta (e^{\frac{\beta U}{2}} + 1)^2} \right) \\
 &+ \frac{U^3 \omega_1 \left(-\frac{U \omega_2 \delta_{\omega_1 - \omega_3}}{U^2 + 4\omega_2^2} - \frac{4(\omega_1 + \omega_2 - \omega_3)}{\beta(U^2 + 4(\omega_1 + \omega_2 - \omega_3)^2)} \right)}{U^2 + 4\omega_1^2} - \frac{4U^3 \omega_2 \omega_3}{\beta(U^2 + 4\omega_2^2)(U^2 + 4\omega_3^2)} \\
 &- \frac{U^3 (e^{\frac{\beta U}{2}} - 1)}{2\beta (e^{\frac{\beta U}{2}} + 1) (U^2 + (\omega_2 - \omega_3)^2)}.
 \end{aligned} \tag{8.12}$$

As in this chapter the calculations and especially sums over Matsubara frequencies are rather complex, *Wolfram Mathematica* [13] was used for lengthy computations. The notebooks containing the calculations regarding the Bethe-Salpeter and Schwinger-Dyson equation are linked in the bibliography [14]. Therefore, in this thesis only ansatz, input values and results to the two-particle irreducible vertices are written out explicitly. For more information, one should refer to the mentioned *Wolfram Mathematica* notebooks. Next, the vertex in the antiparallel channel for all spin arguments equal

$$\begin{aligned}
 \gamma_{\text{a}|\uparrow\uparrow;\uparrow\uparrow}(\omega_1, \omega_2, \omega_3) &= I_{\text{a}|\uparrow\uparrow;\uparrow\uparrow}(\omega_1, \omega_5, \omega_5 + \omega_3 - \omega_2) G(\omega_5 + \omega_3 - \omega_2) G(\omega_5) \Gamma_{\uparrow\uparrow;\uparrow\uparrow}(\omega_5 + \omega_3 - \omega_2, \omega_2, \omega_3) \\
 &+ I_{\text{a}|\uparrow\downarrow;\uparrow\downarrow}(\omega_1, \omega_5, \omega_5 + \omega_3 - \omega_2) G(\omega_5 + \omega_3 - \omega_2) G(\omega_5) \Gamma_{\downarrow\uparrow;\uparrow\downarrow}(\omega_5 + \omega_3 - \omega_2, \omega_2, \omega_3)
 \end{aligned} \tag{8.13}$$

is computed. Considering the second summand of Eq. (8.13), we have not calculated an expression for $\Gamma_{\downarrow\uparrow;\uparrow\downarrow}$ in chapter 5. Fortunately, the Hubbard atom is crossing-symmetric and therefore there is a relation between $\Gamma_{\downarrow\uparrow;\uparrow\downarrow}$ and $\Gamma_{\uparrow\downarrow;\uparrow\downarrow}$:

$$\Gamma_{\downarrow\uparrow;\uparrow\downarrow}(\omega_1, \omega_2, \omega_3) = -\Gamma_{\uparrow\downarrow;\uparrow\downarrow}(\omega_1, \omega_2, \omega_1 + \omega_2 - \omega_3) \tag{8.14}$$

However, concerning the two-particle reducible channels one needs to be careful. For them, the relations

$$\gamma_{\text{a}|\uparrow\downarrow;\uparrow\downarrow}(\omega_1, \omega_2, \omega_3) = -\gamma_{\text{t}|\uparrow\downarrow;\uparrow\downarrow}(\omega_1, \omega_2, \omega_1 + \omega_2 - \omega_3) \tag{8.15}$$

$$\gamma_{\text{p}|\uparrow\downarrow;\uparrow\downarrow}(\omega_1, \omega_2, \omega_3) = -\gamma_{\text{p}|\uparrow\downarrow;\uparrow\downarrow}(\omega_1, \omega_2, \omega_1 + \omega_2 - \omega_3) \tag{8.16}$$

hold. With this, the second summand from Eq. (8.13) is formulated as

$$\begin{aligned}
 &I_{\text{a}|\uparrow\downarrow;\uparrow\downarrow}(\omega_1, \omega_5, \omega_5 + \omega_3 - \omega_2) G(\omega_5 + \omega_3 - \omega_2) G(\omega_5) \Gamma_{\downarrow\uparrow;\uparrow\downarrow}(\omega_5 + \omega_3 - \omega_2, \omega_2, \omega_3) \\
 &= -I_{\text{a}|\uparrow\downarrow;\uparrow\downarrow}(\omega_1, \omega_5, \omega_1 + \omega_2 - \omega_3) G(\omega_5 + \omega_3 - \omega_2) G(\omega_5) \Gamma_{\uparrow\downarrow;\uparrow\downarrow}(\omega_5 + \omega_3 - \omega_2, \omega_2, \omega_5).
 \end{aligned} \tag{8.17}$$

Inserting the quantities Eq. (8.6), Eq. (8.7), Eq. (8.8) and Eq. (8.9), the two-particle reducible

vertex in the antiparallel channel for all spin arguments equal $\gamma_{a|\uparrow\uparrow;\uparrow\uparrow}$ is expressed as

$$\begin{aligned}
 \gamma_{a|\uparrow\uparrow;\uparrow\uparrow}(\omega_1, \omega_2, \omega_3) &= -\frac{U^3 (e^{\frac{\beta U}{2}} - 1)}{2\beta (e^{\frac{\beta U}{2}} + 1) (U^2 + (\omega_2 - \omega_3)^2)} \\
 &+ U^4 \delta_{\omega_1 + \omega_2} \left(\frac{\omega_1 (\omega_1 + \omega_2 - \omega_3)}{(U^2 + 4\omega_1^2) (U^2 + 4(\omega_1 + \omega_2 - \omega_3)^2)} + \frac{\omega_2 \omega_3}{(U^2 + 4\omega_2^2) (U^2 + 4\omega_3^2)} \right) \\
 &- U^4 \delta_{\omega_1 - \omega_3} \left(\frac{2\omega_1 (\omega_1 + \omega_2 - \omega_3)}{(U^2 + 4\omega_1^2) (U^2 + 4(\omega_1 + \omega_2 - \omega_3)^2)} + \frac{\omega_2 \omega_3}{(U^2 + 4\omega_2^2) (U^2 + 4\omega_3^2)} \right) \\
 &+ \delta_{\omega_2 - \omega_3} \left(\frac{U^4 \omega_1 (\omega_1 + \omega_2 - \omega_3)}{(U^2 + 4\omega_1^2) (U^2 + 4(\omega_1 + \omega_2 - \omega_3)^2)} + \frac{U^3 (e^{\frac{\beta U}{2}} - 1)}{2\beta (e^{\frac{\beta U}{2}} + 1) (U^2 + (\omega_2 - \omega_3)^2)} \right. \\
 &\left. - \frac{U (\beta U e^{\frac{\beta U}{2}} + e^{\beta U} - 1)}{2\beta (e^{\frac{\beta U}{2}} + 1)^2} \right). \tag{8.18}
 \end{aligned}$$

Next, the two-particle reducible vertex in the parallel channel according to Eq. (8.2) is calculated for the Hubbard atom as

$$\gamma_{p|12;34} = \frac{1}{2} I_{p|12;68} G_{65} G_{87} \Gamma_{57;34}. \tag{8.19}$$

The Bethe-Salpeter equation for spin arguments $\uparrow\downarrow\uparrow\downarrow$ reads

$$\begin{aligned}
 \gamma_{p|\uparrow\downarrow;\uparrow\downarrow}(\omega_1, \omega_2, \omega_3) &= \frac{1}{2} I_{p|\uparrow\downarrow;\uparrow\downarrow}(\omega_1, \omega_2, \omega_5) G(\omega_5) G(\omega_1 + \omega_2 - \omega_5) \Gamma_{\uparrow\downarrow;\uparrow\downarrow}(\omega_5, \omega_2 + \omega_1 - \omega_5, \omega_3) \\
 &+ \frac{1}{2} I_{p|\uparrow\downarrow;\uparrow\downarrow}(\omega_1, \omega_2, \omega_5) G(\omega_5) G(\omega_1 + \omega_2 - \omega_5) \Gamma_{\downarrow\uparrow;\downarrow\uparrow}(\omega_5, \omega_2 + \omega_1 - \omega_5, \omega_3). \tag{8.20}
 \end{aligned}$$

For the second summand of Eq. (8.20), the relations due to crossing symmetry Eq. (8.15) and Eq. (8.16) are again applied. With this, the summand is expressed in terms of diagrams from chapter 5 as

$$\begin{aligned}
 &\frac{1}{2} I_{p|\uparrow\downarrow;\uparrow\downarrow}(\omega_1, \omega_2, \omega_5) G(\omega_5) G(\omega_1 + \omega_2 - \omega_5) \Gamma_{\downarrow\uparrow;\downarrow\uparrow}(\omega_5, \omega_2 + \omega_1 - \omega_5, \omega_3) \\
 &= \frac{1}{2} I_{p|\uparrow\downarrow;\uparrow\downarrow}(\omega_1, \omega_2, \omega_1 + \omega_2 - \omega_5) G(\omega_5) G(\omega_1 + \omega_2 - \omega_5) \Gamma_{\uparrow\downarrow;\uparrow\downarrow}(\omega_5, \omega_2 + \omega_1 - \omega_5, \omega_1 + \omega_2 - \omega_3). \tag{8.21}
 \end{aligned}$$

Determining the irreducible parts in the parallel channel I_p as shown in Fig. 8.1, we evaluate the frequency sum over ω_5 and obtain the expression

$$\begin{aligned}
 \gamma_{p|\uparrow\downarrow;\uparrow\downarrow}(\omega_1, \omega_2, \omega_3) &= \frac{1}{2} \left(\frac{8U^3 \omega_1 \omega_2}{\beta (U^2 + 4\omega_1^2) (U^2 + 4\omega_2^2)} + \frac{U^3 (e^{\beta U} - 1)}{\beta (e^{\frac{\beta U}{2}} + 1)^2 (U^2 + (\omega_1 + \omega_2)^2)} \right. \\
 &+ \frac{8U^3 \omega_3 (\omega_1 + \omega_2 - \omega_3)}{\beta (U^2 + 4\omega_3^2) (U^2 + 4(\omega_1 + \omega_2 - \omega_3)^2)} + \left(\frac{U^2 (\beta U e^{\frac{\beta U}{2}} + e^{\beta U} - 1)}{4 (e^{\frac{\beta U}{2}} + 1)^2} - \frac{2U^4 \omega_1^2}{(U^2 + 4\omega_1^2)^2} \right. \\
 &+ \left. \left. \frac{U (\beta U e^{\frac{\beta U}{2}} (U^2 + (\omega_1 + \omega_2)^2) + e^{\beta U} (\omega_1 + \omega_2)^2 - (\omega_1 + \omega_2)^2)}{\beta (e^{\frac{\beta U}{2}} + 1)^2 (U^2 + (\omega_1 + \omega_2)^2)} \right) \delta_{\omega_1 + \omega_2} \right. \\
 &\left. - \frac{2U^4 \omega_1 \omega_2 \delta_{\omega_1 - \omega_3}}{(U^2 + 4\omega_1^2) (U^2 + 4\omega_2^2)} \right). \tag{8.22}
 \end{aligned}$$

In the parallel channel, $\gamma_{p|\uparrow\uparrow\uparrow\uparrow}$ only consists of one component, with an irreducible part in the parallel channel depicted in Fig. 8.1. The corresponding mathematical term is evaluated easily, as

the whole term is proportional to Kronecker-deltas, which can be seen from [14]:

$$\begin{aligned}\gamma_{\text{p}\uparrow\uparrow;\uparrow}(\omega_1, \omega_2, \omega_3) &= \frac{1}{2} I_{\text{p}\uparrow\downarrow;\uparrow}(\omega_1, \omega_2, \omega_5) G(\omega_5) G(\omega_1 + \omega_2 - \omega_5) \Gamma_{\downarrow\uparrow;\uparrow}(\omega_5, \omega_2 + \omega_1 - \omega_5, \omega_3) \\ &= \frac{2U^4 \omega_1 \omega_2 (\delta_{\omega_2 - \omega_3} - \delta_{\omega_1 - \omega_3})}{(U^2 + 4\omega_1^2)(U^2 + 4\omega_2^2)}\end{aligned}\quad (8.23)$$

According to Eq. (8.2), the transverse-antiparallel vertex for the Hubbard atom is calculated as

$$\gamma_{\text{t}|12;34} = -I_{\text{t}|52;64} G_7 G_5 \Gamma_{17;38} \delta_{67} \delta_{85}.\quad (8.24)$$

Evaluating the spin summations, $\gamma_{\text{t}|\uparrow\downarrow;\uparrow\downarrow}$ is given by

$$\begin{aligned}\gamma_{\text{t}|\uparrow\downarrow;\uparrow\downarrow}(\omega_1, \omega_2, \omega_3) &= -I_{\text{t}|\uparrow\downarrow;\uparrow\downarrow}(\omega_5, \omega_2, \omega_3 + \omega_5 - \omega_1) G(\omega_3 + \omega_5 - \omega_1) G(\omega_5) \Gamma_{\uparrow\uparrow;\uparrow}(\omega_1, \omega_3 + \omega_5 - \omega_1, \omega_3) \\ &\quad - I_{\text{t}|\downarrow\downarrow;\downarrow\downarrow}(\omega_5, \omega_2, \omega_3 + \omega_5 - \omega_1) G(\omega_3 + \omega_5 - \omega_1) G(\omega_5) \Gamma_{\uparrow\downarrow;\uparrow\downarrow}(\omega_1, \omega_3 + \omega_5 - \omega_1, \omega_3).\end{aligned}\quad (8.25)$$

Explicitly, $\gamma_{\text{t}|\uparrow\downarrow;\uparrow\downarrow}$ reads

$$\begin{aligned}\gamma_{\text{t}|\uparrow\downarrow;\uparrow\downarrow}(\omega_1, \omega_2, \omega_3) &= -\frac{4U^3 \omega_1 \omega_3}{\beta(U^2 + 4\omega_1^2)(U^2 + 4\omega_3^2)} - \frac{4U^3 \omega_2 (\omega_1 + \omega_2 - \omega_3)}{\beta(U^2 + 4\omega_2^2)(U^2 + 4(\omega_1 + \omega_2 - \omega_3)^2)} \\ &\quad + U^4 \delta_{\omega_1 + \omega_2} \left(-\frac{\omega_1 \omega_3}{(U^2 + 4\omega_1^2)(U^2 + 4\omega_3^2)} - \frac{\omega_2 (\omega_1 + \omega_2 - \omega_3)}{(U^2 + 4\omega_2^2)(U^2 + 4(\omega_1 + \omega_2 - \omega_3)^2)} \right) \\ &\quad + \frac{U^2 (\beta U e^{\frac{\beta U}{2}} + e^{\beta U} - 1) \delta_{\omega_1 - \omega_3}}{8(e^{\frac{\beta U}{2}} + 1)^2} \\ &\quad + U^4 \delta_{\omega_2 - \omega_3} \left(\frac{\omega_1 \omega_3}{(U^2 + 4\omega_1^2)(U^2 + 4\omega_3^2)} + \frac{\omega_2 (\omega_1 + \omega_2 - \omega_3)}{(U^2 + 4\omega_2^2)(U^2 + 4(\omega_1 + \omega_2 - \omega_3)^2)} \right).\end{aligned}\quad (8.26)$$

Lastly, we require the component $\gamma_{\text{t}|\uparrow\uparrow;\uparrow\uparrow}$ computed from the Bethe-Salpeter equations, which is given by

$$\begin{aligned}\gamma_{\text{t}|\uparrow\uparrow;\uparrow\uparrow}(\omega_1, \omega_2, \omega_3) &= -I_{\text{t}|\uparrow\downarrow;\uparrow\downarrow}(\omega_5, \omega_2, \omega_3 + \omega_5 - \omega_1) G(\omega_3 + \omega_5 - \omega_1) G(\omega_5) \Gamma_{\uparrow\uparrow;\uparrow}(\omega_1, \omega_3 + \omega_5 - \omega_1, \omega_3) \\ &\quad - I_{\text{t}|\downarrow\downarrow;\downarrow\downarrow}(\omega_5, \omega_2, \omega_3 + \omega_5 - \omega_1) G(\omega_3 + \omega_5 - \omega_1) G(\omega_5) \Gamma_{\uparrow\downarrow;\uparrow\downarrow}(\omega_1, \omega_3 + \omega_5 - \omega_1, \omega_3).\end{aligned}\quad (8.27)$$

Again, for a full treatment of Eq. (8.27), see [14]. Here, we restrict ourselves to only stating the result

$$\begin{aligned}\gamma_{\text{t}|\uparrow\uparrow;\uparrow\uparrow}(\omega_1, \omega_2, \omega_3) &= \frac{U^3 (e^{\frac{\beta U}{2}} - 1)}{2\beta (e^{\frac{\beta U}{2}} + 1) (U^2 + (\omega_1 - \omega_3)^2)} \\ &\quad - U^4 \delta_{\omega_1 + \omega_2} \left(\frac{\omega_1 \omega_3}{(U^2 + 4\omega_1^2)(U^2 + 4\omega_3^2)} + \frac{\omega_2 (\omega_1 + \omega_2 - \omega_3)}{(U^2 + 4\omega_2^2)(U^2 + 4(\omega_1 + \omega_2 - \omega_3)^2)} \right) \\ &\quad + \delta_{\omega_1 - \omega_3} \left(\frac{U (\beta U e^{\frac{\beta U}{2}} + e^{\beta U} - 1)}{2\beta (e^{\frac{\beta U}{2}} + 1)^2} - \frac{U^4 \omega_2 (\omega_1 + \omega_2 - \omega_3)}{(U^2 + 4\omega_2^2)(U^2 + 4(\omega_1 + \omega_2 - \omega_3)^2)} \right) \\ &\quad + U^4 \delta_{\omega_2 - \omega_3} \left(\frac{\omega_1 \omega_3}{(U^2 + 4\omega_1^2)(U^2 + 4\omega_3^2)} + \frac{2\omega_2 (\omega_1 + \omega_2 - \omega_3)}{(U^2 + 4\omega_2^2)(U^2 + 4(\omega_1 + \omega_2 - \omega_3)^2)} \right).\end{aligned}\quad (8.28)$$

Normally, γ_r with $r \in \{\text{a, p, t}\}$ and R would be summed for the full vertex. However, if this

was done with the expressions for γ_{r1} from this section, which will subsequently be denoted with an additional 1 as index, the resulting vertex would not fulfill the symmetry requirements. The additional index numbers the contributions to the full four-point vertex upon symmetrization. Explicitly, the four-point vertex needs to fulfill the following relations:

$$\Gamma_{12;34}(\omega_1, \omega_2, \omega_3) = \Gamma_{12;34}(-\omega_1, -\omega_2, -\omega_3) \quad (8.29)$$

$$\Gamma_{12;34}(\omega_1, \omega_2, \omega_3) = \Gamma_{21;43}(\omega_2, \omega_1, \omega_1 + \omega_2 - \omega_3) \quad (8.30)$$

$$\Gamma_{12;34}(\omega_1, \omega_2, \omega_3) = \Gamma_{34;12}(\omega_3, \omega_1 + \omega_2 - \omega_3, \omega_1) \quad (8.31)$$

In principle, a suitable vertex is constructed as follows: First, the Bethe-Salpeter equations are evaluated with exchanged frequency arguments of the irreducible and full vertices. To obtain the symmetric vertex

$$\Gamma_{\text{BSE}}(\omega_1, \omega_2, \omega_3) = \frac{1}{2}(\Gamma_{\text{BSE1}}(\omega_1, \omega_2, \omega_3) + \Gamma_{\text{BSE2}}(\omega_1, \omega_2, \omega_3)), \quad (8.32)$$

the results from both forms of Bethe-Salpeter equations need to be added. Above, Γ_{BSE1} stands for the original vertex computed in this section, whereas the index BSE2 denotes the vertex contribution necessary to account for all diagrams. Γ_{BSE2} would be obtained from switching the role of the irreducible parts I and Γ , as when inserting perturbation theory results the contraction order of these quantities does make a difference. Luckily, computing the Bethe-Salpeter equations all over again can be avoided by switching frequency arguments in the results from the first calculations depending on the respective channel, to obtain Γ_{BSE2} :

$$\gamma_{a2}(\omega_1, \omega_2, \omega_3) = \gamma_{a1}(\omega_2, \omega_1, \omega_1 + \omega_2 - \omega_3) \quad (8.33)$$

$$\gamma_{p2}(\omega_1, \omega_2, \omega_3) = \gamma_{p1}(\omega_3, \omega_1 + \omega_2 - \omega_3, \omega_3) \quad (8.34)$$

$$\gamma_{t2}(\omega_1, \omega_2, \omega_3) = \gamma_{t1}(\omega_2, \omega_1, \omega_1 + \omega_2 - \omega_3) \quad (8.35)$$

Applying Eq. (8.32) then leads to the final form of the four-point-vertices, which fulfill all symmetry requirements. Fig. 8.2 illustrates the vertex contributions from the Bethe-Salpeter equations. The expressions to their full extent are found on the next page. They are explicitly written out, as the results are important for the next chapter.

$$\begin{aligned}
 \Gamma_{\uparrow\downarrow;\uparrow\downarrow}(\omega_1, \omega_2, \omega_3) = & \frac{U}{8} \left[\frac{8}{\beta} + \frac{32U^2\omega_1\omega_2}{\beta(U^2 + 4\omega_1^2)(U^2 + 4\omega_2^2)} - \frac{32U^2\omega_1(\omega_1 + \omega_2 - \omega_3)}{\beta(U^2 + 4\omega_1^2)(U^2 + 4(\omega_1 + \omega_2 - \omega_3)^2)} \right. \\
 & - \frac{32U^2\omega_1\omega_3}{\beta(U^2 + 4\omega_1^2)(U^2 + 4\omega_3^2)} - \frac{32U^2\omega_2(\omega_1 + \omega_2 - \omega_3)}{\beta(U^2 + 4\omega_2^2)(U^2 + 4(\omega_1 + \omega_2 - \omega_3)^2)} \\
 & + \frac{4U^2(e^{\beta U} - 1)}{\beta(e^{\frac{\beta U}{2}} + 1)^2(U^2 + (\omega_1 + \omega_2)^2)} + \frac{32U^2\omega_3(\omega_1 + \omega_2 - \omega_3)}{\beta(U^2 + 4\omega_3^2)(U^2 + 4(\omega_1 + \omega_2 - \omega_3)^2)} \\
 & - \frac{16U^2\omega_2\omega_3}{\beta(U^2 + 4\omega_2^2)(U^2 + 4\omega_3^2)} - \frac{16U^2\omega_2\omega_3}{(U^2 + 4\omega_2^2)(\beta U^2 + 4\beta\omega_3^2)} - \frac{4U^2(e^{\frac{\beta U}{2}} - 1)}{\beta(e^{\frac{\beta U}{2}} + 1)(U^2 + (\omega_2 - \omega_3)^2)} \\
 & + \delta_{\omega_1 + \omega_2} \left(\frac{4(\beta U e^{\frac{\beta U}{2}}(U^2 + (\omega_1 + \omega_2)^2) + e^{\beta U}(\omega_1 + \omega_2)^2 - (\omega_1 + \omega_2)^2)}{\beta(e^{\frac{\beta U}{2}} + 1)^2(U^2 + (\omega_1 + \omega_2)^2)} - \frac{4U^3\omega_1^2}{(U^2 + 4\omega_1^2)^2} \right. \\
 & - \frac{8U^3\omega_1\omega_3}{(U^2 + 4\omega_1^2)(U^2 + 4\omega_3^2)} - \frac{8U^3\omega_2(\omega_1 + \omega_2 - \omega_3)}{(U^2 + 4\omega_2^2)(U^2 + 4(\omega_1 + \omega_2 - \omega_3)^2)} - \frac{4U^3\omega_3^2}{(U^2 + 4\omega_3^2)^2} \\
 & \left. + \frac{U(\beta U e^{\frac{\beta U}{2}} + e^{\beta U} - 1)}{(e^{\frac{\beta U}{2}} + 1)^2} \right) + \delta_{\omega_1 - \omega_3} \left(-\frac{12U^3\omega_1\omega_2}{(U^2 + 4\omega_1^2)(U^2 + 4\omega_2^2)} \right. \\
 & - \frac{4U^3\omega_3(\omega_1 + \omega_2 - \omega_3)}{(U^2 + 4\omega_3^2)(U^2 + 4(\omega_1 + \omega_2 - \omega_3)^2)} + \frac{U(\beta U e^{\frac{\beta U}{2}} + e^{\beta U} - 1)}{(e^{\frac{\beta U}{2}} + 1)^2} \left. \right) + \delta_{\omega_2 - \omega_3} \left(\frac{4U^3\omega_1^2}{(U^2 + 4\omega_1^2)^2} \right. \\
 & + \frac{4U^2(e^{\frac{\beta U}{2}} - 1)}{\beta(e^{\frac{\beta U}{2}} + 1)(U^2 + (\omega_2 - \omega_3)^2)} + \frac{8U^3\omega_1\omega_3}{(U^2 + 4\omega_1^2)(U^2 + 4\omega_3^2)} + \frac{4U^3\omega_2^2}{(U^2 + 4\omega_2^2)^2} \\
 & \left. + \frac{U(\beta U e^{\frac{\beta U}{2}} + e^{\beta U} - 1)}{(e^{\frac{\beta U}{2}} + 1)^2} - \frac{4(\beta U e^{\frac{\beta U}{2}} + e^{\beta U} - 1)}{\beta(e^{\frac{\beta U}{2}} + 1)^2} + \frac{8U^3\omega_2(\omega_1 + \omega_2 - \omega_3)}{(U^2 + 4\omega_2^2)(U^2 + 4(\omega_1 + \omega_2 - \omega_3)^2)} \right) \Big] \\
 \end{aligned} \tag{8.36}$$

$$\begin{aligned}
 \Gamma_{\uparrow\uparrow;\uparrow\uparrow}(\omega_1, \omega_2, \omega_3) = & \frac{1}{2}U \left[\frac{U^2(e^{\frac{\beta U}{2}} - 1)}{\beta(e^{\frac{\beta U}{2}} + 1)(U^2 + (\omega_1 - \omega_3)^2)} - \frac{U^2(e^{\frac{\beta U}{2}} - 1)}{\beta(e^{\frac{\beta U}{2}} + 1)(U^2 + (\omega_2 - \omega_3)^2)} \right. \\
 & + \frac{2U^3(\omega_1 - \omega_2)\delta_{\omega_1 + \omega_2}(U^2 - 4\omega_1\omega_2)(\omega_1 + \omega_2 - 2\omega_3)(U^2 + 4\omega_3(-\omega_1 - \omega_2 + \omega_3))}{(U^2 + 4\omega_1^2)(U^2 + 4\omega_2^2)(U^2 + 4\omega_3^2)(U^2 + 4(\omega_1 + \omega_2 - \omega_3)^2)} \\
 & + \delta_{\omega_1 - \omega_3} \left(-\frac{U^3\omega_1\omega_2}{(U^2 + 4\omega_1^2)(U^2 + 4\omega_2^2)} - \frac{3U^3\omega_1(\omega_1 + \omega_2 - \omega_3)}{(U^2 + 4\omega_1^2)(U^2 + 4(\omega_1 + \omega_2 - \omega_3)^2)} \right. \\
 & - \frac{U^3\omega_1\omega_3}{(U^2 + 4\omega_1^2)(U^2 + 4\omega_3^2)} - \frac{U^3\omega_2(\omega_1 + \omega_2 - \omega_3)}{(U^2 + 4\omega_2^2)(U^2 + 4(\omega_1 + \omega_2 - \omega_3)^2)} \\
 & \left. - \frac{U^3\omega_3(\omega_1 + \omega_2 - \omega_3)}{(U^2 + 4\omega_3^2)(U^2 + 4(\omega_1 + \omega_2 - \omega_3)^2)} - \frac{3U^3\omega_2\omega_3}{(U^2 + 4\omega_2^2)(U^2 + 4\omega_3^2)} + \frac{\beta U e^{\frac{\beta U}{2}} + e^{\beta U} - 1}{\beta(e^{\frac{\beta U}{2}} + 1)^2} \right) \\
 & + \delta_{\omega_2 - \omega_3} \left(\frac{U^2(e^{\frac{\beta U}{2}} - 1)}{\beta(e^{\frac{\beta U}{2}} + 1)(U^2 + (\omega_2 - \omega_3)^2)} + \frac{U^3\omega_1\omega_2}{(U^2 + 4\omega_1^2)(U^2 + 4\omega_2^2)} - \frac{\beta U e^{\frac{\beta U}{2}} + e^{\beta U} - 1}{\beta(e^{\frac{\beta U}{2}} + 1)^2} \right. \\
 & + \frac{U^3\omega_2\omega_3}{(U^2 + 4\omega_2^2)(U^2 + 4\omega_3^2)} + \frac{U^3\omega_1(\omega_1 + \omega_2 - \omega_3)}{(U^2 + 4\omega_1^2)(U^2 + 4(\omega_1 + \omega_2 - \omega_3)^2)} + \frac{3U^3\omega_1\omega_3}{(U^2 + 4\omega_1^2)(U^2 + 4\omega_3^2)} \\
 & \left. + \frac{3U^3\omega_2(\omega_1 + \omega_2 - \omega_3)}{(U^2 + 4\omega_2^2)(U^2 + 4(\omega_1 + \omega_2 - \omega_3)^2)} + \frac{U^3\omega_3(\omega_1 + \omega_2 - \omega_3)}{(U^2 + 4\omega_3^2)(U^2 + 4(\omega_1 + \omega_2 - \omega_3)^2)} \right) \Big] \\
 \end{aligned} \tag{8.37}$$

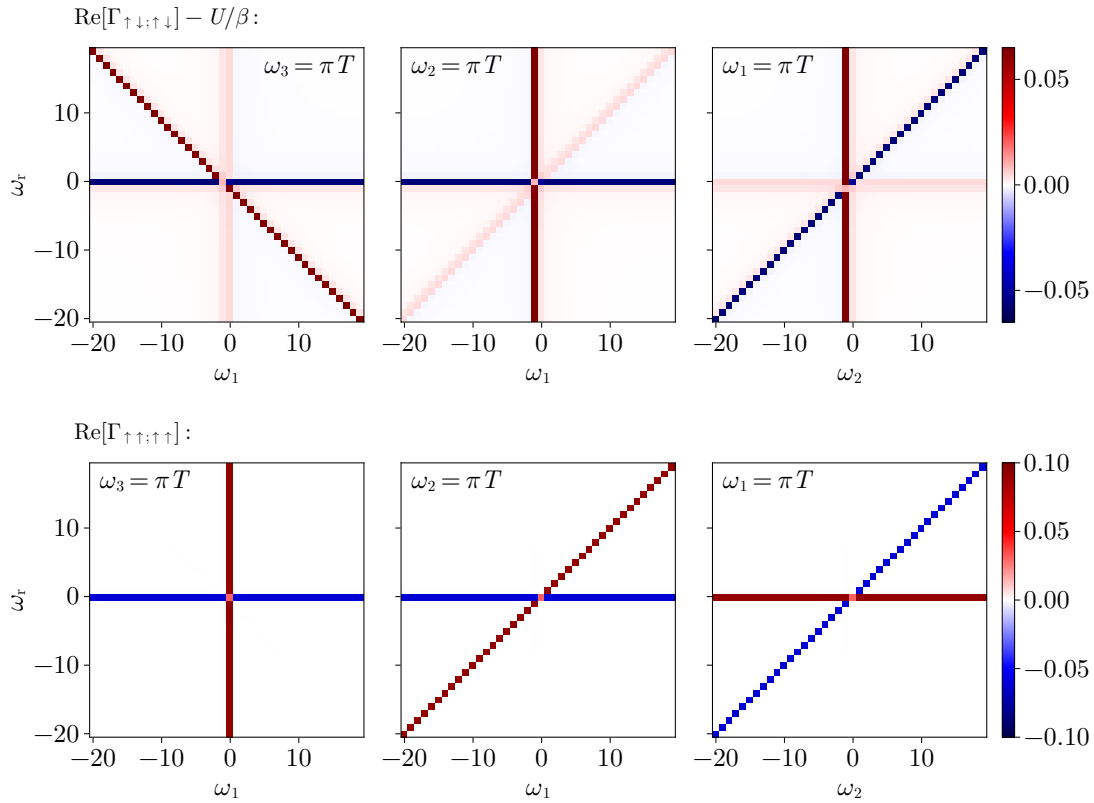


Figure 8.2: Contributions to the four-point vertex derived from the Bethe-Salpeter equations for the parameter set $U = 0.5, \beta = 1$. The label ω_r stands for the frequency index, for which the frequency was not set equal to $\frac{\pi}{\beta}$ and not plotted along the x-axis (label below each plot). For both combinations of spin arguments considered, the imaginary part is equal to zero.

As a consistency check, the expressions Eq. (8.36) and Eq. (8.37) can be expanded in terms of orders in the interaction strength and compared to the expansion of the exact quantities Eq. (7.16) and Eq. (7.16). Since the Bethe-Salpeter equations are exact relations and second-order perturbation theory results were used as initial values, the expansion vertex contributions should agree with the expansion of the exact vertices up to third-order in the interaction strength. First, the exact solution is expanded. Expanding the vertex from the Bethe-Salpeter equations up to third-order, leads to

$$\begin{aligned} \Gamma_{\uparrow\downarrow;\downarrow\uparrow}(\omega_1, \omega_2, \omega_3) &= \frac{1}{4}U^2(\delta_{\omega_1+\omega_2} - \delta_{\omega_2-\omega_3}) + \frac{U}{\beta} \\ &- \frac{\beta}{8}U^3 \left(\frac{2(\omega_1^2 + \omega_1(\omega_2 - \omega_3) + \omega_2^2 - \omega_2\omega_3 + \omega_3^2)}{\beta^2\omega_1\omega_2\omega_3(\omega_1 + \omega_2 - \omega_3)} - \frac{\delta_{\omega_1+\omega_2}}{2} - \frac{\delta_{\omega_1-\omega_3}}{2} - \frac{\delta_{\omega_2-\omega_3}}{2} \right) + \mathcal{O}(U^4), \end{aligned} \quad (8.38)$$

$$\Gamma_{\uparrow\uparrow;\uparrow\uparrow}(\omega_1, \omega_2, \omega_3) = \frac{1}{4}U^2(\delta_{\omega_1-\omega_3} - \delta_{\omega_2-\omega_3}) + \mathcal{O}(U^4). \quad (8.39)$$

Indeed, the expansion coefficients up to third-order are the same as for the exact solution. Therefore, the Bethe-Salpeter equations were applied correctly and the result for the four-point vertex can be used to determine the violation of the U(1) Ward identity in the next chapter.

8.3 Self-Energy from the Schwinger-Dyson Equation

For evaluating the U(1) Ward identity, an expression for the self-energy is needed. In numerical implementations, the self-energy is calculated from the vertex obtained after a Parquet iteration. However, the Matsubara summations appearing turned out to be prohibitively complex. Therefore, we do it differently: Again, second-order perturbation theory results are selected as initial value of the four-point vertex for the Schwinger-Dyson equation.

To begin, the Schwinger-Dyson equation Eq. (8.5) is rewritten for the Hubbard atom as

$$\Sigma_1 = -\Gamma_{0|12;12}G_2 - \frac{1}{2}\Gamma_{0|12;57}G_2G_7G_5\Gamma_{57;12}. \quad (8.40)$$

Taking into consideration that for the vertex with all spin arguments equal the first-order contribution in the interaction strength vanishes and that frequency conservation holds, Eq. (8.40) is written out explicitly as

$$\begin{aligned} \Sigma(\omega) = & -\sum_{\omega_2} (\Gamma_0 G(\omega_2)) - \frac{1}{2} \sum_{\omega_2, \omega_5} (\Gamma_0 G(\omega_2) G(\omega + \omega_2 - \omega_5) G(\omega_5) \Gamma_{\uparrow\downarrow; \uparrow\downarrow}(\omega_5, \omega + \omega_2 - \omega_5, \omega) \\ & + \Gamma_0 G(\omega_2) G(\omega + \omega_2 - \omega_5) G(\omega_5) \Gamma_{\downarrow\uparrow; \downarrow\uparrow}(\omega_5, \omega + \omega_2 - \omega_5, \omega)). \end{aligned} \quad (8.41)$$

To express the second summand in terms of vertex contributions from chapter 5, relations due to crossing-symmetry Eq. (8.14) are applied:

$$\begin{aligned} & \Gamma_0 G(\omega_2) G(\omega + \omega_2 - \omega_5) G(\omega_5) \Gamma_{\downarrow\uparrow; \downarrow\uparrow}(\omega_5, \omega + \omega_2 - \omega_5, \omega) \\ & = \Gamma_0 G(\omega_2) G(\omega + \omega_2 - \omega_5) G(\omega_5) \Gamma_{\uparrow\downarrow; \uparrow\downarrow}(\omega_5, \omega + \omega_2 - \omega_5, \omega_2) \end{aligned} \quad (8.42)$$

Inserting Eq. (8.42) into Eq. (8.41), an expression for the self-energy can be calculated. Next, the frequency summation was evaluated.

$$\Sigma_{\text{SDE}}(\omega) = \frac{1}{2}U \left(-1 - \frac{2iU\omega \left(U^2 \left(26e^{\frac{\beta U}{2}} + e^{\beta U} + 1 \right) + 4\omega^2 \left(e^{\frac{\beta U}{2}} + 1 \right)^2 \right)}{\left(e^{\frac{\beta U}{2}} + 1 \right)^2 \left(U^2 + 4\omega^2 \right) \left(9U^2 + 4\omega^2 \right)} \right) \quad (8.43)$$

The corresponding explicit calculations can be found in the respective *Wolfram Mathematica* notebook linked in the bibliography [14]. Graphically, the real and imaginary part of the self-energy from the Schwinger-Dyson equation are depicted in Fig. 8.3.

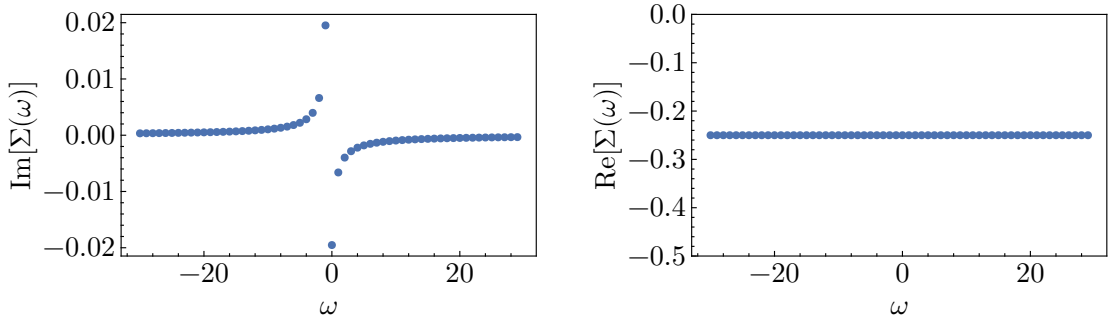


Figure 8.3: Real and imaginary part of the self-energy from the Schwinger-Dyson equation at $\beta = 1$, $U = 0.5$. The real part consists only of the Hartree-term, which is constant and equal to $-\frac{U}{2}$.

Similar to section 8.2, the self-energy obtained from the Schwinger-Dyson equation up to third-order in the interaction strength

$$\Sigma_{\text{SDE}}(\omega) = -\frac{U}{2} - \frac{iU^2}{4\omega} + \mathcal{O}(U^4) \quad (8.44)$$

should now agree with the exact self-energy Eq. (7.15). Comparing this to the expansion of Eq. (7.15), note that as expected they are in fact equal.

Summarizing, we have now found approximations to four-point vertex and self-energy, following the basic principles of Parquet formalism with some adjustments to generate expressions which may still be handled analytically. The violation of the U(1) Ward identity for these new quantities is investigated in the subsequent chapter.

9 Fulfillment of the Ward Identity after BSE and SDE

In the following, the quantities from the Bethe-Salpeter equations and Schwinger-Dyson equation are substituted into the U(1) Ward identity. Originally, it was planned to analyze the violation of this equation with the primary goal to improve the Parquet approximation and cancel the violation. An additional term, which was added to the approximation of the two-particle irreducible vertex, was to be figured out through an educated guess from the mathematical form of the violation. This term then should have ensured the fulfillment of the identity.

However, doing this posed a prohibitive challenge due to the complexity of the calculation. It caused especially great difficulty to evaluate the Matsubara frequency summation necessary for evaluating the left-hand side of the U(1) Ward identity Eq. (6.38). The primary reason for this was the extraordinary number of function poles, which the Green's function derived from the self-energy Eq. (8.43) introduced to the left-hand side of the Ward identity. Hence, the respective contributions possessed many residues (see appendix B) and the evaluated expression was way too long to possibly find a suitable alternative to the Parquet approximation Γ_0 or even draw any conclusions from. Therefore, we resorted to an alternative approach, which is the subject of chapters 10 and 11.

Regarding the vertex and self-energy from the previous section, the corresponding violation is computed numerically. Explicitly, the Ward identity reads

$$(i\omega_2 - i\omega_1) \sum_{\sigma, \omega} G(\omega) G(\omega + \omega_1 - \omega_2) \Gamma_{\text{BSE}}(\omega, \omega_1, \omega + \omega_1 - \omega_2) = \Sigma_{\text{SDE}}(\omega_2) - \Sigma_{\text{SDE}}(\omega_1). \quad (9.1)$$

Above, G refers to the single-particle Green's function, which is given by $G = \frac{1}{[G_0]^{-1} - \Sigma_{\text{SDE}}}$. For ease of notation, spin indices were omitted. The general form of the Ward identity with all indices is given by Eq. (6.39).

For obtaining a numerical value for the violation, the summation

$$\sum_{\sigma, n} G\left(\frac{2\pi n + \pi}{\beta}\right) \Gamma\left(\frac{2\pi n + \pi}{\beta}, \omega_1, \frac{2\pi n + \pi}{\beta} + \omega_1 - \omega_2\right) G\left(\frac{2\pi n + \pi}{\beta} + \omega_1 - \omega_2\right) \quad (9.2)$$

has to be performed. Here, n denotes the index of the summation frequency ω . From n , the corresponding ω can be evaluated according to Eq. (3.37). Due to the structure of the Green's functions (see Fig. 9.1), a large range for the summation index has to be used in approximating 9.2 to ensure convergence. More specifically, the bare vertex multiplied by the product of Green's functions is alternating and not symmetric to $n = 0$ and thus poses difficulties upon summation.

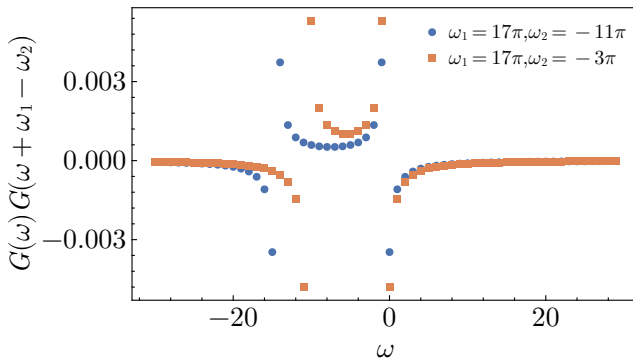


Figure 9.1: Product of Green's functions from the U(1) Ward identity for the self-energy from the Parquet equations for $U = 0.5, \beta = 1$.

To aid convergence, one can add and subtract terms from Eq. (3.37) and evaluate the summation

of simpler ‘problematic’ terms analytically. For example, Eq. (3.37) could be transformed as

$$\sum_{\sigma,\omega} \left(G(\omega)G(\omega + \omega_1 - \omega_2) [\Gamma(\omega, \omega_1, \omega + \omega_1 - \omega_2) - U] \right. \\ \left. + U[G(\omega)G(\omega + \omega_1 - \omega_2) - G_0(\omega)G_0(\omega + \omega_1 - \omega_2)] + UG_0(\omega)G_0(\omega + \omega_1 - \omega_2) \right). \quad (9.3)$$

Above, the only term causing convergence problems is given by the last summand $UG_0(\omega)G_0(\omega + \omega_1 - \omega_2)$, which due to the simple structure of the bare propagator can be summed analytically via the usual Residue theorem ansatz.

In principle, to simplify the evaluation of Eq. (3.37), the summation frequency can be shifted such that the sum would be (almost) symmetrical to the extremal values of the Green’s functions. This type of shift does not change the value of the infinite summation. However, one needs to ensure that the shifted summation frequency still possesses the properties of a fermionic Matsubara frequency. In summary, without changing the original expression Eq. (3.37) the only option to guarantee accurate numerical results is to choose a large range for the summation index. This motivates the switch from *Wolfram Mathematica* to the programming language *Julia* [15] for the upcoming numerical calculations, as in practice it reduces computation time drastically. Moreover, with the package *MatsubaraFunctions.jl* [16] Matsubara functions and frequency summations can be implemented very conveniently. Results from evaluating the violation Eq. (9.1) are depicted in Fig. 9.2, Fig. 9.3 and Fig. 9.4 for different temperatures. The *Julia* implementation is linked in the bibliography [14].

For all parameter choices, the violations are roughly an order of magnitude smaller than the actual values of left-hand side and right-hand side of the Ward identity. For $\omega_1 = \omega_2$, the Ward identity is trivially fulfilled due to the self-energy difference on the right-hand side evaluating to zero and the proportionality of the left-hand side to the factor $(i\omega_2 - i\omega_1)$. This results in the diagonal from the top-right to the bottom-left in the density plots of the Ward identity difference. Both the self-energy and the summation over the vertex contribution $\Gamma_{\uparrow\uparrow;\uparrow\uparrow}$ display a ‘cross-like’ structure, whereas the vertex contribution $\Gamma_{\uparrow\downarrow;\uparrow\downarrow}$ accounts for the diagonal structure in the Ward identity difference and assumes large values for large frequency differences. Therefore, for large differences $|\omega_2 - \omega_1|$ the violation increases, which is rather unexpected. Regarding different interaction strengths, this increase especially influences the violation for small $\frac{U}{T}$. This suggests convergence problems caused by the summation of the product $\Gamma_0 G(\omega)G(\omega + \omega_1 - \omega_2)$ included in $\Gamma_{\uparrow\downarrow;\uparrow\downarrow}$ as cause of the increase, as for low temperatures first-order terms in U are dominant. Some approaches to dealing with these issues were discussed above but not implemented at the time of writing.

All in all, the Ward identity does not hold for the quantities Σ_{SDE} and Γ_{BSE} , whereas the absolute value of the violation increases with the interaction strength. While for small U the violation of the Ward identity seems to be due to the asymptotics of the last summand, for larger U a cross-like structure appears in the violation. The first issue should be fixable with some effort, whereas the second one is non-trivial. In the following, we try to develop a systematic method to ensure fulfillment the U(1) Ward identity by improving on the two-particle irreducible vertex approximation.

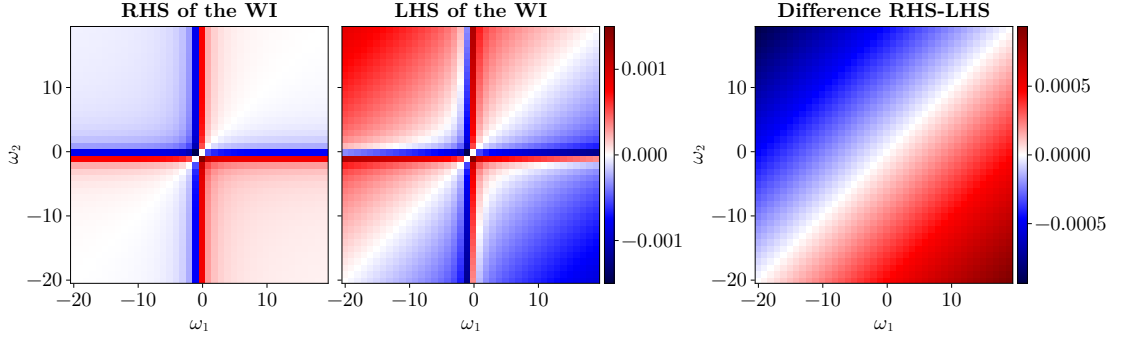


Figure 9.2: From left to right: Imaginary part of the right-hand side of the U(1) Ward identity (self-energy difference), imaginary part of the left-hand side of the U(1) Ward identity and violation of the U(1) Ward identity for $U = 0.1$, $\beta = 1$.

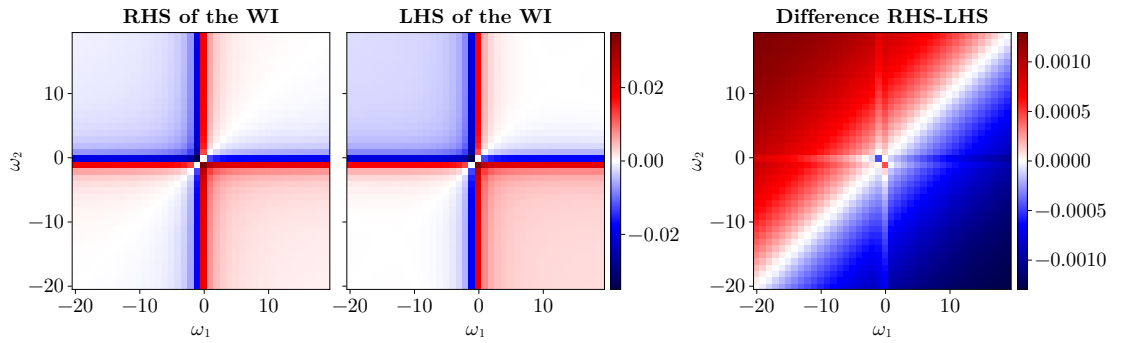


Figure 9.3: From left to right: Imaginary part of the right-hand side of the U(1) Ward identity (self-energy difference), imaginary part of the left-hand side of the U(1) Ward identity and violation of the U(1) Ward identity for $U = 0.5$, $\beta = 1$.

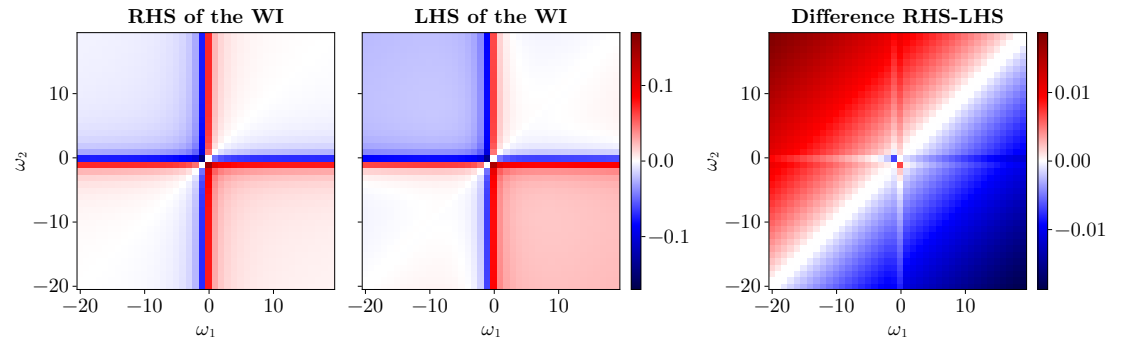


Figure 9.4: From left to right: Imaginary part of the right-hand side of the U(1) Ward identity (self-energy difference), imaginary part of the left-hand side of the U(1) Ward identity and violation of the U(1) Ward identity for $U = 1$, $\beta = 1$.

10 Analytical Approximation for the Irreducible Four-Point Vertex

Finding an ansatz to approximate the two-particle irreducible vertex, which ensures that the U(1) Ward identity holds, is now done analytically for a simple case. In general, this section should serve as a proof of concept. It is meant to give some ideas on possible approaches to mathematically finding rest terms ansatzes. In later sections, the procedure is repeated similarly for a more complex case.

However, we first restrict ourselves to compensating the violation of the Ward identity in second-order perturbation theory in the particle-hole symmetric regime. Inserting second-order quantities separately, the Ward identity is fulfilled (see chapter 7.1) but it is not when zero-, first- and second-order diagrams are substituted at the same time and the Green's function is computed from the second-order self-energy according to the Dyson equation, analogous to the evaluation of the Green's function in the last chapter. The quantities considered are then given by the four-point vertex contributions Eq. (8.8) and Eq. (8.9), the self-energy Eq. (8.7) and the single-particle Green's function:

$$G = \frac{1}{[G_0]^{-1} - \Sigma_2} = -\frac{4i\omega}{U^2 + 4\omega^2} \quad (10.1)$$

Now, when calculating the Ward identity violation, violations in orders higher than second-order

$$\begin{aligned} & \Sigma(\omega_2) - \Sigma(\omega_1) - (i\omega_2 - i\omega_1) \sum_{\omega} G(\omega)G(\omega + \omega_1 - \omega_2)\Gamma_{\uparrow\uparrow;\uparrow\uparrow}(\omega, \omega_1, \omega + \omega_1 - \omega_2, \omega_2) \\ & + \Gamma_{\uparrow\downarrow;\uparrow\downarrow}(\omega, \omega_1, \omega + \omega_1 - \omega_2, \omega_2) \\ & = \frac{1}{4}U^2(i\omega_2 - i\omega_1) \left(\frac{2 \tanh\left(\frac{\beta U}{4}\right)}{U^2 + (\omega_1 - \omega_2)^2} - \frac{16\omega_1\omega_2}{(U^2 + 4\omega_1^2)(U^2 + 4\omega_2^2)} + \frac{1}{\omega_1\omega_2} \right) \\ & \equiv (i\omega_2 - i\omega_1)\epsilon(\omega_1, \omega_2) \end{aligned} \quad (10.2)$$

arise. Our objective is now, to add something to the vertex to cancel the violation $\epsilon(\omega_1, \omega_2)$. Therefore, let us at first discuss the mathematical form of rest terms for the four-point vertex: Due to symmetry requirements, the four-point vertex needs to fulfill Eq. (8.29), Eq. (8.30) and Eq. (8.31). Hence, our ansatz for R also needs to possess these properties. This imposes the condition

$$\begin{aligned} R_{\uparrow\downarrow;\uparrow\downarrow}(\omega_1, \omega_2, \omega_3) &= f(\omega_1, \omega_2, \omega_3) + f(\omega_2, \omega_1, \omega_1 + \omega_2 - \omega_3) + f(\omega_1 + \omega_2 - \omega_3, \omega_3, \omega_2) \\ &+ f(\omega_3, \omega_1 + \omega_2 - \omega_3, \omega_1) \end{aligned} \quad (10.3)$$

on R . Here, f is an arbitrary function of Matsubara frequencies ω_1 , ω_2 and ω_3 . In general, the rest term $R_{\uparrow\uparrow;\uparrow\uparrow}$ is given by

$$R_{\uparrow\uparrow;\uparrow\uparrow}(\omega_1, \omega_2, \omega_3) = R_{\uparrow\downarrow;\uparrow\downarrow}(\omega_1, \omega_2, \omega_3) + R_{\uparrow\downarrow;\uparrow\downarrow}(\omega_1, \omega_2, \omega_3). \quad (10.4)$$

Hence, from crossing symmetry the relation

$$R_{\uparrow\uparrow;\uparrow\uparrow}(\omega_1, \omega_2, \omega_3) = R_{\uparrow\downarrow;\uparrow\downarrow}(\omega_1, \omega_2, \omega_3) - R_{\uparrow\downarrow;\uparrow\downarrow}(\omega_2, \omega_1, \omega_3) \quad (10.5)$$

between the rest term $R_{\uparrow\downarrow;\uparrow\downarrow}$ and $R_{\uparrow\uparrow;\uparrow\uparrow}$ arises, which is defined as the rest term corresponding to the vertex contribution $\Gamma_{\uparrow\uparrow;\uparrow\uparrow}$. Additionally, time-reversal symmetry needs to be regarded, as it is not automatically ensured by choosing a rest term of the form Eq. (10.1). It is trivially fulfilled, if R depends only on even products of its frequency arguments. Taking Eq. (10.3) and Eq. (10.5)

into consideration, instead of looking for a suitable R we search for a function f to construct the two-particle irreducible vertex approximation from.

Let us now revisit the explicit expression of the violation Eq. (10.2). Note, that the violation is made up of three distinct summands. They are now considered separately to find rest terms and corresponding functions f , which cancel them.

Of course, there are many different options to cancel each summand of $\epsilon(\omega_1, \omega_2)$. Nevertheless, even for a violation consisting of only three rather compact summands it proves itself to be difficult to find an ansatz for new expressions which sum up to the violation when evaluating the infinite Matsubara sum. Though definitely possible, a much faster way is given by choosing a function f and therefore a rest term fully proportional to Kronecker-delta symbols. Especially, choosing an f containing either the factor $\delta_{\omega_1-\omega_2}$, which vanishes in the Ward identity due to the prefactor $i(\omega_2 - \omega_1)$, or containing $\delta_{\omega\pm\omega_1}, \delta_{\omega\pm\omega_2}$, which cancel out the Matsubara frequency summation over ω . Another advantage of choosing rest terms proportional to Kronecker-delta functions is them being very convenient in further calculations and especially frequency summations including the modified four-point vertices.

For the first summand, a suitable f is given by

$$f_1(\omega_1, \omega_2, \omega_3) = \frac{U^2 (U^2 + 4\omega_2^2) (U^2 + 4\omega_3^2) \delta_{\omega_1-\omega_3} \tanh\left(\frac{\beta U}{4}\right)}{128\omega_2\omega_3 (U^2 + (\omega_1 - \omega_2)^2)}. \quad (10.6)$$

It can be verified that this function indeed cancels the first summand of the violation ϵ by constructing the rest terms according to Eq. (10.3) and Eq. (10.5). As the full expressions of the rest terms are again rather elaborate, the end results to the rest terms counteracting the full ϵ are found at the end of this paragraph. The verification that with the modified four-point vertex the U(1) Ward identity holds was performed with *Wolfram Mathematica* [13] and is illustrated in a notebook linked in the bibliography [14].

The function f_2 corresponding to the rest term canceling the second summand of $\epsilon(\omega_1, \omega_2)$ is given by

$$f_2(\omega_1, \omega_2, \omega_3) = \frac{1}{32} U^2 \delta_{\omega_2-\omega_3}. \quad (10.7)$$

At last, the function to construct a rest term corresponding to the third summand is determined:

$$f_3(\omega_1, \omega_2, \omega_3) = \frac{U^2 (U^2 + 4\omega_2^2) (U^2 + 4\omega_3^2) \delta_{\omega_1-\omega_3}}{256\omega_1\omega_2^2\omega_3} \quad (10.8)$$

Next, the rest terms are constructed from the functions introduced above. If they were added to the four-point vertex contributions, the U(1) Ward identity would hold for these quantities by construction. The subsequent page is dedicated to showing the full ansatz for the irreducible terms.

$$\begin{aligned}
 R_{\uparrow\downarrow,\uparrow\downarrow}(\omega_1, \omega_2, \omega_3) = & \frac{1}{256} U^2 \left(\delta_{\omega_1 - \omega_3} \left(\frac{2(U^2 + 4\omega_1^2) \tanh\left(\frac{\beta U}{4}\right) (U^2 + 4(\omega_1 + \omega_2 - \omega_3)^2)}{\omega_1 (U^2 + (\omega_1 - \omega_2)^2) (\omega_1 + \omega_2 - \omega_3)} \right. \right. \\
 & + \frac{2(U^2 + 4\omega_1^2) \tanh\left(\frac{\beta U}{4}\right) (U^2 + 4(\omega_1 + \omega_2 - \omega_3)^2)}{\omega_1 (\omega_1 + \omega_2 - \omega_3) (U^2 + (\omega_1 + \omega_2 - 2\omega_3)^2)} + \frac{2(U^2 + 4\omega_2^2) (U^2 + 4\omega_3^2) \tanh\left(\frac{\beta U}{4}\right)}{\omega_2 \omega_3 (U^2 + (\omega_1 - \omega_2)^2)} \\
 & - \frac{2(U^2 + 4\omega_2^2) (U^2 + 4\omega_3^2) \tanh\left(\frac{\beta U}{4}\right)}{\omega_2 \omega_3 (U^2 + (\omega_1 + \omega_2 - 2\omega_3)^2)} + \frac{(U^2 + 4\omega_1^2) (U^2 + 4(\omega_1 + \omega_2 - \omega_3)^2)}{\omega_1^2 \omega_2 (\omega_1 + \omega_2 - \omega_3)} \\
 & + \frac{(U^2 + 4\omega_1^2) (U^2 + 4(\omega_1 + \omega_2 - \omega_3)^2)}{\omega_1 \omega_3 (\omega_1 + \omega_2 - \omega_3)^2} + \frac{(U^2 + 4\omega_2^2) (U^2 + 4\omega_3^2)}{\omega_1 \omega_2^2 \omega_3} \\
 & \left. \left. + \frac{(U^2 + 4\omega_2^2) (U^2 + 4\omega_3^2)}{\omega_2 \omega_3^2 (\omega_1 + \omega_2 - \omega_3)} \right) + 32 \delta_{\omega_2 - \omega_3} \right)
 \end{aligned} \tag{10.9}$$

$$\begin{aligned}
 R_{\uparrow\uparrow,\uparrow\uparrow}(\omega_1, \omega_2, \omega_3) = & \frac{1}{256} U^2 \left(\delta_{\omega_2 - \omega_3} \left(- \frac{2(U^2 + 4\omega_1^2) (U^2 + 4\omega_3^2) \tanh\left(\frac{\beta U}{4}\right)}{\omega_1 \omega_3 (U^2 + (\omega_1 - \omega_2)^2)} \right. \right. \\
 & - \frac{2(U^2 + 4\omega_1^2) (U^2 + 4\omega_3^2) \tanh\left(\frac{\beta U}{4}\right)}{\omega_1 \omega_3 (U^2 + (\omega_1 + \omega_2 - 2\omega_3)^2)} - \frac{2(U^2 + 4\omega_2^2) \tanh\left(\frac{\beta U}{4}\right) (U^2 + 4(\omega_1 + \omega_2 - \omega_3)^2)}{\omega_2 (U^2 + (\omega_1 - \omega_2)^2) (\omega_1 + \omega_2 - \omega_3)} \\
 & - \frac{2(U^2 + 4\omega_2^2) \tanh\left(\frac{\beta U}{4}\right) (U^2 + 4(\omega_1 + \omega_2 - \omega_3)^2)}{\omega_2 (\omega_1 + \omega_2 - \omega_3) (U^2 + (\omega_1 + \omega_2 - 2\omega_3)^2)} - \frac{(U^2 + 4\omega_1^2) (U^2 + 4\omega_3^2)}{\omega_1^2 \omega_2 \omega_3} \\
 & - \frac{(U^2 + 4\omega_1^2) (U^2 + 4\omega_3^2)}{\omega_1 \omega_3^2 (\omega_1 + \omega_2 - \omega_3)} - \frac{(U^2 + 4\omega_2^2) (U^2 + 4(\omega_1 + \omega_2 - \omega_3)^2)}{\omega_1 \omega_2^2 (\omega_1 + \omega_2 - \omega_3)} \\
 & \left. \left. - \frac{(U^2 + 4\omega_2^2) (U^2 + 4(\omega_1 + \omega_2 - \omega_3)^2)}{\omega_2 \omega_3 (\omega_1 + \omega_2 - \omega_3)^2} + 32 \right) \right. \\
 & + \delta_{\omega_1 - \omega_3} \left(\frac{2(U^2 + 4\omega_1^2) \tanh\left(\frac{\beta U}{4}\right) (U^2 + 4(\omega_1 + \omega_2 - \omega_3)^2)}{\omega_1 (U^2 + (\omega_1 - \omega_2)^2) (\omega_1 + \omega_2 - \omega_3)} \right. \\
 & + \frac{2(U^2 + 4\omega_1^2) \tanh\left(\frac{\beta U}{4}\right) (U^2 + 4(\omega_1 + \omega_2 \omega_3)^2)}{\omega_1 (\omega_1 + \omega_2 - \omega_3) (U^2 + (\omega_1 + \omega_2 - 2\omega_3)^2)} + \frac{2(U^2 + 4\omega_2^2) (U^2 + 4\omega_3^2) \tanh\left(\frac{\beta U}{4}\right)}{\omega_2 \omega_3 (U^2 + (\omega_1 - \omega_2)^2)} \\
 & + \frac{2(U^2 + 4\omega_2^2) (U^2 + 4\omega_3^2) \tanh\left(\frac{\beta U}{4}\right)}{\omega_2 \omega_3 (U^2 + (\omega_1 + \omega_2 - 2\omega_3)^2)} + \frac{(U^2 + 4\omega_1^2) (U^2 + 4(\omega_1 + \omega_2 - \omega_3)^2)}{\omega_1^2 \omega_2 (\omega_1 + \omega_2 - \omega_3)} \\
 & + \frac{(U^2 + 4\omega_1^2) (U^2 + 4(\omega_1 + \omega_2 - \omega_3)^2)}{\omega_1 \omega_3 (\omega_1 + \omega_2 - \omega_3)^2} + \frac{(U^2 + 4\omega_2^2) (U^2 + 4\omega_3^2)}{\omega_1 \omega_2^2 \omega_3} \\
 & \left. \left. + \frac{(U^2 + 4\omega_2^2) (U^2 + 4\omega_3^2)}{\omega_2 \omega_3^2 (\omega_1 + \omega_2 - \omega_3)} - 32 \right) \right)
 \end{aligned} \tag{10.10}$$

Let us now compare the modified vertex in second-order with the new approximations Eq. (10.9) and Eq. (10.10) added to the exact four-point vertex contributions introduced in section 7.2.

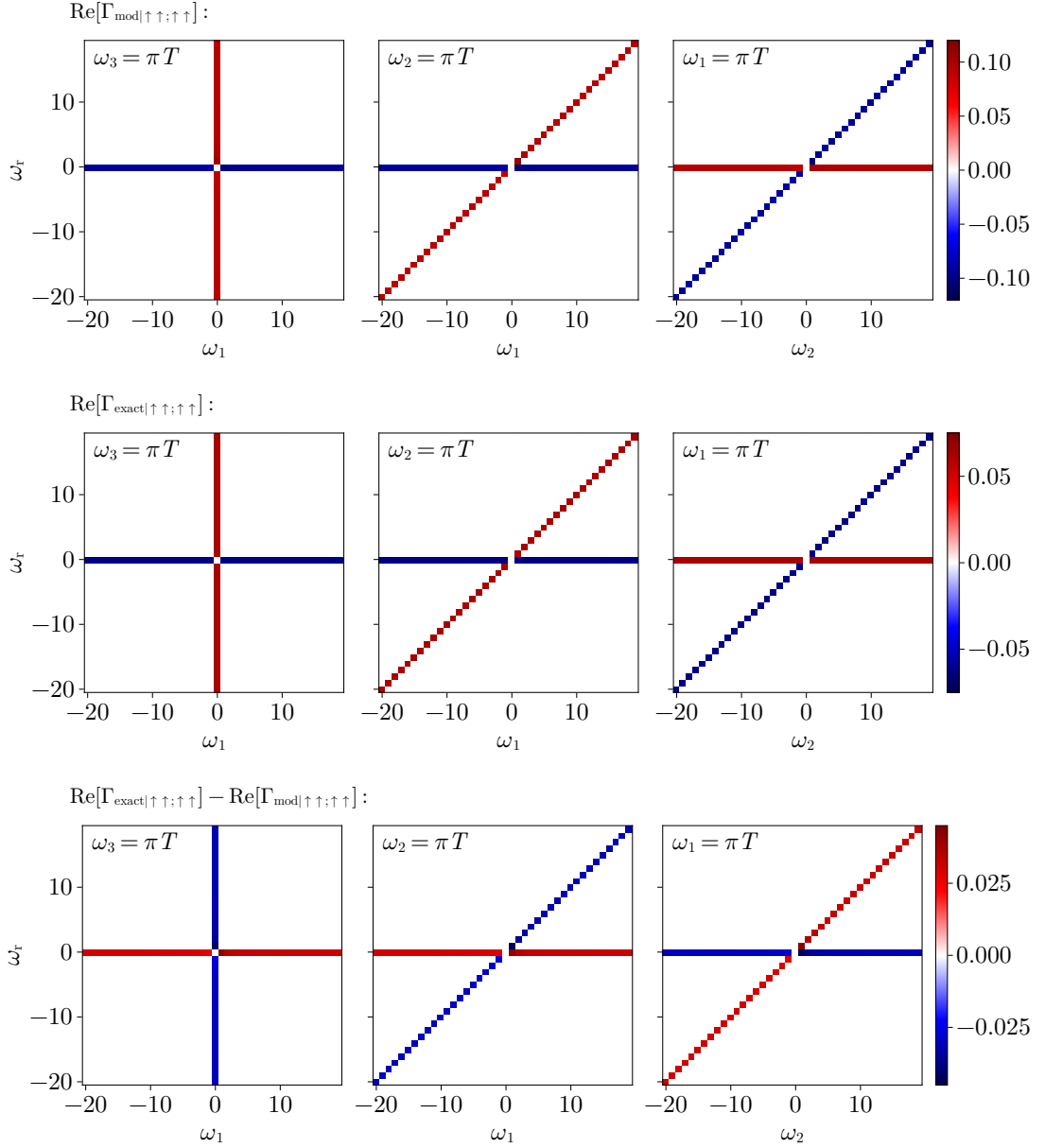


Figure 10.1: Comparison of the modified four-point vertex contribution $\Gamma_{\text{mod}|\uparrow\uparrow;\uparrow\uparrow}$, which is given by the four-point vertex $\Gamma_{\uparrow\uparrow;\uparrow\uparrow}$ in second-order in the interaction strength in term Eq. (10.8) added to it to the exact vertex contribution $\Gamma_{\text{exact}|\uparrow\uparrow;\uparrow\uparrow}$. The comparison considers the particle-hole symmetric regime for the parameters $\beta = 1$, $U = 0.5$. The axis labeling is explained in the caption of Fig. 8.2.

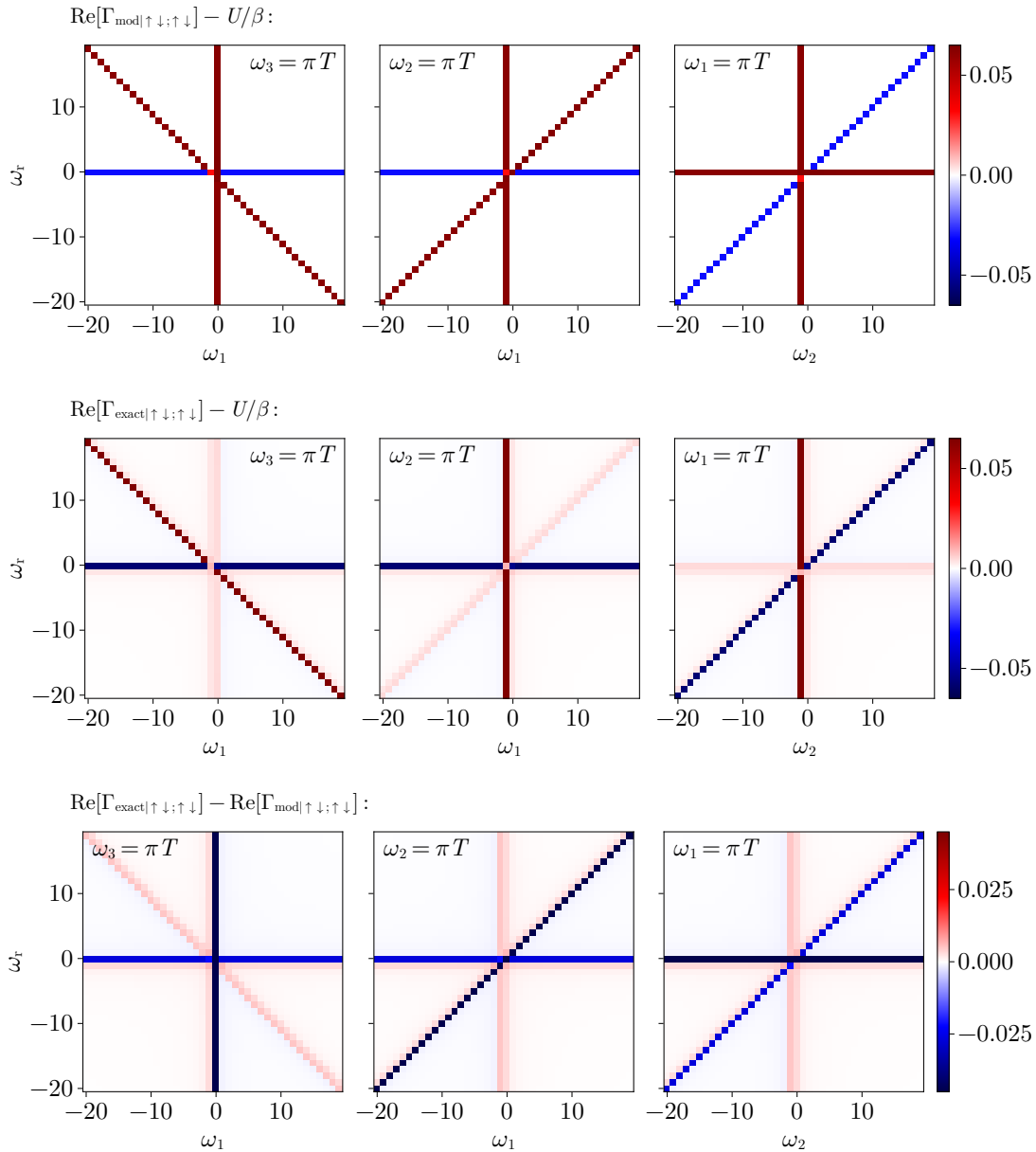


Figure 10.2: Comparison of the modified four-point vertex contribution $\Gamma_{\text{mod}|\uparrow\downarrow;\uparrow\downarrow}$, which is given by the four-point vertex $\Gamma_{\uparrow\downarrow;\uparrow\downarrow}$ in second-order in the interaction strength with rest term Eq. (10.8) added to it to the exact vertex contribution $\Gamma_{\text{exact}|\uparrow\downarrow;\uparrow\downarrow}$. The comparison considers the particle-hole symmetric regime for the parameters $\beta = 1$, $U = 0.5$. The axis labeling is explained in the caption of Fig. 8.2.

It is apparent that the exact vertex and the modified vertices structure-wise look very similar for all spin arguments equal. This stems from them both being mostly proportional to Kronecker-delta coefficients in the particle-hole symmetric regime. Nevertheless, the absolute value of the modified vertex contribution $\Gamma_{\text{mod}|\uparrow\uparrow;\uparrow\uparrow}$ is about a factor 2 larger in comparison to the exact solution for the parameters specified in the caption of Fig. 10.1. Regarding the vertex contribution $\Gamma_{\text{mod}|\uparrow\downarrow;\uparrow\downarrow}$, the modified and the exact vertex contributions are in the same order of magnitude for the parameters chosen, as can be seen in Fig. (10.2). Again, extremal values of the vertex contributions are found on the diagonals due to proportionality to Kronecker-delta symbols.

Although this has shown that taking an educated guess on the form of R to fulfill the Ward

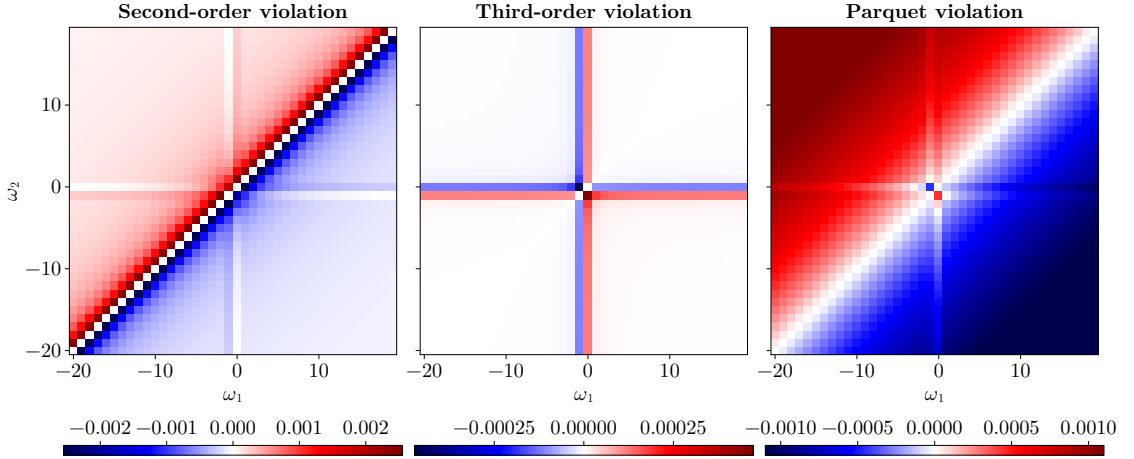


Figure 10.3: Comparison of the violations of the U(1) Ward identity for vertex and self-energy in second and third-order and derived from Schwinger-Dyson and Bethe-Salpeter equations for $U = 0.5$, $\beta = 1$.

identity is in principle possible, the rest terms derived in this chapter are not beneficial to our main objective: Cancellation of the violation for vertex and self-energy from BSE and SDE. To see why, the violation $\epsilon(\omega_1, \omega_2)$ compensated in this section is expanded as

$$\epsilon(\omega_1, \omega_2) = \frac{\beta U^3}{8(\omega_1 - \omega_2)^2} + \mathcal{O}(U^4) \quad (10.11)$$

in orders of the interaction strength.

Corrections from the rest terms Eq. (10.9) and Eq. (10.10) start in third-order. Since the vertex and self-energy from BSE and SDE are exact quantities up to third-order, adding rest terms constructed from the functions f_1 to f_3 from this chapter would overcompensate violations in third-order. Especially for small U , the coefficient of $\epsilon(\omega_1, \omega_2)$ proportional to U^3 dominates higher-order corrections and accounts for an even larger violation of the Ward identity for Γ_{BSE} and Σ_{SDE} . As perturbation theory itself is only valid for small interactions $\frac{U}{\beta}$ per definition, it is not to be expected that a modification of Γ_{BSE} with the same rest terms as above would change anything for the better. A comparison of the violations in second-order and the violation from last chapter is depicted in Fig. 10.3.

As a rest term for the violation of the Ward identity including Γ_{BSE} and Σ_{SDE} needs to account for violations in fourth-order and upwards, finding a rest term based on third-order might be able to cancel the violation from chapter 9 at least in parts. Therefore, the exact vertex and self-energy Eq. (7.15), Eq. (7.16) and Eq. (7.17) are expanded up to third-order in the interaction strength:

$$\Sigma(\omega) = -\frac{U}{2} - \frac{iU^2}{4\omega} \quad (10.12)$$

$$\Gamma_{\uparrow\uparrow, \uparrow\uparrow}(\omega_1, \omega_2, \omega_3) = \frac{1}{4}U^2(\delta_{\omega_1 - \omega_3} - \delta_{\omega_2 - \omega_3}) \quad (10.13)$$

$$\Gamma_{\uparrow\downarrow,\uparrow\downarrow}(\omega_1, \omega_2, \omega_3) = \frac{1}{\beta} \left(U + \frac{1}{4} U^2 (\beta \delta_{\omega_1+\omega_2} - \beta \delta_{\omega_2-\omega_3}) + U^3 \left(\frac{1}{16} \beta^2 \delta_{\omega_1+\omega_2} + \frac{1}{16} \beta^2 \delta_{\omega_1-\omega_3} \right. \right. \\ \left. \left. + \frac{1}{16} \beta^2 \delta_{\omega_2-\omega_3} + \frac{-\omega_1^2 + \omega_3(\omega_1 + \omega_2) - \omega_1\omega_2 - \omega_2^2 - \omega_3^2}{4\omega_1\omega_2\omega_3(\omega_1 + \omega_2 - \omega_3)} \right) \right) \quad (10.14)$$

Again, the Green's function is obtained according to the Dyson equation. Evaluating the Ward identity as in Eq. (10.2) for the third-order quantities yields the violation

$$\epsilon'(\omega_1, \omega_2) \equiv \frac{U^2}{8\omega_1\omega_2} \left(\frac{16\omega_1^2\omega_2^2(\beta U - 2)}{(U^2 + 4\omega_1^2)(U^2 + 4\omega_2^2)} - \frac{\tanh\left(\frac{\beta U}{4}\right)(U^2 + 4(\omega_1 - \omega_2)^2)}{U^2 + (\omega_1 - \omega_2)^2} + 2 \right). \quad (10.15)$$

Expanding $\epsilon'(\omega_1, \omega_2)$ indeed shows that its lowest-order term in the interaction strength arises in fourth-order. Before computing rest terms which sum up to $\epsilon'(\omega_1, \omega_2)$, let us compare the violations of the Ward identity from this and last chapter depicted in Fig. 10.3.

The comparison Fig. 10.3 makes it obvious that cancelling the violation in the Ward identity for the vertex and self-energy from BSE and SDE is not possible by making assumptions about the two-particle irreducible vertex based on standard diagrammatic perturbation theory. The third-order violation is also not able to compensate the violation from chapter 9. One observes a 'cross-shaped' pattern in the third-order as well as the numerical violation. However, the latter is dominated by diagonal features coming from the suboptimal numerical treatment of the asymptotics of the bare contribution.

In summary, the results from this chapter tell us that for determining rest terms compensating the numerical violation from chapter 9, the ansatzes cannot be based on perturbation theory but ideally should come from the numerical violation directly. Moreover, we were able to get a feeling on how rest terms for the four-point vertex can be determined in a fast and easy way. In the next chapter, this is applied to the numerical violation.

11 Numerical Approximation for the Irreducible Four-Point Vertex

Having obtained some experience on finding rest terms in the previous section, we will repeat the procedure to obtain a numerical addition to the four-point vertex Γ_{BSE} , with which the version of the U(1) Ward identity from chapter 9 holds.

As before, there are two main difficulties in finding additional terms which cancel the violation. For one, approximations for the two-particle irreducible vertex need to fulfill the symmetries of the four-point vertex. This is automatically ensured by choosing a specific form of ansatz for the rest term. One possible form is given by Eq. (10.3). Therefore, the goal is again to find a suitable function f from which we can construct the rest terms according to Eq. (10.3) and Eq. (10.5).

Furthermore, the Matsubara frequency summation poses difficulties in determining rest terms. Whereas for the analytic case (chapter 10) it was possible to make assumptions on R based on the mathematical structure of the violation, we cannot do this for numerical values. In principle, the equation

$$\sum_{\omega, \sigma} G(\omega)G(\omega + \omega_1 - \omega_2)R(\omega, \omega_1, \omega + \omega_1 - \omega_2) = \frac{\Delta_{\text{WI}}(\omega_1, \omega_2)}{(i\omega_2 - i\omega_1)} \quad (11.1)$$

needs to be solved for R . Here, Δ_{WI} denotes the violation of the Ward identity and the summation index σ indicates a summation over spin arguments. Note, that when $|\omega_1 - \omega_2| = 0$ one seemingly would have to divide by zero to determine R . However, as the Ward identity is trivially fulfilled for $|\omega_1 - \omega_2| = 0$, R is just set to zero on this diagonal in the frequency plane.

There are different options to deal with the summation on the left-hand side of Eq. (11.1). However, in any case assumptions about the form of R or equivalently the form of f , from which R is constructed, need to be made. A frequency proportionality such as $f \propto \frac{1}{\omega_1\omega_2\omega_3}$ could be considered, which contains prefactors ensuring the sums converge. Alternatively, we could avoid the frequency summation completely by postulating f being fully proportional to Kronecker-delta symbols. Due to the prefactor $(i\omega_2 - i\omega_1)$ in Eq. (11.1) for the Hubbard atom, or more general $([G_0(\omega)]^{-1} - [G_0(\omega + \omega_1 - \omega_2)]^{-1})$, terms proportional to $\delta_{\omega_1 - \omega_2}$ generally vanish in the U(1) Ward identity, whereas terms proportional to $\delta_{\omega \pm \omega_1}, \delta_{\omega \pm \omega_2}$ cancel the Matsubara frequency summation. To find f , the latter method of postulating proportionality to Kronecker-deltas is chosen because of its simplicity and generality, as it is applicable to any form of numerical violation. If f is demanded to be proportional to only one Kronecker-delta symbol, there are two options

$$f_1(\omega_1, \omega_2, \omega_3) = \delta_{\omega_1 - \omega_3} \tilde{f}_1(\omega_1, \omega_2, \omega_3) \quad (11.2)$$

$$f_2(\omega_1, \omega_2, \omega_3) = \delta_{\omega_2 - \omega_3} \tilde{f}_2(\omega_1, \omega_2, \omega_3) \quad (11.3)$$

which cancel out the summation upon construction of a rest term R . Although a combination of f_1 and f_2 is also thinkable, we will restrict ourselves to either choosing the proportionality of option f_1 or f_2 . If the four-point vertex is constructed from f_1 according to Eq. (10.3) and Eq. (10.5), the

left-hand side of Eq. (11.1) simplifies to

$$\begin{aligned}
 & \sum_{\omega, \sigma} G(\omega)G(\omega + \omega_1 - \omega_2)R(\omega, \omega_1, \omega + \omega_1 - \omega_2) \\
 &= \sum_{\omega} G(\omega)G(\omega + \omega_1 - \omega_2) (R_{\uparrow\downarrow; \uparrow\downarrow}(\omega, \omega_1, \omega + \omega_1 - \omega_2) + R_{\uparrow\uparrow; \uparrow\uparrow}(\omega, \omega_1, \omega + \omega_1 - \omega_2)) \\
 &= \sum_{\omega} G(\omega)G(\omega + \omega_1 - \omega_2) [2\delta_{\omega_1 - \omega_2} (\tilde{f}_1(\omega, \omega_1, \omega + \omega_1 - \omega_2) + \tilde{f}_1(\omega_1, \omega, \omega_2)) \\
 &+ \tilde{f}_1(\omega + \omega_1 - \omega_2, \omega_2, \omega) + \tilde{f}_1(\omega_2, \omega + \omega_1 - \omega_2, \omega_1)) - \delta_{\omega - \omega_2} (\tilde{f}_1(\omega_1, \omega, \omega + \omega_1 - \omega_2) \\
 &+ \tilde{f}_1(\omega, \omega_1, \omega_2) + \tilde{f}_1(\omega + \omega_1 - \omega_2, \omega_2, \omega_1) + \tilde{f}_1(\omega_2, \omega + \omega_1 - \omega_2, \omega))] \\
 &= -2G(\omega_1)G(\omega_2) (\tilde{f}_1(\omega_1, \omega_2, \omega_1) + \tilde{f}_1(\omega_2, \omega_1, \omega_2)) = -4G(\omega_1)G(\omega_2)\tilde{f}_1(\omega_1, \omega_2, \omega_1).
 \end{aligned} \tag{11.4}$$

The same procedure is repeated for the rest term constructed from f_2 :

$$\begin{aligned}
 & \sum_{\omega, \sigma} G(\omega)G(\omega + \omega_1 - \omega_2)R(\omega, \omega_1, \omega + \omega_1 - \omega_2) \\
 &= \sum_{\omega} G(\omega)G(\omega + \omega_1 - \omega_2) [2\delta_{\omega - \omega_2} (\tilde{f}_1(\omega, \omega_1, \omega + \omega_1 - \omega_2) + \tilde{f}_1(\omega_1, \omega, \omega_2)) \\
 &+ \tilde{f}_1(\omega + \omega_1 - \omega_2, \omega_2, \omega) + \tilde{f}_1(\omega_2, \omega + \omega_1 - \omega_2, \omega_1)) - \delta_{\omega_1 - \omega_2} (\tilde{f}_1(\omega_1, \omega, \omega + \omega_1 - \omega_2) \\
 &+ \tilde{f}_1(\omega, \omega_1, \omega_2) + \tilde{f}_1(\omega + \omega_1 - \omega_2, \omega_2, \omega_1) + \tilde{f}_1(\omega_2, \omega + \omega_1 - \omega_2, \omega))] \\
 &= 4G(\omega_1)G(\omega_2) (\tilde{f}_2(\omega_2, \omega_1, \omega_1) + \tilde{f}_2(\omega_1, \omega_2, \omega_2)) = 8G(\omega_1)G(\omega_2)\tilde{f}_2(\omega_2, \omega_1, \omega_1)
 \end{aligned} \tag{11.5}$$

Regarding their respective structure, the expressions Eq. (11.4) and Eq. (11.5) for f_1 and f_2 only differ in prefactors and sign. From the derivations of the functions above, depending on the option 1 or 2 either only the vertex correction $R_{\uparrow\uparrow; \uparrow\uparrow}$ (option f_1) or both $R_{\uparrow\uparrow; \uparrow\uparrow}$ and $R_{\uparrow\downarrow; \uparrow\downarrow}$ (option f_2) contribute to the compensation of the violation.

In both Eq. (11.4) and Eq. (11.5), the last equality is based on f being a crossing-symmetric function, which we can assume, if we define f in a specific way. Suppose, we are looking for a function \tilde{f}_1 for which the condition $\tilde{f}_1(\omega_1, \omega_2, \omega_1) = \tilde{f}_1(\omega_2, \omega_1, \omega_2)$ holds. Therefore, we define f_1 to be of the form

$$f_1(\omega_1, \omega_2, \omega_3) \equiv (f'_1(\omega_1, \omega_2, \omega_1) + f'_1(\omega_2, \omega_1, \omega_2)) \delta_{\omega_1 - \omega_3} \tag{11.6}$$

with $\tilde{f}_1(\omega_1, \omega_2, \omega_3) = f'_1(\omega_1, \omega_2, \omega_1) + f'_1(\omega_2, \omega_1, \omega_2)$. Per construction, this fulfills the requirements we demanded. Similarly, one can construct \tilde{f}_2 such that $\tilde{f}_2(\omega_2, \omega_1, \omega_1) = \tilde{f}_2(\omega_1, \omega_2, \omega_2)$ holds. Still, in the following we write \tilde{f} instead of explicitly inserting for example Eq. (11.6). Even so, the above definitions of the functions \tilde{f}_1 and \tilde{f}_2 make our previous transformations valid.

To obtain an expression for $\tilde{f}_1(\omega_1, \omega_2, \omega_1)$ and $\tilde{f}_2(\omega_2, \omega_1, \omega_1)$, we solve Eq. (11.1) for \tilde{f} by substituting the numerical values for the violation from Parquet. The resulting functions \tilde{f}_i are depicted in Fig. 11.1. One can clearly recognize the increase to higher frequencies as with the violation of the Ward identity Fig. 9.2. On the other hand, the increase in violation around the corners of the ‘cross-shaped’ feature is not observable and both functions f_1 and f_2 assume very small values for either ω_1 or ω_2 having a frequency index close to zero. However, the structure of the functions f_1 and f_2 should not be compared directly to the structure of the violation, as in the Ward identity the four-point vertices constructed from f_1 and f_2 are multiplied by Green’s functions, which take on extremal values for small frequencies (see chapter 9).

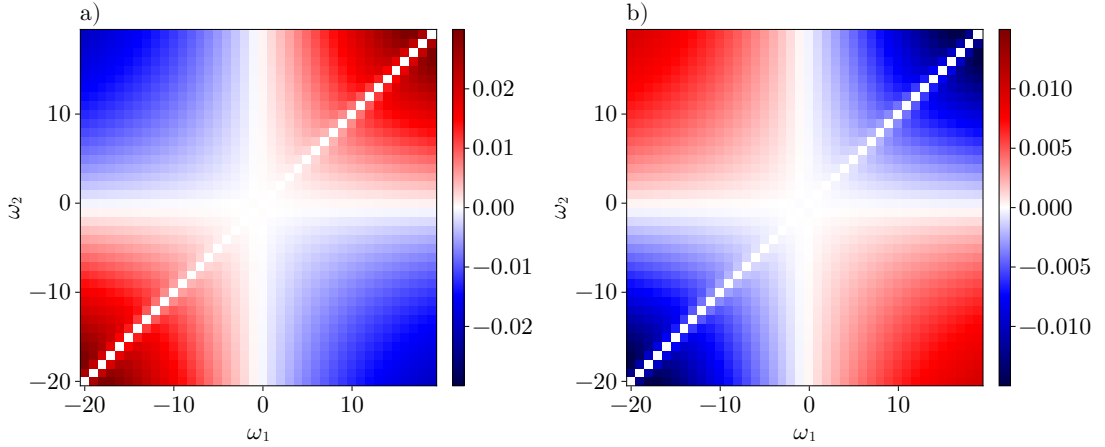


Figure 11.1: Functions which can be used to construct the rest term for the four point vertex form. a) Density plot of $\tilde{f}_1(\omega_1, \omega_2, \omega_1)$ b) Density plot of $\tilde{f}_2(\omega_2, \omega_1, \omega_1)$. For these plots, the parameters $U = 0.5, \beta = 1$ were chosen.

If a rest term R is now constructed from one of the functions introduced above, the U(1) Ward identity is fulfilled. As the rest terms should serve as correction to the four-point vertex, it is not enough to only know the rest term's frequency dependence on two arguments ω_1 and ω_2 . The general expressions $R(\omega_1, \omega_2, \omega_3)$ and $f(\omega_1, \omega_2, \omega_3)$ are needed, whereas f denotes either f_1 or f_2 . Fortunately, $R(\omega_1, \omega_2, \omega_3)$ can be inferred from $\tilde{f}_1(\omega_1, \omega_2, \omega_1)$ or $\tilde{f}_2(\omega_2, \omega_1, \omega_1)$ using symmetry considerations and the proportionality to Kronecker-delta symbols. To construct in example a rest term from $\tilde{f}_1(\omega_1, \omega_2, \omega_1)$ for the U(1) Ward identity according to Eq. (10.3), the terms

$$\begin{aligned}
 f_1(\omega_2, \omega_1, \omega_1 + \omega_2 - \omega_3) &= \tilde{f}_1(\omega_2, \omega_1, \omega_1 + \omega_2 - \omega_3) \delta_{\omega_1 - \omega_3} = \tilde{f}_1(\omega_2, \omega_1, \omega_2) \delta_{\omega_1 - \omega_3} \\
 f_1(\omega_3, \omega_1 + \omega_2 - \omega_3, \omega_1) &= \tilde{f}_1(\omega_3, \omega_1 + \omega_2 - \omega_3, \omega_1) \delta_{\omega_1 - \omega_3} = \tilde{f}_1(\omega_1, \omega_2, \omega_1) \delta_{\omega_1 - \omega_3} \\
 f_1(\omega_1 + \omega_2 - \omega_3, \omega_3, \omega_2) &= \tilde{f}_1(\omega_1 + \omega_2 - \omega_3, \omega_3, \omega_2) \delta_{\omega_1 - \omega_3} = \tilde{f}_1(\omega_2, \omega_1, \omega_2) \delta_{\omega_1 - \omega_3}
 \end{aligned} \tag{11.7}$$

are needed. With \tilde{f}_1 defined as in Eq. (11.6), the general form of the rest terms for the four-point vertex reads

$$R_{\uparrow\downarrow; \uparrow\downarrow}(\omega_1, \omega_2, \omega_3) = 4\tilde{f}_1(\omega_1, \omega_2, \omega_1) \delta_{\omega_1 - \omega_3} \tag{11.8}$$

$$R_{\uparrow\uparrow; \uparrow\uparrow}(\omega_1, \omega_2, \omega_3) = 4\tilde{f}_1(\omega_1, \omega_2, \omega_1) \delta_{\omega_1 - \omega_3} - 4\tilde{f}_1(\omega_2, \omega_1, \omega_2) \delta_{\omega_2 - \omega_3}. \tag{11.9}$$

Accordingly, a rest term corresponding to f_2 could be obtained.

Therefore, we guessed a general rest term, which ensures the fulfillment of the U(1) Ward identity of the Hubbard atom. However, this method of guessing functions to construct rest terms from can be generalized to other models as well. Why obtaining alternatives for the irreducible vertex approximation such as described above might be helpful to improve on the qualities of approximations from Parquet formalism, is reviewed in the conclusion (chapter 12).

12 Conclusion and Outlook

To summarize, this thesis has derived and investigated the $U(1)$ Ward identity for the Hubbard atom in the context of perturbation theory and the Parquet formalism. For this purpose, diagrammatic approximations were calculated, stretching the limits of analytic calculations in the context of perturbative expansions. Regarding this specific aspect of the text, it is concluded that higher-order perturbation theory computations in the general case are only feasible numerically. In the second part of this thesis, these perturbation theory results were used to develop a systematic method to analytically and numerically guess irreducible four-point vertex approximations, which ensure the fulfillment of the $U(1)$ Ward identity.

In principle, this method of finding ansatzes of rest terms could be applied after each Parquet iteration. If convergence of the Parquet equations could be achieved, this would yield a high-quality approximation of the four-point vertex, which fulfills the $U(1)$ Ward identity and thus particle conservation. As the approach is not restricted to the Hubbard atom, it could be tested for other models as well. Setting up the code to try including the rest terms in actual numerical parquet iterations is beyond the scope of this thesis but definitely worth a try.

Another possible continuation of the results from this thesis would be a refinement of the rest-term ansatzes. Currently, they are restricted to rest terms proportional to Kronecker-deltas, whereas in practice the part of the two-particle irreducible vertex not proportional to Kronecker-delta symbols is of even greater interest. Possibly, one could look for a systematic method to make educated guesses on these types of rest terms either analytically or numerically as well. On the other hand, as from each continuous symmetry arises a corresponding Ward identity, one could also try to find rest terms approximations based on the fulfillment of multiple of these identities. As the Hubbard atom possesses a total-irreducible four-point vertex contribution not proportional to Kronecker-delta symbols [12] as well as an additional $SU(2)$ symmetry, it again would fit the criteria of an exemplary model to explore the ideas in this paragraph further. Not least due to its simplicity but also due to its exact solvability, the Hubbard atom has proven itself to be the perfect choice of model when testing out new methods or to learn basics on diagrammatic perturbation theory.

All in all, the fulfillment of Ward identities in the context of diagrammatic approximation methods as the Parquet formalism is of high significance to obtain physically realistic results. As many diagrammatic methods are not designed to automatically ensure Ward identities to hold, fundamental conservation principles are often violated for approximated quantities, which makes further investigation necessary.

Bibliography

- [1] A. Altland and B. Simons, *Condensed Matter Field Theory*, 3rd ed. (Cambridge University Press, 2023).
- [2] D. P. Arovas, E. Berg, S. A. Kivelson, and S. Raghu, “The Hubbard Model,” *Annual Review of Condensed Matter Physics* **13**, Publisher: Annual Reviews, 239–274 (2022).
- [3] E. Pavarini, P. Coleman, and E. Koch, *Many-Body Physics: From Kondo to Hubbard* (Forschungszentrum Jülich GmbH Zentralbibliothek, Verlag, 2015).
- [4] E. Koridon and L. Ligthart, *Solving the one-dimensional Hubbard model with the Bethe Ansatz*, 2018.
- [5] F. A. Berezin, *The method of second quantization* (New York, Academic Press, 1966).
- [6] J. W. Negele, *Quantum Many-particle Systems* (CRC Press, 2018).
- [7] F. Kugler, “Renormalization group approaches to strongly correlated electron systems” (2019).
- [8] L. G. Molinari, *Notes on Wick’s theorem in many-body theory*, 2023.
- [9] J. C. Ward, “An Identity in Quantum Electrodynamics,” *Phys. Rev.* **78**, 182–182 (1950).
- [10] Y. Takahashi, “On the generalized Ward identity,” *Il Nuovo Cimento (1955-1965)* **6**, 371–375 (1957).
- [11] P. Kopietz, L. Bartosch, L. Costa, A. Isidori, and A. Ferraz, “Ward identities for the Anderson impurity model: derivation via functional methods and the exact renormalization group,” *Journal of Physics A: Mathematical and Theoretical* **43**, 385004 (2010).
- [12] P. Thunström, O. Gunnarsson, S. Ciuchi, and G. Rohringer, “Analytical investigation of singularities in two-particle irreducible vertex functions of the Hubbard atom,” *Phys. Rev. B* **98**, 235107 (2018).
- [13] Wolfram Research Inc., *Mathematica*, version 14.0.
- [14] J. Bialk, *JuliaBialk/WardIdentityNotebooks*, version v1.0.0, 2024.
- [15] J. Bezanson, A. Edelman, S. Karpinski, and V. B. Shah, “Julia: A Fresh Approach to Numerical Computing,” *CoRR abs/1411.1607* (2014).
- [16] D. Kiese, A. Ge, N. Ritz, J. Von Delft, and N. Wentzell, “MatsubaraFunctions.jl: An equilibrium Green’s function library in the Julia programming language,” *SciPost Physics Codebases*, **24** (2024).
- [17] R. Hunt, *University of Cambridge - Lecture Notes - Mathematical Methods II (Natural Sciences Tripos, Part IB), Chapter 1*.
- [18] I. Gelfand, S. Fomin, and R. Silverman, *Calculus of Variations*, Dover Books on Mathematics (Dover Publications, 2000).
- [19] J. von Delft and O. Yevtushenko, *Condensed Matter Field Theory – Lecture Notes*, 2020.
- [20] U. Behn, “On the Ward Identities for the Hubbard Model. Particle-Number Conservation and the Analytical Structure of the Self-Energy,” *physica status solidi (b)* **88**, 699–704 (1978).
- [21] N. Beisert, *ETH Zurich - Lecture Notes - Quantum Field Theory i, Chapter 4*.

A Introduction to Functional Derivation

This section serves as short review of the calculus of functionals, which are necessary for the calculations in this thesis. The following text will mainly be a short summary of [17] and the first chapter of [18]. A lot of statements are not proven and one should refer to the literature for this exact purpose.

One can think of a functional as a function of functions and their variables. Geometrically speaking, a functional of one variable is a function of curves and a functional of several variables can even take surfaces as input. Whereas calculus of functionals has many applications in physics, we mostly need concepts to derive generating functionals with respect to field variables in order to derive correlation functions and other related quantities. As our generating functionals are dependent on many field variables, we will focus on functionals of several variables. For simplification, we only consider functionals of two variables containing up to first order derivatives

$$J[z] = \int \int_R dx dy F\left(x, y, z(x, y), \frac{\partial z(x, y)}{\partial x}, \frac{\partial z(x, y)}{\partial y}\right) \quad (\text{A.1})$$

but the concepts can be easily generalized. Here, $z(x, y)$ is an arbitrary function which is a variable of the functional $J[z]$. R is some region where F is well-defined. Probably, even if there was no formal introduction to functionals yet, every physics student has come across the term variation or calculus of variations for example in theoretical mechanics. A variation can be interpreted as a differential of a functional. It can be obtained by incrementing the functional $J[z]$ by a nearby⁷ function $h(x, y)$ and subtracting the original functional, which has not been incremented:

$$\Delta J = J[z + h] - J[z] = \int \int_R dx dy F\left(x, y, z + h, \frac{\partial(z+h)}{\partial x}, \frac{\partial(z+h)}{\partial y}\right) - F\left(x, y, z, \frac{\partial z}{\partial x}, \frac{\partial z}{\partial y}\right) \quad (\text{A.2})$$

Expanding the integrand up to first order yields the variation of J :

$$\delta J \equiv \int \int_R dx dy \frac{\partial F}{\partial z} h + \frac{\partial F}{\partial(\partial_x z)} \frac{\partial h}{\partial x} + \frac{\partial F}{\partial(\partial_y z)} \frac{\partial h}{\partial y} \quad (\text{A.3})$$

Additionally, one can prove that the variation of a functional is unique [18]. Similar to determining extrema of functions, at stationary points of a functional its variation is zero. Determining stationary points of functionals is a concept often needed in physics for example in the Hamiltonian principle where one considers the variation of the action.

If there exists an analog to differentials in functional calculus, it is only natural that there is also an analog to the derivatives of functions, which is called the functional derivative. At first, let's consider the fraction

$$\frac{J[z + h] - J[z]}{\Delta \sigma}. \quad (\text{A.4})$$

Again, h is a function nearby to z . This time however, we impose an additional constraint on h : it is only nonzero in a neighborhood of point (x_0, y_0) . The denominator $\Delta \sigma$ stands for the "area" or "volume" between z and h . Now, let $\Delta \sigma$ and simultaneously the region where h is nonzero go to zero. If Eq. (A.4) converges to a limit under these conditions, this limit is the variational or functional derivative at point (x_0, y_0) and is denoted by $\left. \frac{\delta J}{\delta z} \right|_{x=x_0}$. In fact, the same rules which are usually defined for normal differentiation such as sum rule, product rule, chain rule etc. also hold

⁷What nearby means, is determined by the space the variables are defined on and the respective norm. Functions are defined as components in function space. For example, one can choose the space of all functions with continuous derivatives \mathcal{D}_1 , for which the norm is given by the maximum absolute value of a function. However, one normally chooses the space based on the concrete form of the respective functional one wants to describe. More on function spaces and suitable choices for functionals can be found in [18].

for functional differentiation [18]. Therefore, even if the functional derivative is technically different, in the case of this thesis we can often treat it almost in the same way as derivatives of functions.

B Evaluation of Matsubara Sums

While working in Matsubara frequency formalism, one often encounters infinite summations of the form

$$S = \sum_{n=-\infty}^{\infty} f(i\omega_n) \quad (\text{B.1})$$

with f being a rational function of the Matsubara frequency $\omega_n = \frac{(2n+1)\pi}{\beta}$. In this section, it will be explained how fermionic Matsubara sums can be evaluated in a convenient way following the outline given in chapter 4 of [1]. As in appendix A, the mathematical reasoning behind the calculations will not be discussed rigorously.

The basic idea behind simplifying the computation of terms as Eq. (B.1) is replacing summation by the evaluation of an integral by using Cauchy's residue theorem. It implies that on a connected open subset U of \mathbb{C} the integration of a holomorphic function over a closed path is equal to the residues at the poles of the function enclosed by the path. To apply this theorem to our case, note that every polynomial $g(z), z \in U$ is holomorphic. According to the composition rules for holomorphic functions, the quotient of two holomorphic functions is holomorphic as well and therefore the rational function f from Eq. (B.1) is holomorphic. Next, we choose a holomorphic weighting function, which has poles located exactly at the values $i\omega_n$. Functions, which fulfill this property are for example given by:

$$h_1(z) = \frac{\beta}{1 + e^{-\beta z}} \quad (\text{B.2})$$

$$h_2(z) = \frac{-\beta}{1 + e^{\beta z}} \quad (\text{B.3})$$

We verify the defining property for a suitable weighting function by inserting $z = i\omega_n$:

$$e^{\beta \frac{i(2n+1)\pi}{\beta}} = e^{-\beta \frac{i(2n+1)\pi}{\beta}} = -1 \quad (\text{B.4})$$

Hence, at $z = i\omega_n$ the denominator is 0 and the weighting function has poles for all $n \in \mathbb{N}$. The selection of a specific weighting function only plays a role if the Matsubara sum to be evaluated does not converge. For example, h_1 controls the divergence in the left half of the complex plane, whereas h_2 is used to control convergence in the right half. However, if the frequency sum converges, the final result should not depend on the choice of the weighting function. After choosing between for example h_1 and h_2 , we can express the sum as a contour integral in the complex plane according to residue theorem as

$$\sum_{n=-\infty}^{\infty} f(i\omega_n) = -\frac{1}{2\pi i} \oint f(z)h(z)dz. \quad (\text{B.5})$$

The minus sign in front of the integral arises, as for fermions the Matsubara frequencies are encircled counter-clockwise. The transformation to a contour integral is represented graphically in Fig. B.1. Cauchy's residue theorem also states that deforming the integration contour doesn't change the value of the integral, if the same poles are enclosed by the deformed integration path. Thus, we deform the contour in Fig. B.1a such that the value of the integral in Eq. (B.5) can be determined easily. The choice of the contour is dependent on the specific Matsubara summation to be evaluated. In the case of no branch cuts, which is the case for most Matsubara summations in this thesis, a suitable choice is given by Fig. (B.1)b). In the following, this choice is discussed exemplary. The

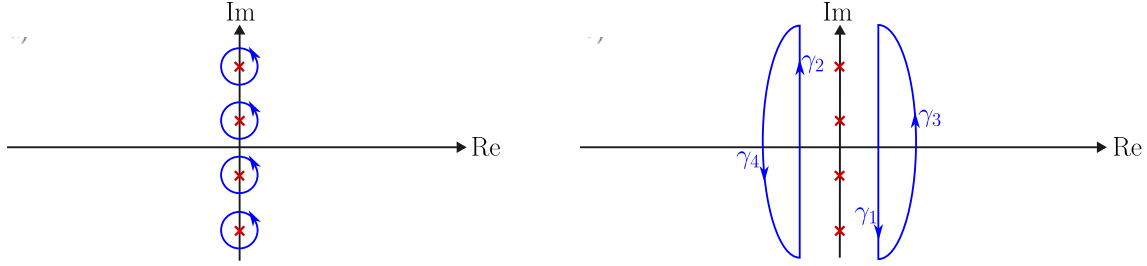


Figure B.1: Schematic overview of how residue theorem can be used to determine the value of Matsubara frequency sums, similar to Figure 4.2 from chapter 4 of [1]. a) location of the function poles $i\omega_n$ on the imaginary axis. b) instead of just integrating along the imaginary axis, the contour is closed such that residue theorem can be applied.

integration path in Fig. B.1b is separated:

$$-\frac{1}{2\pi i} \oint f(z)h(z)dz = \frac{1}{2\pi i} \left(\int_{\gamma_1} f(z)h(z)dz + \int_{\gamma_2} f(z)h(z)dz - \int_{\gamma_3} f(z)h(z)dz - \int_{\gamma_4} f(z)h(z)dz \right) \quad (\text{B.6})$$

γ_3 and γ_4 are half-circles with their radius R going to infinity in order to encircle all Matsubara frequencies on the imaginary axis. In the limit $R \rightarrow \infty$, their contribution to the integral Eq. (B.6) vanishes. This can be seen by inserting the parametrization of a circle into the integral and evaluating the limit, for example for γ_3

$$\lim_{R \rightarrow \infty} \int_{\gamma_3} d\phi R f(Re^{i\phi}) \frac{-\beta}{1 + e^{Re^{i\phi}}} = \int_{\gamma_3} d\phi \lim_{R \rightarrow \infty} \left(R f(Re^{i\phi}) \frac{-\beta}{1 + e^{Re^{i\phi}}} \right) = 0. \quad (\text{B.7})$$

Above, limit and integral are exchanged under the assumption that the integral converges, which will not be proven here. The last equality follows from the domination of the exponential function in the limit $R \rightarrow \infty$ over any rational function of the radius. Applying this reasoning to the integral over the other half-circle, its contribution vanishes as well and therefore

$$-\frac{1}{2\pi i} \oint f(z)h(z)dz = \frac{1}{2\pi i} \int_{\gamma_1} f(z)h(z)dz + \int_{\gamma_2} f(z)h(z)dz. \quad (\text{B.8})$$

Using residue theorem and relating the contour integral back to the original frequency summation, one obtains

$$\sum_{n=-\infty}^{\infty} f(i\omega_n) = - \sum_{\text{poles } z_0} \text{Res}(f(z)h(z), z_0). \quad (\text{B.9})$$

As the function $f(z)h(z)$ has a finite number of poles z_0 , we successfully have reduced an infinite frequency summation to a summation over a finite number of residues, which are computed as

$$\text{Res}(f(z)h(z), z_0) = \frac{1}{(m-1)!} \lim_{z \rightarrow z_0} \frac{d^{m-1}}{dz^{m-1}} ((z - z_0)^m f(z)h(z)) \quad (\text{B.10})$$

with m being the order of the function pole z_0 .

This concludes the explanations on evaluation of simple types of Matsubara sums. Cases of more complex frequency sums leading to branch cuts need to be considered individually.

Affidativ

I hereby declare that this thesis is my own work, and that I have not used any sources and aids other than those stated in the thesis.

Hiermit erkläre ich, die vorliegende Arbeit selbständig verfasst zu haben und keine anderen als die in der Arbeit angegebenen Quellen und Hilfsmittel benutzt zu haben.

Munich, July 24, 2024
München, 24. Juli 2024

Julia Bialk